FOLDING OF THE HUMAN TELOMERE SEQUENCE DNA IN NON-AQUEOUS AND OTHERWISE VISCOUS SOLVENTS

A Thesis
Presented to
Academic Faculty

By

Ford M. Lannan

In Partial Fulfillment
Of the Requirements for the Degree
Master of Science in the
School of Chemistry and Biochemistry

Georgia Institute of Technology

May 2012

FOLDING OF THE HUMAN TELOMERE SEQUENCE DNA IN NON-AQUEOUS AND OTHERWISE VISCOUS SOLVENTS

Approved by:

Dr. Nicholas V. Hud
School of Chemistry & Biochemistry
Georgia Institute of Technology

Dr. Loren D. Williams
School of Chemistry & Biochemistry
Georgia Institute of Technology

Dr. Roger Wartell
School of Biology
Georgia Institute of Technology

Date Approved: March 22, 2012

This is dedicated to…

My wife, Kate Lannan for her enduring faith in my life's path and for the unwavering loyalty and patience during my transition from a soldier to a scientist

and

My parents, Tom and Corliss Lannan whom I must thank for all the support they provided while I was growing up. Without you both, I would not be the man I am today

ACKNOWLEDGEMENTS

First and foremost, I wish to thank Professor Nicholas V. Hud who provided me with this project knowing the constraints of my "Army" timeline. He truly set me up for success, and is one of the main reasons I was able to graduate with a master's degree with an accompanying thesis in the timeframe allotted to me. Moreover, I have been consistently privy to his insight into complex problems and humbled by his ability to convey the answers to these problems in a simple and meaningful way. I have successfully undergone a transition from a soldier to a scientist, which is truly a testament to his contributions to my growth in the field of Chemistry and Biochemistry.

I am eternally grateful to Irena Mamajanov, PhD., whom I have leaned on the most during my investigations presented below. She is truly a gifted chemist and I would not have been able to accomplish what I have to this point without her selflessness and gracious help during the conduct of my research.

I would also like to thank all the members of the Hud Lab, past and present; specifically, Aaron Engelhart, Ragan Buckley, Brian Cafferty, Brandon Laughlin, Michael Chen and Denise Enekwa and the Center for Chemical Evolution (CCE) for friendship, understanding and help along the way; and for funding my research. I am constantly amazed at the tight knit community within the Hud Lab and the CCE as a whole.

Moreover, I would like to thank my additional committee members, Professors Loren D. Williams and Roger Wartell. I much appreciated their time and effort when it

came to furthering my understanding of Chemistry and Biochemistry. Thanks for the fruitful discussions in regards to my research and assistance along the way.

Lastly, I wish to thank Professors Charles L. Liotta and Charles A. Eckert for helpful discussions pertaining to the solvents used in this work and Elizabeth J. Biddinger, PhD., as well as Emily Peterson of the Breedveld lab for assistance with viscosity measurement.

TABLE OF CONTENTS

LIST OF TABLES

LIST OF FIGURES

LIST OF SYMBOLS AND ABBREVIATIONS

DES	Deep Eutectic Solvent
ChCl	Choline Chloride
PEG 200	Polyethylene glycol; Average Molecular Weight 200 amu
Ur	Urea
UV	Ultraviolet
m*m*	millimolal (moles • kg^{-1} solvent)
nm	Nanometer
WL	Wavelength
HTS	Human Telomere Sequence
Htelo1	$d[TAG_3(TTAG_3)_3]$
CD	Circular Dichroism
T_m	Transition Midpoint
G	Guanine Base
A	Adenine Base
C	Cytosine Base
T	Thymine Base
U	Uracil Base
FRET	Fluorescence Resonance Energy Transfer
T-Jump	Temperature Jump
Kcal	Kilocalorie
Mol	Mole

ΔH	Change in Enthalpy
ΔS	Change in Entropy
ΔG	Change in Free Energy
SPR	Surface Plasmon Resonance
η	Dynamic viscosity (eta)
τ	Rate onstant (tau)
GGBA	Guanosine Glycosidic Bond Angles

SUMMARY

G-quadruplex forming human telomere sequence (HTS) DNA has been widely studied due to the telomere's implied role in biological processes, including cellular ageing and cancer physiology. The goal of these previous efforts has been to characterize the physiologically relevant structures and their stability and dynamics in order to develop therapeutic applications. Unfortunately, understanding the biologically relevant form of the human telomere DNA is complicated by the fact that HTS-derived sequences are highly polymorphic. To further complicate the issue, recent investigations have demonstrated the ability of "cell-like" co-solvents to alter the preferred G-quadruplex fold of HTS DNA.[1-3] Overall, the origins of G-quadruplex structure selection, the relative contributions of crowding versus dehydration, and the possible effects of co-solvents on kinetically determined folding pathways remain unresolved.

Towards answering these questions, I investigated HTS DNA G-quadruplex in extreme anhydrous and high viscosity conditions utilizing a deep eutectic solvent (DES) consisting of choline chloride and urea. Herein, I report that the water-free DES supports an extremely stable parallel stranded structure, consistent with observations that diminished water activity is the main cause of structural transitions to the "parallel-propeller" form.[2] Furthermore, my research shows that the highly viscous nature of the solvent enables significant diffusion based control over HTS g-quadruplex folding rates and topology, fully consistent with Kramers rate theory. To the best of my knowledge, this is the first example of the kinetic exploration of G-quadruplex folding utilizing high friction solvent; the results of which display a decreased *intramolecular* folding rate of

HTS DNA to a never before encountered time scale on the order of days at physiological temperature. Moreover, I have demonstrated that the folding pathway of a G-quadruplex can be altered with increased solvent friction. These discoveries are important because they highlight the need to consider the viscosity when exploring the dynamics of human telomeres specifically drug binding and folding of G-quadruplexes in vivo where cellular viscosity has been reported to be as high as 140 cP.[4] Lastly, it appears that tuning solvent viscosity could prove useful to the continued study of G-quadruplex dynamics.

CHAPTER 1

INTRODUCTION

1.1 Abstract

A lesser-known, non-canonical secondary structure of DNA, called G-quadruplex, is of considerable interest and is the focus of this work. G-quadruplex DNA was first characterized by Gellert et al. in 1962. The Davies group introduced the so called G-tetrad and proposed a four stranded helical structure for tetramers of guanylic acid.[5] This chapter will introduce the on-going research on the stability, structure and dynamics of G-quadruplex DNA since this discovery. Moreover, I will present the prevalence of the G-quadruplex in biology and its relevance to human telomeres. Lastly, in this chapter, I will introduce the theory of diffusion-controlled folding reactions that are governed by solvent friction and explain why HTS DNA is a model system to investigate nucleic acid dynamics as a function of solvent viscosity.

1.2 Introduction to the G-quadruplex structure and human telomere sequence DNA

The basic building block of guanine rich G-quadruplex DNA is the G-tetrad, which is composed of four guanine bases that utilize their Hoogsteen and Watson Crick edges to form eight hydrogen bonds per square array. Notably, the exocyclic oxygen of the guanine relieves the buildup of negative charge within the interior of the tetrad by

coordinating a monovalent cation such as Na^+ or K^+. Further stability is achieved by the planarity of the G-tetrads, allowing favorable π-π stacking interactions. Figure 1.1 below displays a general schematic of a G-tetrad

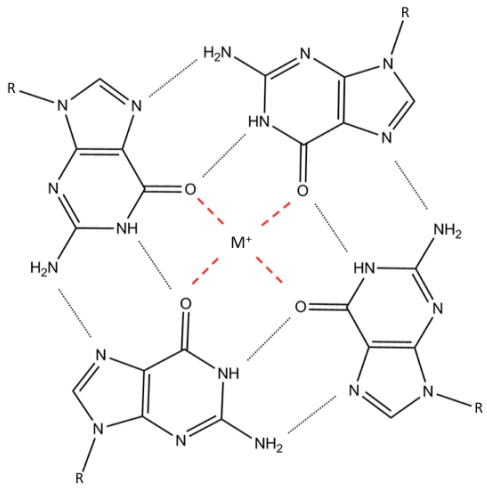

Figure 1.1 Schematic diagram of the guanine quartet. The deoxyribose sugars (R) are not shown for clarity. Black dotted lines indicate hydrogen bonds. Red dashed lines indicate the coordination of the central cation.

While B-form DNA has all anti-glycosidic bond angles and anti-parallel strand orientation, the G-quadruplex can have a mixture of anti- and syn- glycosidic bonds, as well as different strand orientations. Four combinations of strands orientation are possible including: all parallel, 3+1 or so called "hybrid", anti-parallel (up-down-up-down) and anti-parallel (up-up-down-down). The loops connecting the strands may vary as well, and can be described as diagonal (connecting strands on the opposite corner of the G-tetrad), lateral or edgewise (connecting strands on the same face in the anti-parallel direction), or chain reversal (connecting strands on the same face in the parallel direction). See Figure 1.2 for an illustration of the G-quadruplex strand and loop

topologies. Oligonucleotides containing G-rich sequences can form tetra, bi- or unimolecular quadruplexes. The discussion herein will be limited to intramolecular quadruplexes, specifically a four repeat sequence, as this is the minimum number of repeats that allows a unimolecular fold.[6] For this reason, such sequences are the most relevant to biology, and specifically, the human telomere.

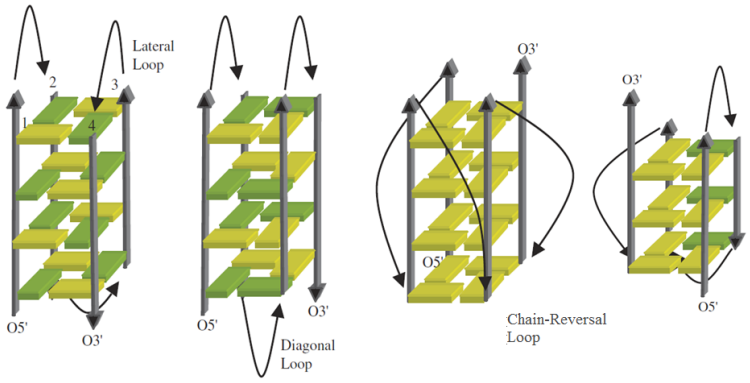

Figure 1.2 Schematic diagrams showing various loop linkers, strand orientations, and resulting glycosidic bond angle arrangements for intramolecular quadruplexes. Green bases indicate syn-, yellow bases indicate anti- orientations. Diagram adapted from reference [7].

The ends of eukaryotic chromosomes are protected from degradation and fusion by telomeres, which are DNA-protein complexes that are maintained by telomerase, a ribonucleoprotein reverse transcriptase.[8, 9] Telomere DNA is comprised of short repeats, *e.g.* $d(TTAGGG)_n$ in humans, with a duplex region and an extended 3'-overhang of the G-rich strand.[10, 11] DNA sequences derived from the telomeres of various species, including the HTS form G-quadruplex structures *in vitro*.[7] G-quadruplex DNA

and RNA is also located throughout other locations in the genome, specifically promoter regions[12], however, for this investigation, the human telomere sequence is the focus.

G-quadruplex formation has been shown to inhibit telomerase, which is overexpressed in many cancer cells.[13, 14]. Therefore, stabilization of the G-quadruplex within the telomeric region would inhibit telomerase and prompt apoptosis in rapidly proliferating cells [15, 16], making the HTS G-quadruplex of particular interest to structural based drug design. Unfortunately, unimolecular G-quadruplexes, including the HTS DNA, are extremely polymorphic depending on sequence, loop size, type of cation bound and solvent conditions. Theoretically, there are 26 different combinations of structures with different loops and strand orientations possible.[17] As of the writing of this text, five different types of structures for HTS DNA have been solved by high-resolution structural studies in vitro.[6, 18-25] Figure 1.3 displays the different solved topologies for the HTS DNA.

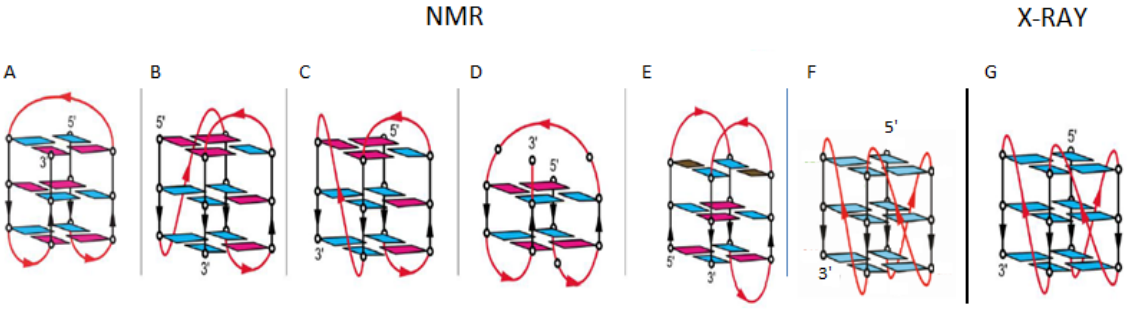

Figure 1.3 Schematic diagrams of intramolecular G-quadruplex consisting of human telomere sequence DNA. (*A*) NMR solved, Na^+ stabilized, basket conformation of sequence d[AGGG(TTAGGG)$_3$] in aqueous conditions,(PDB ID:143D);[19] (*B*) NMR solved, K^+ stabilized, 3+1 hybrid form 1 of sequence d[TAGGG(TTAGGG)$_3$] in aqueous conditions (PDB ID: 2JSM);[23] (*C*) NMR solved, K^+ stabilized, 3+1 hybrid form 2 of sequence d[TAGGG(TTAGGG)$_3$TT] in aqueous conditions (PDB ID: 2JSC);[23] (*D*) NMR solved, K^+ stabilized, basket conformation with only two G-tetrad layers of

sequence d[GGG(TTAGGG)$_3$] in aqueous solution (PDB ID: 2KF8);[24] (E) NMR solved, K^+ stabilized, chair conformation of sequence d[AGGG(CTAGGG)$_3$] in aqueous solution (PDB ID: 2KM3);[26] (F) NMR solved, K^+ stabilized, propeller-type conformation of sequence d[TAGGG(TTAGGG)$_3$] in 40% PEG 200 (v/v) solution (PDB ID: 2LD8);[1] (G) X-ray solved crystal structure of K^+ stabilized propeller-type G-quadruplex observed for the sequence d[AGGG(TTAGGG)^3] (PDB ID:1KF1).[18] Of note, the only difference between hybrids form 1 and form 2 is the position of the chain reversal loop. Cyan guanines are anti-; magenta guanines are syn-; brown colored bases are cytosines; and the TTA loops are the red lines with arrows. This diagram was adapted from reference [1].

The design and screening of ligands that target the G-quadruplexes present within the 3'-overhang of telomere DNA in cancer cells is complicated further by the fact that the actual structure of the G-rich single stranded overhang of human telomere DNA *in vivo* is a matter of considerable debate – a debate driven by the extreme polymorphism of the HTS sequence and further fueled by reports that HTS DNA forms multiple mixed antiparallel/parallel-stranded G-quadruplexes in solution, but a parallel-stranded structure in the crystal state.[27] Recent investigations addressing this question have explored the influence of molecular crowding [1, 28] and reduced water activity [2, 3, 29] on the equilibrium-favored HTS structure, motivated by the hypothesis that the cellular environment (and crystallization milieu) could influence G-quadruplex structure. These studies have demonstrated the ability of co-solvents to drastically alter the topology of G-quadruplexes formed by HTS DNA sequences, but questions still remain concerning the origins of structure selection, the relative contributions of crowding *vs*. dehydration, and regarding which fold is of most biological relevance.[30-39]

1.3 Stability and dynamics of human telomere sequence DNA

Under physiological conditions (37 °C, pH ≈ 7, [100 mM] cation) the intramolecular G-quadruplex formed by human telomere sequence DNA is stable.[40, 41] Factors that stabilize G-quadruplex structures include hydrogen bonding, base stacking, both specific and non-specific ionic interactions, and solvation effects driven by entropic forces.[42] The relative contributions of each of these forces is a matter of debate, however, *ab initio* calculations conclude that interior cation interactions with the exocyclic guanine carbonyl groups provide more enthalpic stability than hydrogen bonds or π-π interactions as a result of base stacking.[43] This conclusion is reinforced by a recent empirical study by Gray and Chaires where they found that quadruplex folding is driven almost entirely by the free energy of cation binding.[44]

Whether contributions from other factors are significant, most data supports the formation of G-quadruplexes as being enthalpically driven. The enthalpy per quartet of HTS DNA with the minimum number of repeats is approximately -15 kcal/mol.[45] Additional residues on the 5' end of the sequence appears to stabilize the quartets, whereas longer repeats destabilize quartet formation but seems to maintain the overall thermal stability.[45, 46]

The type and concentration of cation present within the quadruplex greatly determines the overall stability. Venczel and Sen rank ordered the divalent and monovalent cations as follows $Sr^{2+} > Ba^{2+} > Ca^{2+} > Mg^{2+}$ and $K^{+} > Rb^{+} > Na^{+} > Li^{+}$, Cs^{+}.[47] Of note, smaller sodium ions are able to coordinate in the plane of the G-tetrad, whereas the larger potassium ions must coordinate between the planes. For the purpose

here, physiologically relevant cations are the focus, specifically potassium. Table 1.1 summarizes some representative empirical data from thermodynamic studies of the HTS DNA with K^+, or Na^+ cation added for stabilization.[48]

Table 1.1 Energetics of HTS DNA unfolding

Sequence (5'-)	Cation Concentration	T_m (°C)	-ΔH (kcal/mol)	-ΔS (cal/mol•K)	-ΔG (kcal/mol)	Ref.
$(TTAG_3)_4$	70 mM K^+	63	49	147	3.8	[49]
	70 mM Na^+	49	38	119	1.4	
$AG_3(TTAG_3)_3$	100 mM K^+	63	57	169	4.4	[40]
	100mM Na^+	56	54	163	3.1	
$TTAAG_3(TTAG_3)_3$	100 mM K^+	55	63	193	3.5	[40]
	100 mM Na^+	44	38.5	121	0.9	
$G_3(TTAG3)_3$	100 mM K^+	69.3	77.5	202	7.3	[46]
	100 mM Na^+	63.7	72.7	192	5.8	
$AG_3(TTAG_3)_3^{(A)}$	100 mM K^+	61.8	66.2	186.5	4.9	[50]
	100 mM Na^+	42.8	51.4	153	0.9	
$AG_3(TTAG_3)_3^{(B)}$	25 K^+	111	53.7	N/A	10.7	[2]
	25 Na^+	66	58.1	N/A	7.1	

(A) Obtained through FRET analysis
(B) 50% CH_3CN_3 (v/v)

Clearly potassium displays greater stabilization effects on the HTS quadruplex DNA than sodium. The greater stabilization is mainly attributed to the greater free energy cost of Na^+ dehydration[51] which is a theory based on Crystallographic data (< 1 Å resolution) and NMR studies, indicating that cations within a G-quadruplex are dehydrated.[52]

The length and composition of loops have been shown to affect the stability of G-quadruplexes. The HTS sequence contains a TTA linker. For an intramolecular G-quadruplex with a 3-tetrad stack, there is a one base minimum for loop length, but linkers

of two or less in some sequences have been shown to prevent diagonal loops from forming. Overall, a strong inverse correlation exists between total loop length and T_m.[53] Studies also show loop composition alters stability. For example adenine bases will preferentially stack on G-quartets, whereas thymine maintains rotational freedom, thereby adding no additional stability.[19, 54] However, when considered in tandem, loops prefer thymines as opposed to runs of adenine, which destabilize the overall G-quadruplex structure.[55]

The structure or type of fold of a G-quadruplex greatly affects its overall stability. Parallel G-quadruplexes are more thermodynamically stable than anti-parallel because of both the enthalpy and entropy of formation. However, parallel structures may be less favored from a kinetic standpoint, where one conformation may be transient with time or become kinetically trapped.[56, 57]

Investigation of the intramolecular folding of the HTS G-quadruplex has proven difficult. There are only a few methods that allow accurate monitoring on the time scale needed to properly observe folding kinetics. The various methods used include, stopped flow (SF) devices, fluorescence resonance energy transfer (FRET), temperature jump (T-jump) and surface plasmon resonance (SPR).[7, 42] The general consensus is that the unfolding and formation of *unimolecular* G-quadruplex DNA is kinetically complex. The pathway is usually not a simple two-state process and more often than not, significant intermediates exist along a multistep-folding pathway. The investigation is complicated even more by the fact that the dynamics of the G-quadruplex DNA are dependent on the preferred topology favored in the conditions utilized for investigation. Specifically, Phan and Patel discovered the two-repeat HTS sequence d(TAGGGTTAGGGT) adopts both

parallel and anti-parallel G-quadruplex in K^+ solution and the antiparallel form folded faster but unfolded slower than the parallel form.[58] Table 1.2 below, summarizes representative results of the rates of unfolding and folding of HTS G-quadruplex DNA.

Table 1.2 Kinetics of HTS DNA unfolding and folding

Sequence (5'-)	Method Used	Temperature (°C)	Cations	τ_U (s)	τ_F (s)	Ref.
$d[AG_3(TTAG_3)_3]$	SF	25	[50 mM] K+		0.037	[59]
$d[TTG_3(TTAG_3)_3]$					0.217	
$d[TTG_3(TTAG_3)_3]$					0.063	
$d[(TTAG_3)_4]$	SPR(A)	25	[150 mM] K+	769.2	83.3	[60]
$d[G_3(TTAG3)_3)]$	FRET(B)	20	[100 mM] K+	791		[61]
$d[G_3(TTAG_3)_3)]$	FRET(C)	20	[100 mM] K+	1887		[62]

(A) Monitored unfolding utilizing hybridization to cDNA to form duplex DNA from quadruplex
(B) Monitored unfolding utilizing hybridization to cDNA to form duplex DNA from quadruplex
(C) Monitored unfolding utilizing hybridization to PNA to form duplex DNA/PNA from quadruplex

As seen in Table 1.2, the timescale of folding of the HTS G-quadruplex ranges from 20 ms to 1.5 minutes depending on the method used, sequence, and cation conditions. Despite the difference in rates, these kinetic studies allowed the determination of general proposed folding pathways. First, as suggested by Chaires and Gray, is that the quadruplex folds in a cooperative fashion where K^+ cation binding and folding occurs in a sequential manner. After the initial collapse of the unfolded structure, anti-parallel hairpins maintain equilibrium with less ordered structures. The hairpins then subsequently fold back upon themselves to form transient G-quartets stabilized by H-bonding and cation binding. Then, a slower rate determining isomerization may take

place, at which point, strand orientation and loop type may change.[59] Similar observations by Lee et al. revealed that during folding, the HTS exhibits at least six different conformational states. The first transition is a major compaction event, from a highly disordered ssDNA to short lived, more ordered structures with the same "global folds" as either anti-parallel or parallel quadruplex. These short-lived species exist due to incomplete cation binding between G-quartets and may interconvert between the parallel and anti-parallel topology. Finally, the late stage intermediates are locked into their long lived final states by minor local rearrangements and correct cation binding and coordination.[38]

In contrast to these observations, the Sugiyama group has proposed a "triple strand core model" as the intermediate that would allow folding and subsequent interconversion between different folds of potassium stabilized HTS G-quadruplex. Both *ab initio* methods and single molecule FRET with bromo-guanine substitutions led to the conclusion that an intermediate triplex like structure is more energetically favorable than a modified hairpin (G-G Hoogsteen base pairing) and is just as stable as the complete G-quadruplex. Therefore, according to their model, the pathway would be stepwise in that the initial hairpin would fold into the G-quadruplex structure via triplex formation with K^+ cation association with each step. This would then be followed by the fourth G-tract binding, forming either the chair conformation or the so-called hybrid (3+1) topologies.[63, 64]

Similarly, Ambrus et al. have proposed, a strand reorientation mechanism that could explain switching conformations between the sodium favored anti-parallel basket topology and the hybrid form 1 (3+1) structure upon the addition of potassium ions. The

mechanism would allow the 5'- G-strand of the basket type G-quadruplex to dissociate from the G-tetrad core. The strand could then swing around to the other side of the second G-strand to form an all anti-parallel stranded structural motif with two lateral and one diagonal loop, utilizing a similar triplex type intermediate proposed by the Sugiyama group.[65] Alternatively, if the 3'- G-strand of the hybrid form 1 structure then underwent the same strand re-orientation mechanism, the parallel topology would emerge with all chain reversal loops.

In contrast to the proposed triplex and hairpin proposed intermediates, Zhang et al suggest that a novel basket-type G-quadruplex with only two G-tetrads coordinating one potassium ion as an intermediate state. Using this structure, solved by NMR, they argue that this intermediate would enable a strand-reorientation mechanism that would facilitate switching between anti-parallel and mix stranded hybrid (3+1) structures as well as switching between the form 1 and form 2 of hybrid structures.[66] Their proposed intermediate would form a transient two G-tetrad conformation stabilized by loop interactions. The mechanism would have the 5' strand slide up to dissociate from the core G-Tetrad, forming the transient two-tetrad intermediate, followed by re-association of the strand after a "swing-back" type rearrangement. Similarly, the 3'-G-strand would disassociate and re-associate utilizing the same intermediate and thus transition between the two hybrid forms. This mechanism also explains the transition from the sodium favored anti-parallel basket form and the potassium favored hybrid forms.

The kinetics of the proposed interconversion of G-quadruplex structures is also of significant interest. It is theorized that the variability of the local sodium and potassium concentrations within a cell, and the fact that cell–like conditions are crowded with the

presence of large co-solvents and diminished water activity, enable structural switching of the HTS DNA G-quadruplex.[67-69] Gray et al. characterized the HTS conformational switch from the sodium basket form to the potassium hybrid forms. They concluded that the energy barrier separating the two topologies was small, 1.4-2.4 kcal/mol. They also found that the time course of this transition occurred in three distinct kinetic phases. A rapid phase (< 5 ms), in which the sodium ions are replaced by potassium, followed by slower structural rearrangements with relaxation times of 40-50 seconds and 600-800 seconds at 25 °C.[70] The major structural rearrangement they propose, is the reorientation of one strand and loop with a triplex as an intermediate similar to the mechanism discussed above and proposed by Dai et al[21] and Mashimo et al.[64]

Multiple groups have also monitored the structural transition from the potassium stabilized, hybrid aqueous solution forms to the parallel conformation that is induced upon the introduction of crowding or dehydrating agents. Heddi and Phan observed a much higher activation energy barrier for this transition reported as 32.5 kcal/mol with time constants on the order of 2 hours at physiological temperatures. For the opposite transition, they reported a barrier of 18.9 kcal/mol with a corresponding time constant of 7.5 minutes.[1] From this study it appears that transition from the parallel structure to the hybrid requires less energy than the conversion of the hybrid structure to the parallel one in crowded solution. However, both transitions require substantially more energy of activation (> 17 kcal/mol) than the interconversion between the sodium stabilized basket topology and the potassium favored hybrid forms.

Petraconne et al. recently reported that not all of the HTS G-quadruplex converted to the parallel form when exposed to the molecular crowding agent PEG 200. In contrast,

a significant fraction remained in the hybrid topology at physiological temperatures. They attributed this inconsistency with other groups data[1] to the slightly altered sequence or experimental conditions. Regardless of this discrepancy, their data reinforces that HTS DNA, under crowded conditions, exists in the parallel form.

Xue et al., in their study in a K^+/PEG solution, found that when HTS DNA is liberated from duplex DNA, the strand first adopts the hybrid mixed stranded structure followed by a slow conversion to the thermodynamically favored parallel state. The kinetic mechanism consisted of first unwinding and folding into the hybrid structure, followed by a slow isomerization to the parallel structure with a relaxation time of 50 seconds. Their results suggest that the refolding of HTS G-quadruplex may have kinetically favored conformations.[57] In contrast to these results, Xu et al. found that the refolding from the hybrid to the parallel structure had a relaxation time of 2.9 hours.[71]

Despite all of these findings, the physiological relevant form of HTS is still a matter of debate. From these studies, it is obvious that kinetic control is possible. Moreover, these investigations also indicate a structural transition from the hybrid or anti-parallel forms to the parallel topology occur much further away from equilibrium. Therefore, a much greater potential for control exists for this conversion as opposed to the transitions between the various aqueous hybrid forms stabilized by potassium *vs.* the sodium favored basket topology. However, some investigators may argue that the latter conversion is more assessable due to a smaller energy barrier separating the different forms and therefore more likely. Another level of control is described by the Chaires group, in which they suggest that potassium ions may allosterically regulate HTS DNA conformation and function through an external binding site.[72]

Again, all of these results suggest that HTS DNA dynamics are far from completely understood, and the possibility of kinetic control is worth exploring.[57] Interestingly, the kinetics of a DNA chain folding reaction is generally considered to be under diffusional control.[73-75] Therefore, an introduction into Kramers rate theory and diffusion controlled processes is necessary to further study the dynamics of HTS DNA and to finish the introduction of the work presented in the remainder of the thesis.

1.4 Introduction to diffusion controlled kinetics and Kramers rate theory

In 1940 H.A. Kramers wrote a seminal paper on the diffusion model of chemical reactions.[76] In that paper he outlined explicit theoretical results obtained in the simplified cases of small and large viscosity. Kramers found that in the large viscosity or the strong friction regime, the velocity of a chemical reaction overcoming a one-dimensional barrier is inversely dependent on the frictional forces the molecules are subject to along the reaction coordinate (Equation 1.1).[76]

$$k = (\omega_A \omega_B / \gamma\, 2\pi) e^{\frac{-\Delta G}{k_B T}} \qquad \text{(Equation 1.1)}$$

Where γ represents the friction coefficient, k_B is the Boltzman constant and ωA and ω_B represent the curvature of the free energy barrier at the bottom and the top of the reaction barrier respectively. This conclusion distinguishes Kramers rate theory from other theories such as the Eyring transition-state theory (TST) in that the diffusive mechanism describes multiple random crossings and recrossings of the activation barrier,

whereas TST accounts for a particle in the absence of friction crossing the barrier only once. Therefore, TST often empirically overestimates reaction rates in viscous conditions due to the fact that molecules subject to high friction slow considerably during the multiple recrossing events.[77]

By applying Stokes law, which asserts that the dynamic viscosity (η) of the solvent scales proportionately with the drag force experienced by a particle moving through a fluid, to Kramers rate theory, Equation 1.2 may be written, which conveniently summarizes Kramers theory into a straightforward correlation between k and η.[78]

$$k = \left(\frac{A}{\eta}\right) e^{\frac{-\Delta G}{k_B T}} \qquad \text{(Equation 1.2)}$$

It is important to note that the friction coefficient in Equation 1.1 represents all of the means by which energy can be dissipated out of the reaction coordinate.[77] Moreover, it is an oversimplification to assume that the friction exhibited on the system is completely captured by the bulk macroscopic property of dynamic viscosity.[77] However, often times it is convenient to simplify the microscopic detail in order to study reaction kinetics with the easily measurable viscosity of the solvent. In many cases this approach has proven to be effective in the study of protein folding dynamics, where rate-limiting barrier-crossing processes dominate.[77-89] However, just as many investigations have uncovered other cases in which the mechanisms of friction are independent of viscosity and play a significant role in folding reactions leading to a non-linear correlation between reaction rate and solvent viscosity or at least a weaker dependence (i.e. $k > 1/\eta$).[90-92] These mechanisms include non-frictional solvent effects

or internal friction; which is defined as the dissipation of energy into the folding molecule that do not contribute to the progress along the reaction (folding) coordinate.[77]

In addition, practical difficulties have been identified such as microviscosity differences from bulk viscosity [93, 94] and stability effects [95] caused by added viscogens. Regardless of these findings, Kramers rate theory is generally accepted and has been applied to the investigation of protein folding dynamics and, on a few occasions, to DNA folding kinetics. More recent investigations into folding kinetics have focused on utilizing Kramers rate theory to probe the dynamics of the reaction pathway. These studies include establishing whether the rate-limiting steps of protein folding involve the diffusive motion of the polypeptide and identifying the diffusion controlled stages of protein folding that are not rate limiting.[77] Additionally, more accurate measurement of the kinetic parameters and the probing of non-solvent directed conformational dynamics may be obtained by changing the viscosity of the solvent.[77] Employing this application to G-quadruplex folding, and in particular HTS DNA dynamics, should be valid, as DNA hairpin folding rates have been shown to scale with viscosity, suggesting that nucleic acid chain diffusion is subject to frictional control.[73, 74] Moreover, the polymorphic nature of the HTS DNA allows for the probing of different solvent and co-solvent effects on the folding of an intramolecular G-quadruplex thereby making it a model system. Conversely, Kramers rate theory should provide insight into the convoluted free energy landscape of HTS DNA dynamics.

CHAPTER 2

EXPERIMENTAL TECHNIQUES

2.1 Abstract

This chapter introduces Circular Dichroism as the primary method used in this work to gain information about the G-quadruplex structures of HTS DNA. This chapter then explains how circular dichrosim is used to monitor transitions of quadruplex structure over temperature gradients and throughout a time course. Finally, an introduction to the measurement of dynamic viscosity is made and the difference between the bulk property and local microscopic viscosity is explained.

2.2 Monitoring nucleic acids with circular dichroism

Circular dichroism (CD) is differential absorption when left and right handed circularly polarized light is passed through an optically active substance.[96] A CD instrument measures the wavelength dependence of this absorption difference, termed ellipticity, and thereby provides a characteristic spectrum which enables the assignment of the configuration of a chiral molecule.[97] The chirality of a molecule can be conformational rather than structural, as is the case in the study of the secondary structure of biological macromolecules.

With nucleic acids, the electronic transitions of the chromophoric bases interact to give the characteristic CD spectra. Since CD of nucleic acids is dependent on the base-

base interactions, the technique is sensitive to G-quadruplex secondary structure.[96] Guanines composing the G-tetrads of G-quadruplexes are the chromophores responsible for two absorption bands occurring in the 240-290 nm region as a result of their π-π^* transitions. Chiral excitation coupling occurs between the transition dipole moments caused by the polarized guanines in adjacent stacked G-tetrads.[98] It is hypothesized that stacking quartets of the same or alternating polarity give rise to the two basic types of guanine quadruplex spectra; parallel and antiparallel respectively. Parallel quadruplexes with all anti- or syn- glycosidic bond angles and therefore the same polarity have a dominant positive band at 260 nm and a negative band at 240 nm. Alternatively, antiparallel quadruplexes have a characteristic negative band at 260 nm and a positive band at 290 nm due to the alternating guanosine bond angles and opposite base stacking polarity.

Unfortunately, CD is only an indirect method for the characterization of quadruplex conformation because at this time, there is no valid approach to determine the atomic level structure of a G-quadruplex from a CD spectrum. Structural analysis of G-quadruplex DNA currently relies heavily on empirical comparisons to solved structural motifs.[99] Fortunately, the complex topology and polymorphic nature of the HTS DNA, can be resolved into three characteristic groups and resulting distinct spectra.[100] The groups can be described by classifying the sequence of guanosine glycosidic bond angles (GGBA) along the strand of the stacked guanosine bases. Quadruplex strands that run in the same direction are characterized by the same GGBA and called a “parallel” G-quadruplex as described in Chapter 1. Antiparallel quadruplexes can be divided into two groups. First as described in Chapter 1, a “3+1” quadruplex, which contains both, runs of

GGBA of the same orientation (i.e. anti–anti and syn–syn), as well as different orientations (i.e. syn–anti and anti–syn). The other group, described in Chapter 1 as pure "antiparallel", is comprised of distinct sequences of GGBA. Figure 2.1 provides representative CD spectra for each of these three groups.

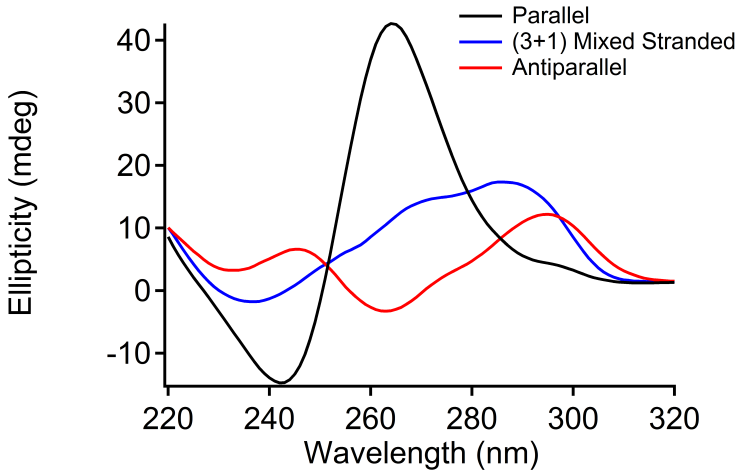

Figure 2.1 CD spectra of the three major forms of HTS DNA G-quadruplex. All samples were 1 mM DNA in nucleotide, contained 100 mM of sodium (antiparallel) or potassium (3+1 and Parallel) Chloride salt and 20 mM of the respective phosphate buffer. Parallel form was induced by addition of PEG 200 to 40% (v/v).

Of note, CD is most useful for distinguishing the parallel stranded topology from the antiparallel or mixed stranded 3+1 conformation. Caution should be exercised when differentiating the two different groups of antiparallel quadruplexes from each other. Moreover, the contribution to CD spectra from different loop types is not negligible and can affect the spectrum in unforeseen ways.[101] Therefore, CD cannot be used to accurately determine the type of loop. As stated above, a direct empirical comparison to a spectrum with a solved structure is needed to effectively determine the exact topology of the G-quadruplex in question.

Circular dichroism is a valid spectroscopic technique to monitor the folding and unfolding of a G-quadruplex. The sensitivity of the instrument allows direct observation of the spectra of folded and unfolded states. Spectral changes allow determination of the thermodynamic properties or kinetic parameters associated with melting transitions.[42] Folding and unfolding reactions of G-quadruplex structures tend to not be simple "two-state" processes, and therefore, must be fit to specific models to obtain thermodynamic or kinetic parameters. In order to test for a two-state transition, isobestic points are usually identified. However, due to experimental limitations, the visual inspection of spectra for the determination of an isobestic point is unreliable.[102] A dual wavelength parametric plot is a more rigorous test of two-state transition.[103] Specifically, a linear or non-linear dependence of spectra are revealed graphically when two wavelengths (usually ca. 265 nm and ca. 295 nm) are plotted against one another. A linear fit of the data would indicate a two-state transition. An additional test of a two-state assumption occurs by singular value decomposition (SVD) analysis. In this analysis, 3D CD Data (ellipticity, wavelength, time) is converted to a matrix. Then SVD of the matrix effectively determines the number of species necessary to account for the changes in the spectra.[104, 105] The dual-wavelength parametric test is used as a two-state transition test for the studies presented herein.

2.2.1 *CD spectrophotometry parameters*

CD spectra were acquired on a Jasco J-810 spectropolarimeter with a Peltier temperature controller (± 0.1 °C accuracy) and 1 mm path length cells. For thermal

denaturation studies, spectra were acquired by scanning 220-320 nm at a rate of 500 nm/min, with averaging of three measurements. For kinetic studies, samples were scanned from 310-235 nm at a rate of 1000 nm/min, with averaging of two measurements.

Single-wavelength progress curves at 260, 290 or 295 nm were used to monitor the folding transition of the HTS G-quadruplex. Kinetic constants were obtained by utilizing the nonlinear least-squares method to fit the data. Standard exponential and double exponential fitting functions of Igor Pro were employed for most fits. However, the fits obtained in Figure 4.11 utilized a three species model derived from the following rate expression:

$$[U] \overset{k_1}{\rightarrow} [K] \overset{k_2}{\rightarrow} [T] \qquad \text{(Equation 2.1)}$$

where U, K and T represent the unfolded state, kinetic state and thermodynamic state of the G-quadruplex, respectively, and k_1 and k_2 represent the rates of conversion between these forms. Utilizing Mathmatica, the resulting integration of the differential rate equations, obtained from Equation 2.1, yielded the following function:

$$f(t) = A \cdot e^{(-k_1 \cdot t)} + B \cdot \frac{(k_1)}{(k_2 - k_1)} \cdot \left(e^{(-k_1 \cdot t)} - e^{(k_2 \cdot t)}\right) + C \qquad \text{(Equation 2.2)}$$

where *f(t)* is the ellipticity intensity at time *t*; *A, B,* and *C* are constants relating to the CD signal of each of the three structural forms (U, K, or T) and k_1 and k_2 are the rate constants. Of note, during least squares fitting utilizing Equation 2.2, the ellipticity values

of the kinetic structure were allowed to vary between the data sets to make up for the multiple species that are likely present at different amounts for each of the different temperatures. For convenience during discussion, the rate constants obtained from fitting kinetic curves have been converted to relaxation times (τ) from the relationship $\tau = 1/k$.

2.3 Viscometer and rheometer measurements

Viscosity is a fundamental physical property of liquids. When a fluid flows, it has an internal resistance to flow. Viscosity is a measure of the resistance to flow that is a function of both temperature and pressure.[106] Viscosity is expressed in two forms: dynamic or kinematic. For the purpose of this work we will focus on the measurement of dynamic (or absolute) viscosity only. Dynamic viscosity is the tangential force per unit area required to slide one layer of fluid against another when two layers are maintained at a unit distance.[106] Macroscopic measurement of dynamic viscosity is obtained from a viscometer or rheometer and is usually expressed in units of centipoise (cP) or pascal-second (Pa•s) (1 cP = 1 mPa•s). The flow characteristics of most liquids are uniform, and described as Newtonian, after Newton's law of viscosity.[107] There are other forms of bulk liquid flow, but they are beyond the scope of this work and shall not be discussed.

The movement of molecules through a viscous medium is described by single particle diffusion. Single particle diffusion is defined by Stoke's law, which is referenced in Chapter 1. Briefly, the drag or frictional force on a spherical particle is proportional to the dynamic viscosity of the solvent. Particle diffusion at the cellular scale however, is more appropriately described by microscopic viscosity, or the local friction experienced

by a molecule undergoing diffusion. This physical property is used to explain the instances where macroscopic viscosity fails to depict the local interactions between molecules and the surrounding environment at the micrometer and nanometer length scales. Both the affect of crowding and the size of co-solute in a solution have been shown to contribute to the measured microscopic viscosity assessed by distorted translational mobility.[108] These factors are especially important in the study of the microscopic viscosity and diffusion of particles within a cell where the environment is non-homogeneous and crowded with biological macromolecules. Compartments inside a cell have been shown to have a viscosity as high as 140 cP, [109] thereby contributing significantly to the diffusion phenomena of intracellular particles, and macromolecules.

2.3.1 Viscosity measurements

Dynamic viscosity of the 90% DES solution was determined using a RheoSys Merlin II rotational viscometer with an integrated temperature controller and cup and bob attachment. The apparatus was calibrated using two viscosity standards (Brookfield, VWR). The instrument error of the 96 cP standard was -0.86%, and +26% for the 9.2 cP standard. Sample solutions of the 90% DES were prepared using airtight bottles and contained 90% DES by mass, 100 m*m* KCl and 20 m*m* KPO_4, pH 7. Viscosity measurements were replicated thrice for each sample. Values reported in Table 2.1 are average values with linearly interpolated instrument error percent.

The viscosities of the more fluid solutions used in this study were determined utilizing an instrument with greater sensitivity, the PHYSICA MCR300, made by Anton

Paar. This instrument utilized a cone and plate attachment and was able to measure the viscosity of liquids under 10 cP, which is below the range of the Merlin II viscometer. The instrument was calibrated to measure the viscosity of water (1 cP) to within ± 5%. Sample solutions of the 40% PEG 200 / 30-15% glycerol (v/v with water) were prepared using airtight bottles and contained 100 mM KCl and 20 mM KPO_4. Viscosity measurements were replicated twice for each sample. Values reported in Table 2.1 are average values of these measurements with standard error.

Table 2.1 Dynamic viscosities of solvents used in this study

Temperature (°C)	Ƞ of 100% DES[a] (cP)	Ƞ of 90% DES[b] (cP)	Ƞ of 40% PEG 200[c] (cP)	Ƞ of 40%PEG 200/30% glycerol[d](cP)	Ƞ of 40%PEG 200/15% glycerol[d](cP)
65	N/A	N/A	1.6	N/A	N/A
60	N/A	12.3± 0.4[c]	1.9	7.1 ± 0.2	3.6 ± 0.1
55	N/A	N/A	2.0	N/A	N/A
50	110	21.4 ±4.4	2.3	9.1 ± 0.1	4.5 ±0.1
45	*146	N/A	2.7	N/A	N/A
40	204	29.7 ±5.9	3.1	13.0 ± 0.2	5.8 ± 0.1
35	*297	N/A	3.6	N/A	N/A
30	452	42.1 ± 6.9	4.2	19.1 ± 0.2	8.1 ± 0.3

[a] values from Abbott et al. data [110], * represents interpolated values of 100% DES from Abbott et al. data.[110]

[b] sample contained 90% ChCl-urea DES by weight, 100 m*m* KCl and 20 m*m* Potassium Phosphate buffer, pH 7. Error values represent instrumental error.

[c] interpolated values of 40% v/v PEG 200 aqueous solution obtained from Bhanot et al. data.[111] Reported error for their study was ≤ 0.5%.

[d] values obtained on Physica MCR 300.

CHAPTER 3

HUMAN TELOMERE SEQUENCE DNA ADOPTS A PARALLEL STRANDED FOLD IN THE WATER FREE CHOLINE CHLORIDE-UREA DEEP EUTECTIC SOLVENT

3.1 Abstract

This chapter introduces the deep eutectic solvent used in this work and then describes the study of the structure and stability of the HTS DNA in this solvent. The analysis upon reintroduction of water concludes the chapter along with a brief discussion of the heat sensitivity of the DES used in this work.

3.2 Introduction: Nucleic acids in deep eutectic solvent (DES)

Generally speaking, room temperature ionic liquids (RTILs) are described as ionic materials that exist as a liquid below 100 °C.[112] Deep eutectic solvents (DES), a class of RTILs, have recently emerged as a new group of non-aqueous solvents.[113] This is mainly due to their environmentally benign nature, non-volatility and general miscibility with a variety of solutes. The term deep eutectic solvent refers to the significant depression of freezing point due to the non-covalent interaction between the components of the solvent. The DES used in this study consists of one part choline chloride and one part urea. The melting point of urea is 133 °C and the melting point of choline chloride is 302 °C, whereas the melting point of the 2:1 mixture is depressed to 12 °C.[110] Previous findings determined that nucleic acids can form stable secondary

structures in water free DES (contains less that 0.25% water as determined by Karl Fischer analysis) composed of choline chloride and urea.[114] These discoveries catalyzed the exploration of HTS DNA in the ChCl-urea DES.

3.2.1 Sample preparation

DNA oligonucleotides were purchased from Integrated DNA Technologies (IDT) (Coralville, IA) G-quadruplex strand sequence is 5'-TAGGG(TTAGGG)$_3$. Precise DNA concentrations were determined on the basis of UV adsorption at 260 nm of the sample measured in water using the molar extinction coefficient of 236,500 L/mol•cm provided by IDT. The ChCl-urea DES was prepared by heating a 1:2 molar mixture of choline chloride (Acros Organics) and urea (Fisher) anhydrous solids while stirring at 80 °C until a homogeneous liquid emerged (ca. 2 hrs). Solutions of nucleic acids in the 100% DES solvent were prepared by mixing an aqueous stock solution, 1 mM in oligonucleotide of DNA with the DES and then subjecting the mixture to vacuum centrifugation until a constant mass was reached (at least 12 hr), a process that was determined (based on gravimetric analysis) to quantitatively remove added water from the anhydrous DES. Prior to experimentation, the G-quadruplex DNA was equilibrated by heating the samples in the relevant solvent/solution for 5 min at 90 °C and then slowly annealing over the course of 12 hours (-6 °C/hr) to room temperature.

3.3 Conformation and Stability of *Htelo1* in 100% ChCl-urea DES

Determination of the folded structure of HTS DNA in the water-free choline chloride-urea (ChCl-urea) DES was difficult due to the high viscosity of the solvent (ca. 1000 cP at 20 °C).[110] High viscosity makes structure determination by NMR impossible. Fortunately, Heddi and Phan published CD spectra for the HTS-derived oligonucleotide d[$TAG_3(TTAG_3)_3$] (*Htelo1*) for solution conditions in which its G-quadruplex structures were also determined using high-resolution NMR spectroscopy.[1] Specifically, in their manuscript they showed that when polyethylene glycol (PEG 200) is added to 40% v/v (40% PEG 200) containing potassium ions, *Htelo1* adopts a parallel-stranded fold. The CD spectrum of *Htelo1* in 40% PEG 200 has a positive band at approximately 265 nm and a negative band at approximately 240 nm (Figure. 3.1). Alternatively, the CD spectrum of *Htelo1* in aqueous buffer containing potassium ions exhibits a positive absorption band near 295 nm and a shoulder at 265 nm (Figure. 3.1). Multiple structures solved by NMR spectroscopy are attributed to the aqueous CD spectrum in Figure 3.1, to include the 3+1 hybrid forms 1 and 2.[24] Moreover, previous work has determined that *Htelo1* exchanges between multiple distinct G-quadruplex structures in aqueous buffer containing potassium ions, all of which have a mix of parallel and antiparallel strand orientations around a core of stacked G-tetrads.[58] Due to the empirical evidence produced by Heddi and Phan in 40% PEG 200, CD spectroscopy can be used to distinguish between the aqueous solution structures and the parallel-stranded structure of *Htelo1*.

The CD spectrum of *Htelo1* in the choline chloride-urea DES, with 100 m*m* KCl added to stabilize any G-quadruplex structures is compared in Figure. 3.1 with the spectra of *Htelo1* in aqueous solution and in 40% PEG 200. The spectrum of *Htelo1* in DES is remarkably close to that observed in 40% PEG 200, establishing that *Htelo1* adopts the same parallel fold in both solvents.

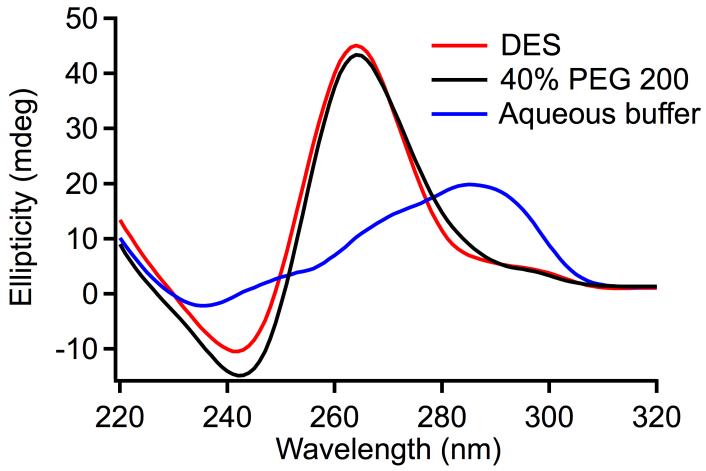

Figure. 3.1 CD spectra of DNA with the HTS-derived sequence d[$TAG_3(TTAG_3)_3$] (*Htelo1*) in various solvents. DES sample was 1 m*m* in nucleotide and contained 100 m*m* KCl. Aqueous buffer solutions contained 20 mM potassium phosphate buffer, pH 7. PEG 200 solution was 40% v/v. Spectra were recorded at 20 °C.

In order to verify the formation of the G-quadruplex structure and elucidate thermodynamic parameters, CD spectra were monitored during subsequent heating and cooling cycles (Figure. 3.2-3.7). Figures 3.8 – 3.10 display the melting and cooling trace analysis of the *Htelo1* samples. A single, cooperative and reversible transition with a temperature midpoint (T_m) of 84 °C (Figure. 3.8) indicates the formation of a stable and folded G-quadruplex. This value is higher than the T_m of 63 °C observed in an aqueous

buffer (Figure. 3.10), but lower than the T_m of 91 °C measured in 40% PEG 200 (Figure 3.11).

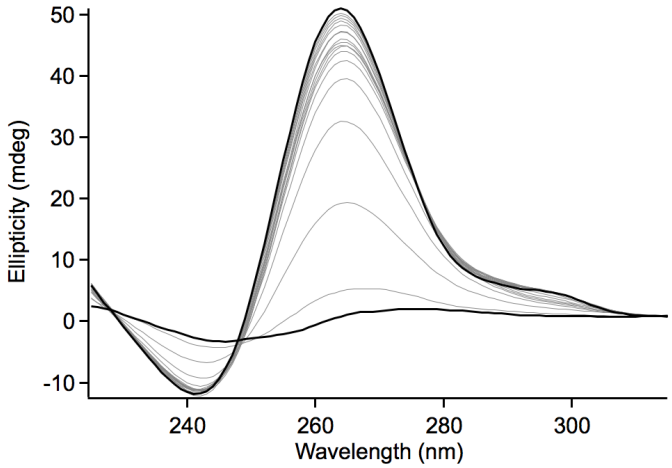

Figure 3.2 CD Spectra of thermal denaturation of *Htelo1* in ChCl-urea DES from 5 °C to 95 °C with 5 °C steps. Sample contained 1m*m* in oligonucleotide DNA and 100 m*m* KCl. Initial and final spectra are displayed with bold black lines.

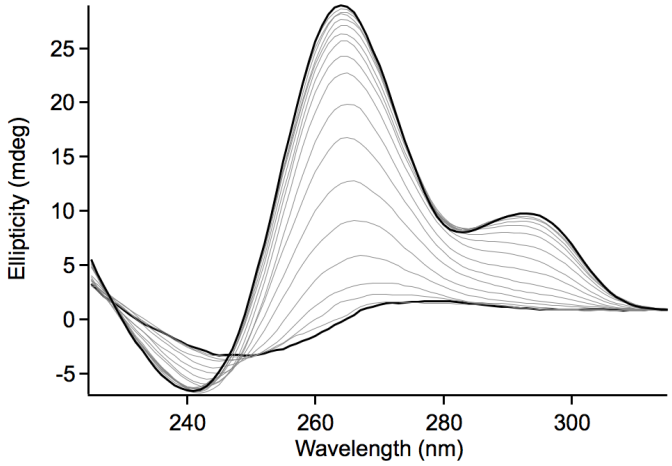

Figure 3.3 CD Spectra of thermal annealing of *Htelo1* in ChCl-urea DES from 5 °C to 95 °C with 5 °C steps. Sample contained 1m*m* in oligonucleotide DNA and 100 m*m* KCl. Initial and final spectra are displayed with bold black lines.

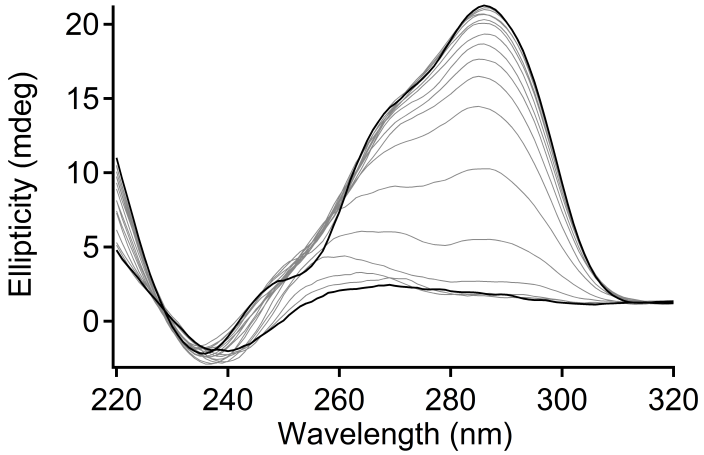

Figure 3.4 CD Spectra of thermal denaturation of *Htelo1* in aqueous buffer from 5 °C to 95 °C with 5 °C steps. Sample contained 1mM in oligonucleotide DNA, 100 mM KCl and 20 mM KPO_4 buffer, pH, 7. Initial and final spectra are displayed with bold black lines.

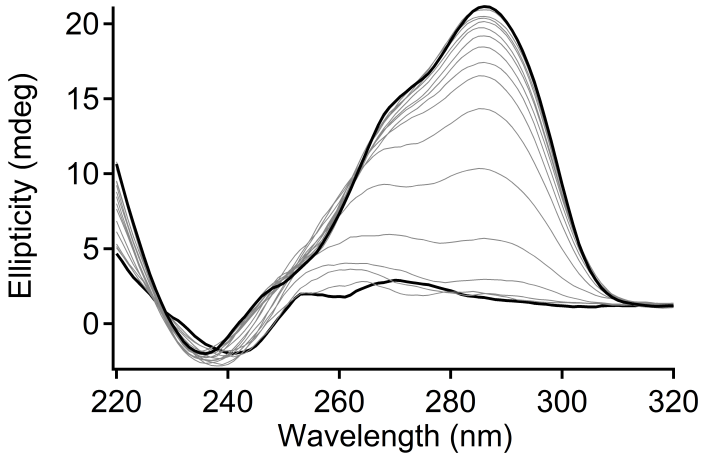

Figure 3.5 CD Spectra of thermal annealing of *Htelo1* in aqueous buffer from 5 °C to 95 °C with 5 °C steps. Sample contained 1mM in oligonucleotide DNA, 100 mM KCl and 20 mM KPO_4 buffer, pH, 7. Initial and final spectra are displayed with bold black lines.

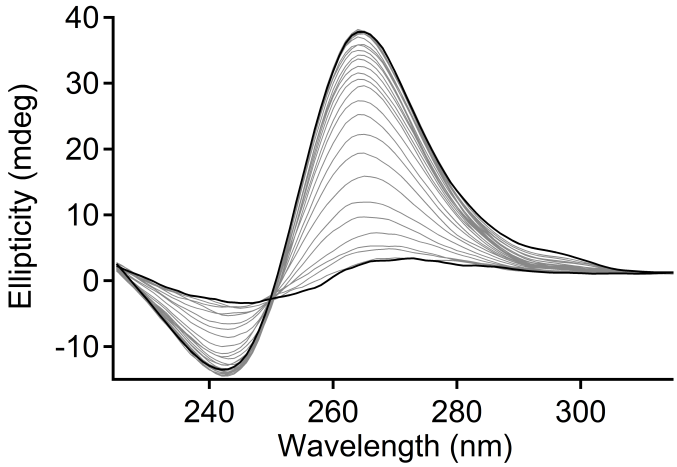

Figure 3.6 CD Spectra of thermal denaturation of *Htelo1* in 40% PEG 200 (v/v) from 50 °C to 106 °C with 2 °C steps. Sample contained 1mM in oligonucleotide DNA, 100 mM KCl and 20 mM KPO_4 buffer, pH, 7. Initial and final spectra are displayed with bold black lines.

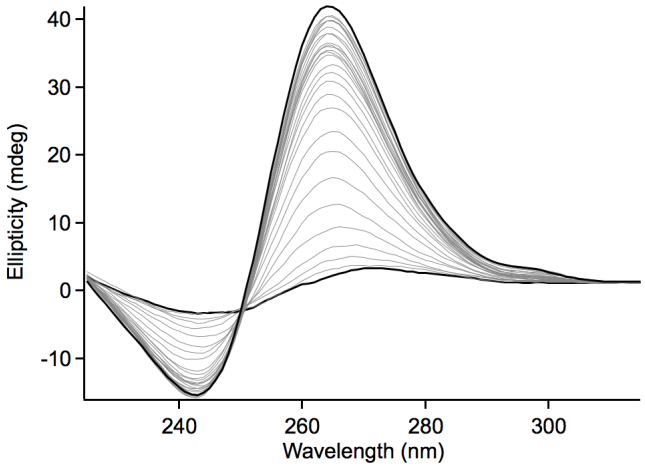

Figure 3.7 CD Spectra of thermal annealing of *Htelo1* in 40% PEG 200 (v/v) from 50 °C to 106 °C with 2 °C steps. Sample contained 1mM in oligonucleotide DNA, 100 mM KCl and 20 mM KPO_4 buffer, pH, 7. Initial and final spectra are displayed with bold black lines.

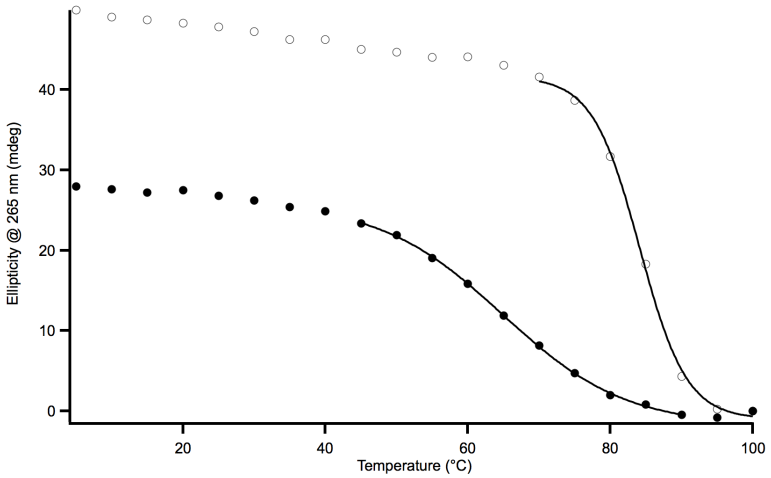

Figure. 3.8 Heating and cooling traces of d[$TAG_3(TTAG_3)_3$](*Htelo1*) in the 100% ChCl-urea DES generated by monitoring CD intensity at 265 nm as a function of temperature. Heating/cooling rates were approximately 1.1 °C/min. Samples were 1 m*m* in nucleotide and contained 100 m*m* KCl. Heating traces shown with open circles; cooling traces shown with filled circles. The sigmoidal fits of traces after a baseline correction to obtain T_m values are shown with black lines.

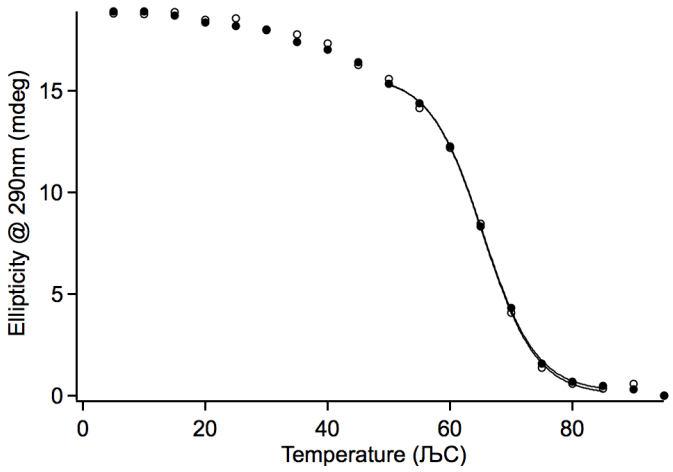

Figure. 3.9 Heating and cooling traces of *Htelo1* in the aqueous buffer generated by monitoring CD intensity at 290 nm as a function of temperature. Heating/cooling rates were approximately 0.3 ºC/min. Samples were 1 mM in nucleotide and contained 100 mM KCl and 20 mM potassium phosphate buffer, pH 7. Heating traces are shown with open circles; cooling traces are shown with filled circles. The sigmoidal fits of traces after a baseline correction to obtain T_m values are shown with black lines.

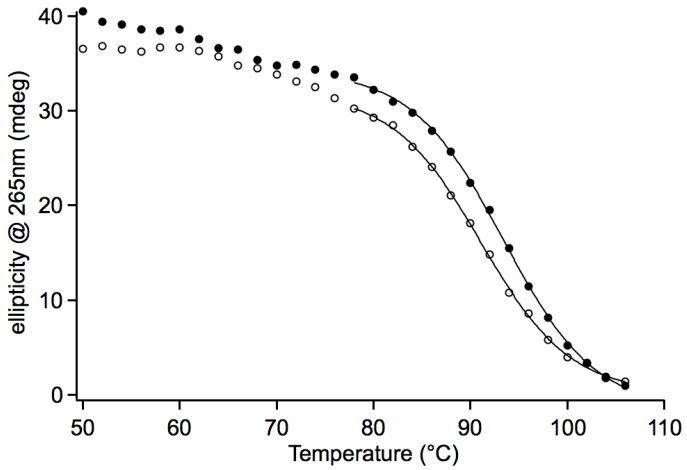

Figure. 3.10 Heating and cooling traces of *Htelo1* in 40% PEG 200 (v/v) generated by monitoring CD intensity at 265 nm as a function of temperature. Heating/cooling rates were approximately 0.68 ºC/min. Samples were 1 mM in nucleotide and contained 40% PEG200 (v/v), 100 mM KCl and 20 mM potassium phosphate buffer, pH 7. Heating traces are shown with open circles; cooling traces are shown with filled circles. Sigmoidal fits of traces after baseline correction to obtain T_m values are shown with black lines.

A surprising observation of the heating and cooling traces of *Htelo1* in the DES is the significant hysteresis phenomenon (>10 °C) exhibited over the other solvents, indicating that the refolding kinetics of *Htelo1* in the DES are slow on the time scale of sample cooling (~ 3 hr). This observation also indicates that neither the heating nor cooling curves correspond to the true equilibrium curves, meaning the temperature midpoint actually exists somewhere between the two traces (84 °C > T_m > 63 °C). Similar studies in aqueous solution under the same conditions and sequence display no hysteresis with similar temperature gradients. To verify the observed hysteresis is a result of the temperature gradient, another thermal melting experiment was conducted with slower cooling rates. (Figures 3.11 and 3.12)

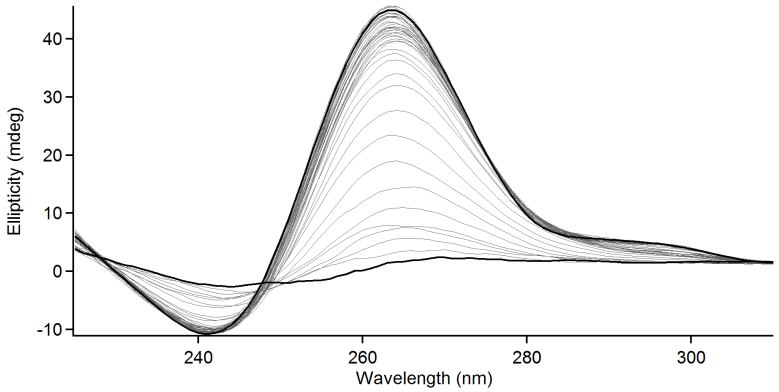

Figure 3.11 CD Spectra of thermal denaturation of *Htelo1* in ChCl-urea DES from 10 °C to 96 °C with 2 °C steps. Sample contained 1m*m* in oligonucleotide DNA and 100 m*m* KCl. Initial and final spectra are displayed with bold black lines.

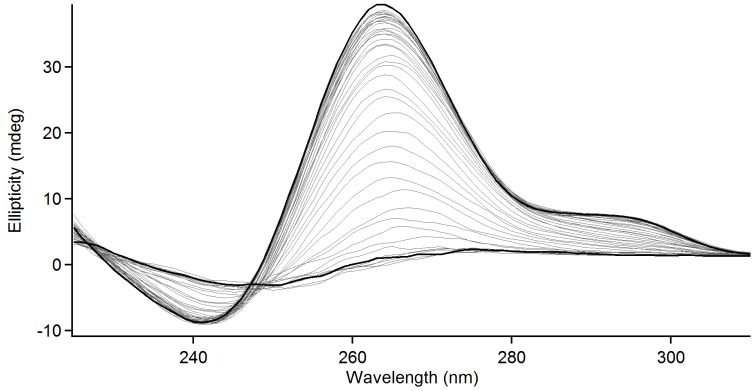

3.12 CD Spectra of the controlled annealing of *Htelo1* in ChCl-urea DES from 10 °C to 96 °C with 2 °C steps. Sample contained 1m*m* in oligonucleotide DNA and 100 m*m* KCl. Initial and final spectra are displayed with bold black lines.

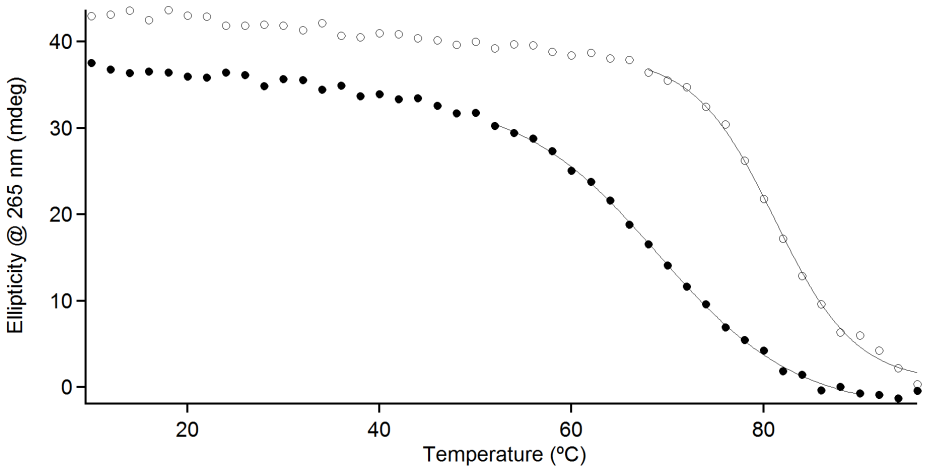

3.13 Heating and cooling traces of d[$TAG_3(TTAG_3)_3$](*Htelo1*) in the 100% ChCl-urea DES generated by monitoring CD intensity at 265 nm as a function of temperature. Heating/cooling rates were approximately .085 °C/min. Samples were 1 m*m* in nucleotide and contained 100 m*m* KCl. Heating traces are shown with open circles; cooling traces are shown filled circles. Sigmoidal fits of traces after baseline correction to obtain T_m values are shown with black lines.

Significant hysteresis was still exhibited by the heating and cooling traces, which implies that the rate of refolding is slow and strongly dependent on temperature, and reliable thermodynamic data requires further analysis. In any case, in order to attain thermodynamic parameters from such melting studies, the concerted two-state transition must exist between the folded and unfolded states.

The presence of isoelliptic points in each series of heating and cooling spectra in Figures 3.2 - 3.7 suggests a two-state transition takes place upon denaturation/ renaturation cycles. However in Figure 3.3, (*Htelo1* annealing in 100% DES) a significant growth of a positive band in the 295 nm region, despite its dissipation upon slower cooling gradients (Figure 3.12) is indicative of more complicated kinetics. To rigorously test these observations, dual wavelength parametric plots of the transitions

were performed on the data in Figures 3.2-3.8.[103] The results of these tests seen in Figures 3.14 -3.16 indicate that a deviation from a simple two-state transition exists during the denaturation of *Htelo1* in all three solvents. A possible explanation of this result is that a significant number of intermediate states of the G-quadruplex exist upon denaturation. This observation is in agreement with previous results obtained in aqueous buffer.[42] Unfortunately, as a result of this phenomenon, thermodynamic and kinetic parameters cannot be accurately obtained and compared between the melting analyses of the three solvents.

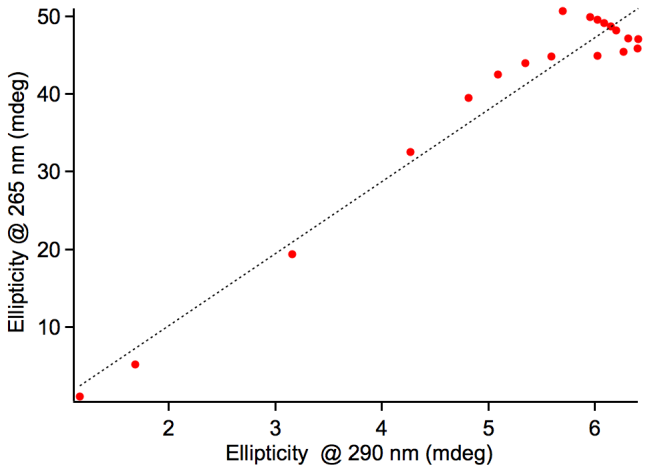

Figure. 3.14 Dual wavelength parametric plot of 265 nm vs. 290 nm for *Htelo1* in Figure 3.2 over the temperature range of 5 °C to 95 °C in 100% ChCl-urea DES. Sample contained 1m*m* in oligonucleotide DNA and 100 m*m* KCl. Linear fit of the data points is indicated by dotted black line.

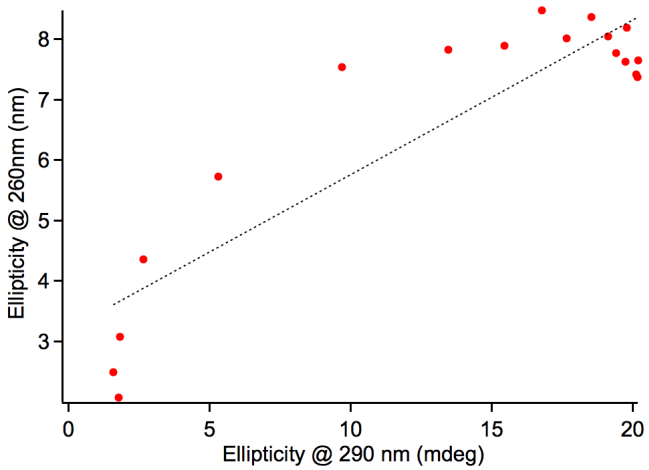

Figure 3.15 Dual wavelength parametric plot of 260 nm vs. 290 nm for *Htelo1* in Figure 3.4 over the temperature range of 5 °C to 95 °C in aqueous buffer. Sample contained 1mM in oligonucleotide DNA, 100 mM KCl and 20 mM KPO_4 buffer, pH, 7. Linear fit of the data points is indicated by dotted black line.

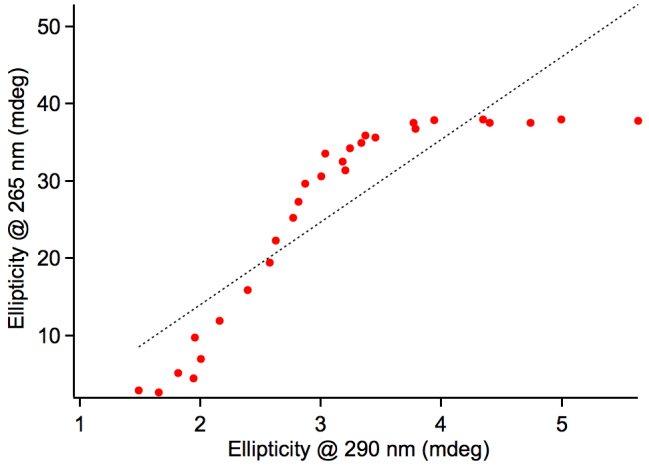

Figure 3.16 Dual wavelength parametric plot of 265 nm vs. 290 nm for *Htelo1* in Figure 3.6 over the temperature range of 50 °C to 106 °C in 40% PEG 200. Sample contained 1mM in oligonucleotide DNA, 100 mM KCl and 20 mM KPO_4 buffer, pH, 7. Linear fit of the data points is indicated by dotted black line.

The inability to garner extended thermodynamic data from the denaturation and renaturation experiments due to a non-two state transition is unfortunate, however, the

general stability of the G-quadruplex in the various solvents can be assessed from observed T_m values (40% PEG 200 > 100% ChCl-urea DES > aqueous buffer). It is not surprising that the parallel stranded structures that exist at equilibrium in the PEG and DES solvents are markedly more stable than the aqueous mixed stranded and anti-parallel forms, as intramolecular parallel G-quadruplexes are inherently more stable than other conformations. It is surprising to note, however, that the *Htelo1* G-quadruplex T_m is 7 °C lower in the ChCl-urea DES than in the PEG. A possible reason for this is destabilization of the quadruplex by urea, which is commonly used as a denaturant for nucleic acids and proteins. The DES contains sufficient amounts of urea (7.4 *m*) to account for the depressed melting transition point. Another possible explanation for the lower T_m is the elimination of bulk water, as the DES contains ≤ 0.25% water as compared to 60% water present in the 40% PEG 200. Of note, molecular crowding agents lower the overall water activity, however, we can assume for the sake of comparison that the quadruplex is exposed to significantly less water in the DES. In order to test these hypotheses, *Htelo1* was analyzed separately in control solutions of urea and choline chloride with equivalent ionic strengths. Figure 3.17 compares the resulting CD spectra of *Htelo1* in the control solvents to that of the 100% ChCl-urea DES and aqueous buffered conditions. From the CD spectra, it appears as though the *Htelo1* DNA in the choline chloride solution conditions maintains a predominantly "aqueous like" CD spectra. In contrast, the urea solvent conditions seem to alter the structure or relative contributions to the CD spectrum of structures present.

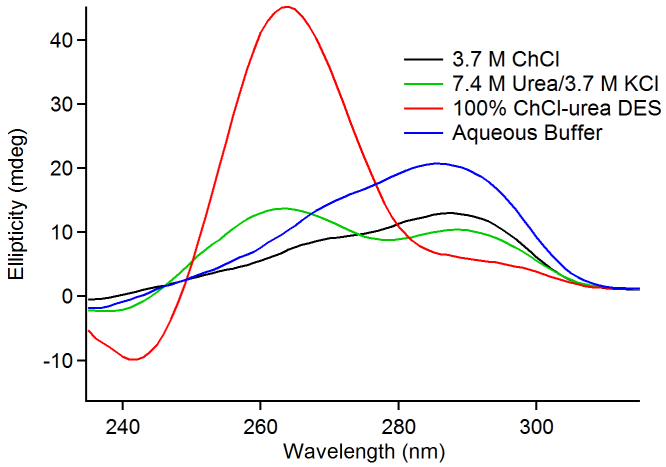

Figure 3.17 CD spectra of *Htelo1* DNA in various solvents. Samples contained 1 m*m* DNA in nucleotide and contained 100 m*m* KCl. Aqueous solutions contained the relative co-solute concentrations as indicated in the figure as well as 20 mM potassium phosphate buffer, pH 7. Spectra were taken at 20 °C.

The T_m of *Htelo1* in the urea control was 67 °C whereas the T_m in the choline chloride control was 77 °C. (Figures 3.18 and 3.19) When compared to the aqueous T_m of 63 °C (Figure 3.9) the stability increased in both control solvents, but was depressed when compared to the T_m of *Htelo1* in 100% DES (82 °C; Figure 3.8).

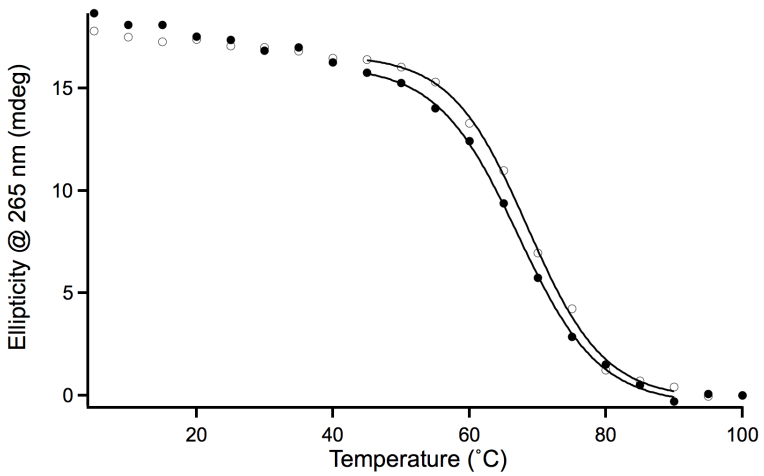

Figure 3.18 Heating and cooling traces of *Htelo1* in 7.4 M urea and 3.7 M KCl generated by monitoring CD intensity at 265 nm as a function of temperature. Heating/cooling rates were approximately 0.6 ºC/min. Samples were 1 mM in nucleotide and contained 100 mM KCl and 20 mM potassium phosphate buffer, pH 7. Heating traces shown with open circles; cooling traces shown with filled circles. Sigmoidal fits of traces after baseline correction to obtain T_m values are shown with black lines.

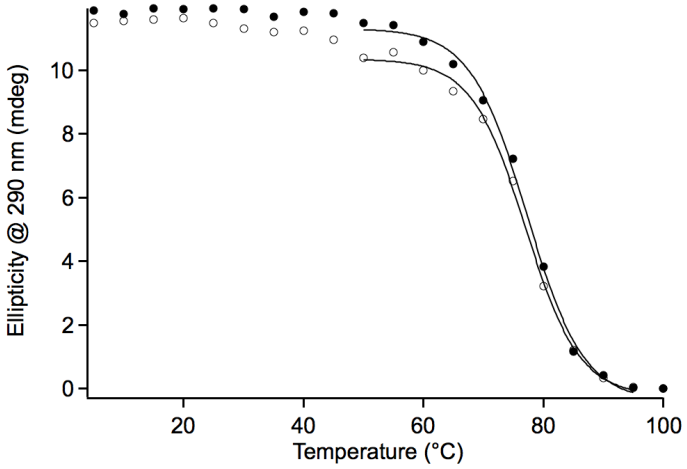

Figure 3.19 Heating and cooling traces of *Htelo1* in 3.7 M choline chloride generated by monitoring CD intensity at 265 nm as a function of temperature. Heating/cooling rates were approximately 0.6 ºC/min. Samples were 1 mM in nucleotide and contained 100 mM KCl and 20 mM potassium phosphate buffer, pH 7. Heating traces shown with open circles; cooling traces shown with filled circles. Sigmoidal fits of traces after baseline correction to obtain T_m values are shown with black lines.

It is difficult to correlate stability associated with each solvent, as the structures that exist in the respective solution conditions can be distinct (Figure 3.17). However, due to the overall increase in T_m in both control solvents with respect to the aqueous buffer, it is problematic to attribute the entirety of the depressed T_m of *Htelo1* in 100% DES to the denaturing properties of urea. Instead, the difference in T_m is most likely a result of the distinct properties of the DES solvent when compared to PEG 200. Alternatively, the T_m of a similar HTS derived sequence (d[A(GGGTTA)$_3$GGG)] in 50% acetonitrile was found to be approximately 111 °C (Table 1.1), markedly increased from both PEG and ChCl-urea DES solutions.[2] Acetonitrile, unlike the PEG, choline chloride and urea, cannot participate in hydrogen bonding and acts more like a dehydrating agent than a molecular crowding medium. The atomic level structure of the HTS-derived sequence in acetonitrile was not solved, but the CD spectrum, 1D ^{1}H NMR and high T_m indicate that the acetonitrile favors the parallel G-quadruplex topology. Due to these findings, hydration seems to play a large role in the favored topology and consequently, the overall stability of the HTS DNA.

3.4 Adding water back to the DES system

In order to further examine the role hydration plays in determination of the conformation and stability of the HTS DNA G-quadruplex, water was systematically added back into the anhydrous DES solvent. The resulting analysis is presented in Figure 3.20.

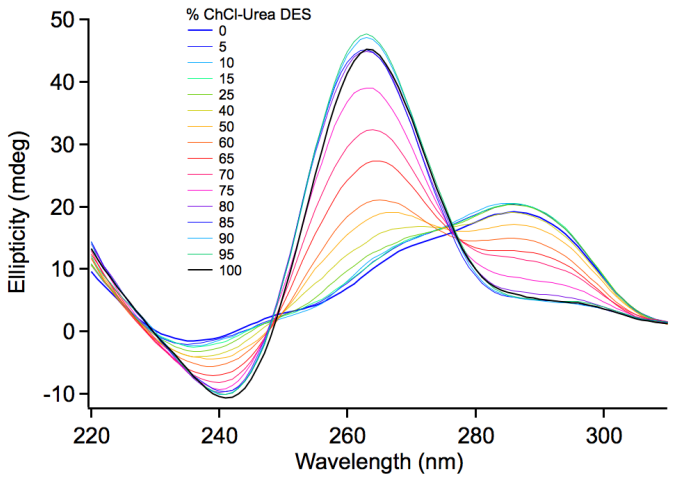

Figure. 3.20 CD spectra of the human telomere sequence in various percentages (w/w) of DES solvent at equilibrium. Final samples after mixing were 1 m*m* in nucleotide and contained 100m*m* KCl and 20 m*m* potassium phosphate buffer, pH 7. Spectra were recorded at 20 °C. Samples were incubated after preparation at 40 °C to expedite reaching HTS structural equilibrium on a practical time scale (ca. < 2 months).

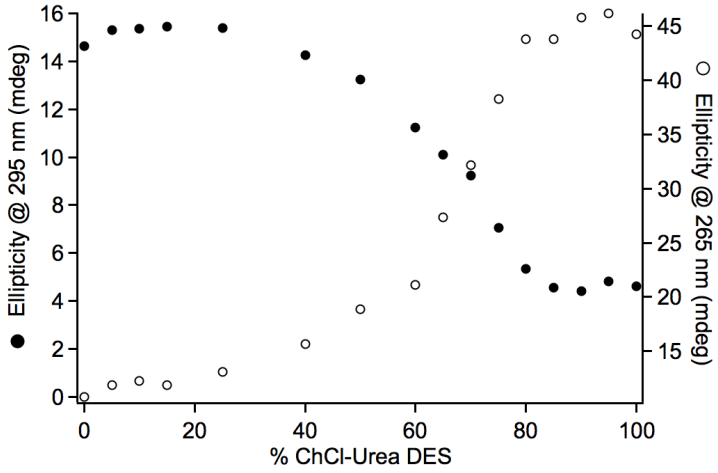

Figure 3.21 Ellipticity at 295 and 265 nm monitored as a function of ChCl-urea DES percentage. CD spectra measured as a function of ChCl-urea/water solvent fractions revealed the *Htelo1* favors complete conversion to the parallel structure for 85-100 % DES. DNA was equilibrated in the buffer solution and then DES was added.

It was determined from this analysis that approximately 85% ChCl-urea DES (w/w with water) is sufficient for the parallel G-quadruplex structure of *Htelo1* to remain as the thermodynamically favored structure. (Figure 3.21) The observation that *Htelo1* adopts its parallel fold in a solution that contains 0 - 15% water supports previous conclusions that dehydration and/or osmotic stress drives HTS DNA to parallel structures.[2] However, the mixtures with PEG 200 or acetonitrile as a co-solvents are qualitatively more effective than ChCl-urea in shifting *Htelo1* to the parallel fold, as the parallel fold of *Htelo1* is favored in a 40% PEG 200 solution that contains 60% water, or a 50% acetonitrile solution that contains 50% water; whereas a water-DES mixture with 40% ChCl-urea shows approximately 10% change or less from the aqueous folded state (Figure. 3.20). The prerequisite for less water in a solvent with ChCl-urea may be the result of choline and urea being able to inhabit some solvent-accessible sites on *Htelo1* in a fashion analogous to water. The amino groups of urea are one of the reasons a deep eutectic is able to form with choline through hydrogen bonding interactions. Likewise, the alcohol group of choline could act as a hydrogen bond donor or the carbonyl groups of urea could act as H-bond acceptors. This interaction could successfully replace water molecules that are H-bound donors or acceptors. In contrast, the larger size of PEG 200 could limit substitution of water-occupied sites on the surface of a G-quadruplex. Moreover, the molecular-level interactions of acetonitrile, which cannot form hydrogen bonds with the G-quadruplex, are expected to also be significantly different from water than those of the DES or PEG components. Furthermore, molecular dynamic (MD) simulations conducted by Heddi and Phan concluded that the hydrophobic rings of the guanine bases are more exposed to solvent in the parallel form of *Htelo1* vs. the

antiparallel or (3+1) hybrid forms of the same sequence where the loops effectively shield the bases.

Overall, these conclusions reinforce that hydration, or lack thereof, is a main contributor to conditions favoring the parallel form of *Htelo1* over other topologies. Additionally, it appears that the unique properties of each solvent (H-bonding capability, dehydrating ability, hydrophilicity vs. hydrophobicity, overall size) accounts for the different thermal stabilities of *Htelo1* G-quadruplex in each milieu.

3.5 DES pH changes as a result of prolonged exposure to high temperatures.

As discussed above, all the samples utilized in DES and PEG 200 were heat denatured to expedite equilibrium conditions. During the course of this study it was discovered that caution must be exercised in such experiments because of the sensitivity of choline chloride-urea DES to heating. When exposed to high temperatures for prolonged periods of time the pH of the DES increases towards more basic levels. Figure 3.22 displays this behavior.

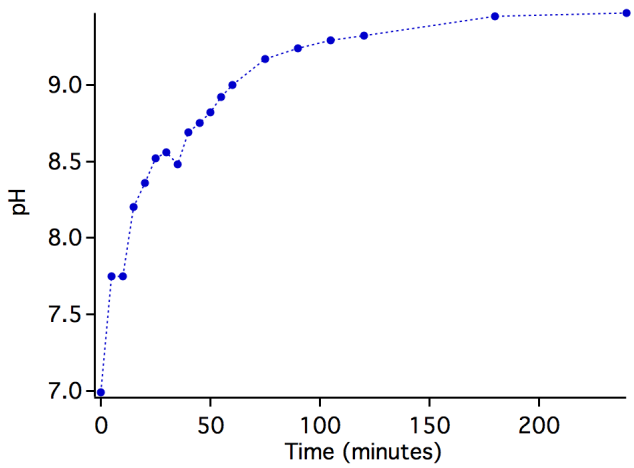

Figure 3.22 DES samples (250 mg) were heated at 95 °C for time indicated then removed from heat block and quick cooled in ice bath. 50% water by weight was added to the sample and allowed to equilibrate for 15 minutes. pH measurement was then taken of each sample. Final sample consisted of 1.85 *m* choline chloride and 3.7 *m* urea.

From this analysis, it may be concluded that heating the DES for prolonged periods of time (> 35 min) leads to an undesirable increase in pH for G-quadruplex studies as the pK_a of a guanine nucleotide is around 9.4.[115] Therefore, a pH in the proximity of this value would affect the stability of the G-quadruplex. A possible explanation for the evolution of basic materials in the DES media is the degradation of urea within the DES to pure ammonia NH_3 and isocyanic acid (HNCO). Previous studies have shown that isocyanic acid is prone to then hydrolyze to produce more ammonia and carbon dioxide. Thereby one mole of urea would produce approximately two moles of ammonia and one mole of carbon dioxide[116]. Further support for this decomposition pathway was observed when the pH of heated ChCl-urea DES was returned to neutrality after being subjected to centrifugation under high vacuum.

Previous reports indicate that urea decomposition of solid urea is possible at 350 °C.[116] If urea decomposition is the cause of the elevated pH, then the eutectic formed between the choline chloride and the urea must severely depress the decomposition temperature of urea. Further investigation into the nature of the heat sensitivity of the DES is beyond the scope of this work. However, for the purposes of this study, empirical evidence shows that the DES is heat sensitive and precautions must be taken when exposing the DES to higher temperatures for prolonged periods of time. As a consequence of this realization, the heat annealing protocol for all DES samples was adjusted in order to preserve sample integrity (section 3.2.1). Also, after heat annealing, samples were exposed to high vacuum centrifugation to remove any evolved species or water in an effort to remain consistent throughout the course of study. The careful treatment of the DES under heating conditions was also considered so as to limit pH fluctuations during experimentation.

CHAPTER 4

HUMAN TELOMERE SEQUENCE DNA DYNAMICS IN THE CHOLINE CHLORIDE-UREA DEEP EUTECTIC SOLVENT

4.1 Abstract

In this chapter the unique kinetic aspects of HTS DNA are explored in the ChCl-urea DES. It is discovered that the HTS DNA folding pathway is altered in the DES and kinetic states are entrapped for prolonged periods of time. Most interestingly, the rate of *Htelo1* refolding to the thermodynamically favored conformation is on the order of months at room temperature.

4.2 The HTS DNA becomes kinetically trapped for extended periods when quick-cooled in the DES.

Once it was determined that different temperature gradients affected the rates of *Htelo1* denaturation/renaturation in 100% DES (Figure 3.8 *vs.* Figure 3.18), the annealing protocol was varied to investigate further the kinetics of *Htelo1* folding at different temperatures from its thermally unfolded state. Figures 4.1 and 4.10 illustrate *Htelo1* samples in the DES that were heated to 90 °C, and quick cooled to various temperatures in less than two minutes. The CD spectrum of *Htelo1* after the first folding event, represented by blue spectrum in Figures 4.1, 4.3, 4.5, 4.7 and 4.9, is different from the equilibrium spectra of *Htelo1* in the DES or in aqueous solution (Figure 3.1). The time series of spectra collected during *Htelo1* folding at various temperatures are displayed in

Figures 4.1-4.10. The spectrum of *Htelo1* in the intermediate state (blue spectrum) has positive bands at 265 and 295 nm at all temperatures investigated, which indicates the presence of one or more G-quadruplex folds that contains both parallel and antiparallel strand orientations.[100]

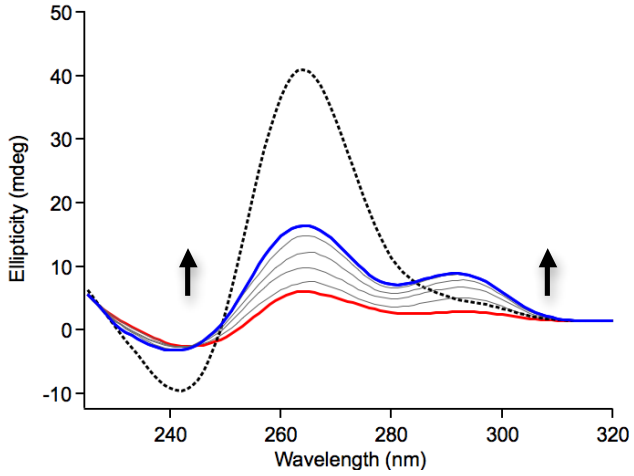

Figure 4.1 Time dependent CD spectra of quick-cooled *Htelo1* in 100%DES. Initial spectrum before heating is shown as black dashed line. After heating to 90 °C for 5 min sample was cooled (-0.65 °C/sec) and placed in CD at 50 °C (red solid line). The *Htelo1* sample reaches a kinetic intermediate (blue solid line) on the order of 1 hour. Sample was 1 m*m* in nucleotide; 100 m*m* KCl.

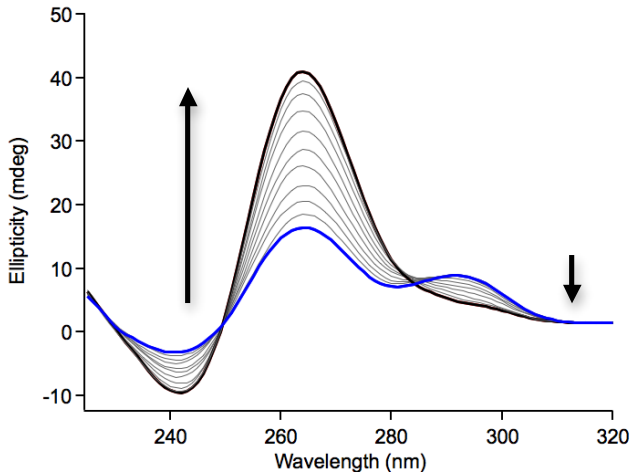

Figure 4.2 Time dependent CD spectra of quick-cooled *Htelo1* sample from Figure 4.1 during second transition while maintained at 50 °C for times between 1 hour (blue line) and 15 hours (black line). Arrows indicate spectral change as a function of time.

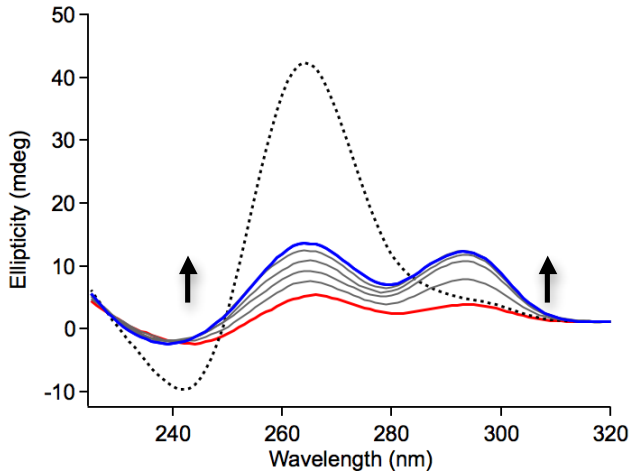

Figure. 4.3 Time dependent CD spectra of quick-cooled *Htelo1* in 100%DES. Initial spectrum before heating is shown as black dashed line. After heating to 90 °C for 5 min sample was cooled (-0.65 °C/sec) and placed in CD at 40 °C (red solid line). The *Htelo1* sample reaches a kinetic intermediate (blue solid line) on the order of 1 hour. Sample was 1 m*m* in nucleotide; 100 m*m* KCl. Arrows indicate spectral change as a function of time.

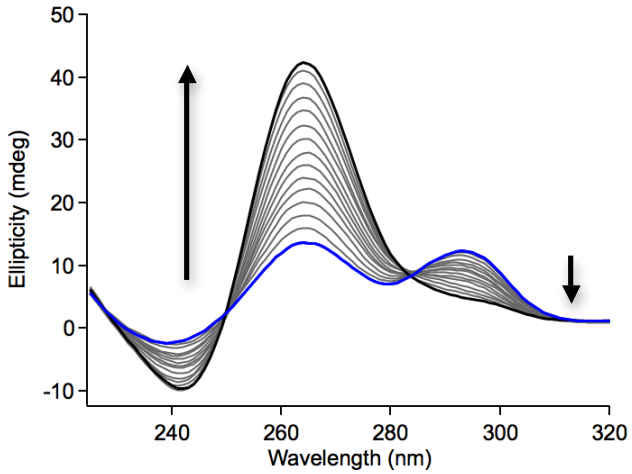

Figure 4.4 Time dependent CD spectra of quick-cooled *Htelo1* sample from Figure 4.1 during second transition while maintained at 40 °C for times between 1 hour (blue line) and 200 hours (black line). Arrows indicate spectral change as a function of time.

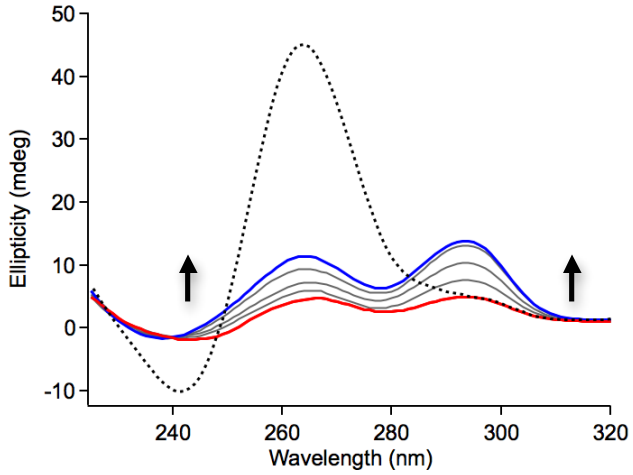

Figure 4.5 Time dependent CD spectra of quick-cooled *Htelo1* in 100%DES. Initial spectrum before heating is shown as black dashed line. After heating to 90 °C for 5 min sample was cooled (-0.65 °C/sec) and placed in CD at 35 °C (red solid line). The *Htelo1* sample reaches a kinetic intermediate (blue solid line) on the order of 1.5 hours. Sample was 1 m*m* in nucleotide; 100 m*m* KCl. Arrows indicate spectral change as a function of time.

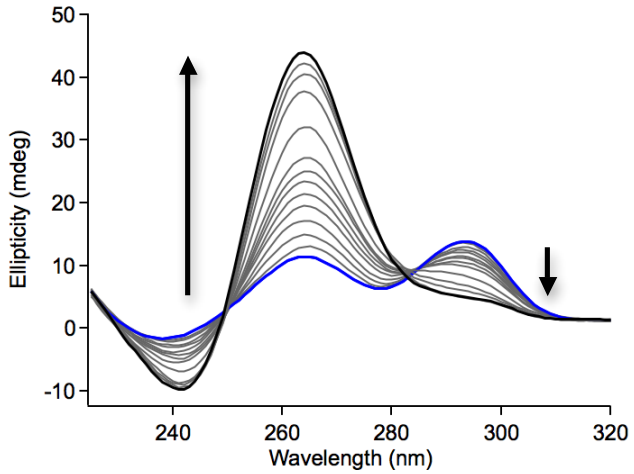

Figure 4.6 Time dependent CD spectra of quick-cooled *Htelo1* sample from figure 4.1 during second transition while maintained at 35 °C for times between 1.5 hours (blue line) and 360 hours (black line). Arrows indicate spectral change as a function of time.

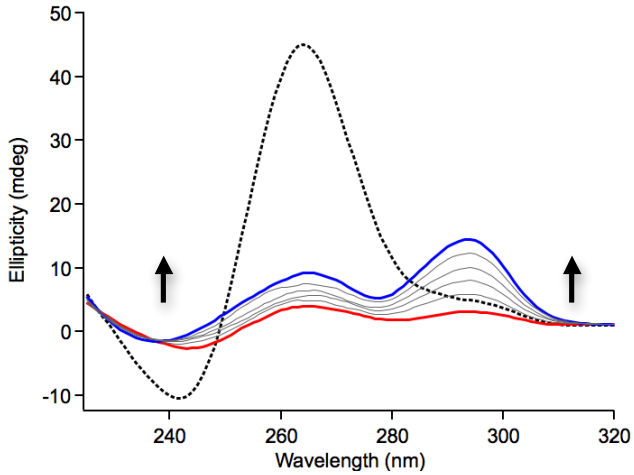

Figure 4.7 Time dependent CD spectra of quick-cooled *Htelo1* in 100%DES. Initial spectrum before heating is shown as black dashed line. After heating to 90 °C for 5 min sample was cooled (-0.65 °C/sec) and placed in CD at 30 °C (red solid line). The *Htelo1* sample reaches a kinetic intermediate (blue solid line) on the order of 1.5 hours. Sample was 1 m*m* in nucleotide; 100 m*m* KCl. Arrows indicate spectral change as a function of time.

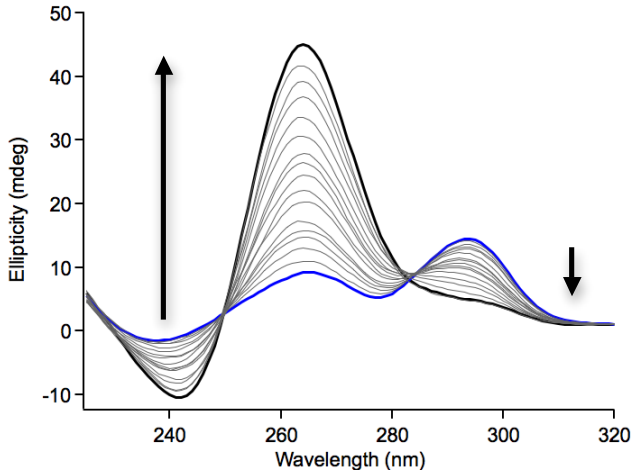

Figure 4.8 Time dependent CD spectra of quick-cooled *Htelo1* sample from Figure 4.1 during second transition while maintained at 30 °C for times between 1.5 hours (blue line) and 1152 hours (final gray line). In this figure, the black line represents the initial spectrum from Figure 4.7 to be used as a comparison. It is assumed that the spectra would have eventually reached this final spectrum; data points were not obtained past 1152 hours. Arrows indicate spectral change as a function of time.

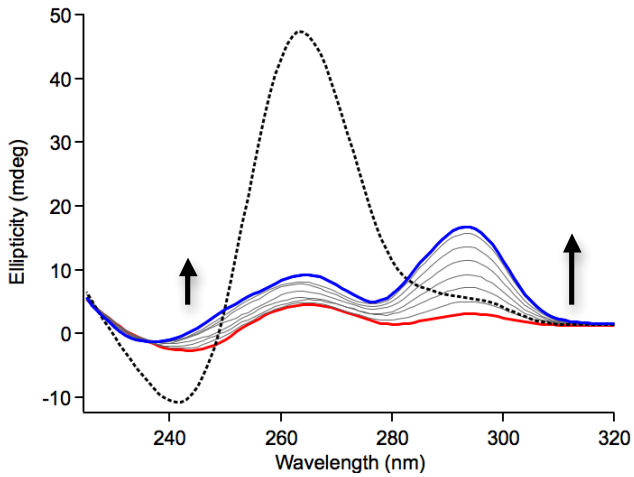

Figure 4.9 Time dependent CD spectra of quick-cooled *Htelo1* in 100%DES. Initial spectrum before heating is shown as black dashed line. After heating to 90 °C for 5 min sample was cooled (-0.65 °C/sec) and placed in CD at 20 °C (red solid line). The *Htelo1* sample reaches a kinetic intermediate (blue solid line) on the order of 3 hours. Sample was 1 m*m* in nucleotide; 100 m*m* KCl.

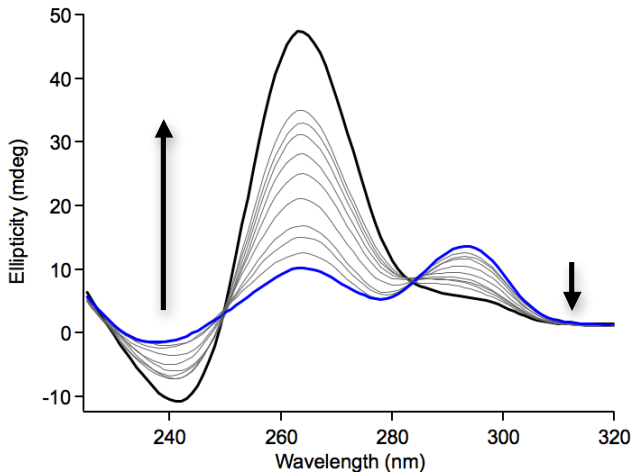

Figure 4.10 Time dependent CD spectra of quick-cooled *Htelo1* sample from Figure 4.1 during second transition while maintained at 20 °C for times between 3 hours (blue line) and 2640 hours (final gray line). In this figure, the black line represents the initial spectrum from Figure 4.9 to be used as a comparison. It is assumed that the spectra would have eventually reached this final spectrum; data points were not obtained past 2640 hours. Arrows indicate spectral change as a function of time.

Interestingly, the intermediate spectrum (blue line) at each temperature could not be fit as a linear combination of the equilibrium aqueous and DES spectra of *Htelo1*. This observation indicates that quick cooling traps *Htelo1* in a different state, or at least an altered distribution of conformations than those adopted in the aqueous buffer. In order to examine the dynamics of the system further, the formation time of G-quadruplex at these various temperatures were plotted vs. ellipticity at 295 nm and 265 nm. (Figure 4.11 and 4.12 respectively). These analyses verified that in the 100% DES, *Htelo1* undergoes at least two refolding events when returning to the thermodynamically favored structure. Specifically, Figure 4.11 illustrates that *Htelo1* initially folds to a structure, or group of structures that are kinetically favored. This initial folding event occurs within one to three hours after being quick-cooled to temperatures between 20 and 50 °C (Figure. 4.11).

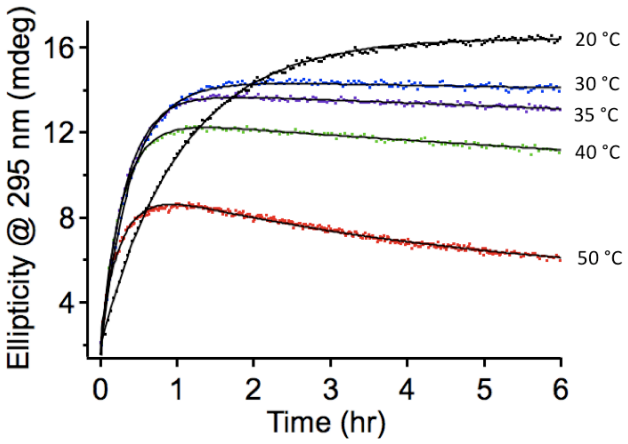

Figure 4.11 CD signal intensity at 295 nm *vs*. time for *Htelo1* maintained at different temperatures after quick cooling from 90 ºC. Samples were 1 m*m* in nucleotide; 100 m*m* KCl. Least squares fits are indicated by solid black lines.

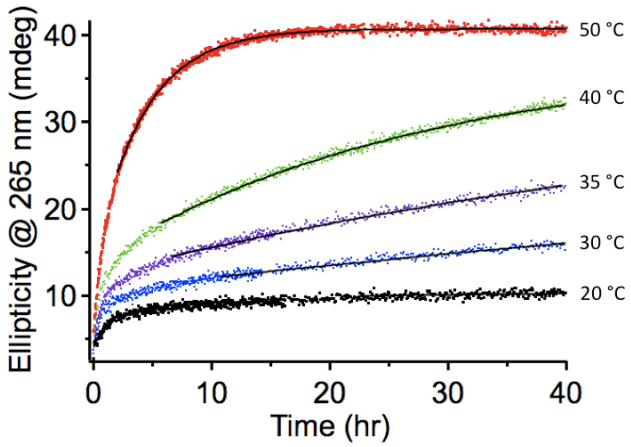

Figure 4.12 CD signal intensity at 265 nm *vs*. time for *Htelo1* maintained at different temperatures after quick cooling from 90 ºC. Samples were 1 m*m* in nucleotide; 100 m*m* KCl. Least squares fits are indicated by solid black lines.

Least-squares fittings of these plots give time constants for this transition (τ_1) of 24 to 16 min for refolding temperatures between 30 and 50 °C, respectively, and approximately 1 hour for 20 °C (Table 4.1). The rise of the 295 nm CD band intensity is

temporary, demonstrating that at least some of the structures adopted by *Htelo1* during the first folding event following quick cooling are merely kinetically favored structures.

Table 4.1: Time constants for *Htelo1* folding following thermal denaturation in 100% ChCl-urea DES

Temperature (°C)	τ_1 (hr)[(a)]	τ_2 (hr)[(b)]
50	0.27	4.2
40	0.27	28
35	0.32	69
30	0.39	165
20	1.00	>1500

(a) From least squares fitting of 295 nm CD intensity *vs*. time.
(b) From least squares fitting of 265 nm CD intensity *vs*. time for time > 2 x τ_1.

The more gradual increase in the 265 nm CD band intensity (Figure. 4.12) continues at all temperatures until the *Htelo1* sample spectrum eventually returns to the initial structure at equilibrium before heating. The 265 nm CD ellipticity effectively monitors this transition of *Htelo1* out of the intermediate state. Least squares fits of 265 nm CD intensity *vs*. time (for time > 2 × τ_1, Figure 4.4) provided rate constants for this second refolding event as a function of temperature (τ_2, Table 4.1). From these results it is obvious that τ_2 displays a significant level of temperature dependence when compared to the τ_1. For example, τ_1 is .27 hours at 50 °C and .39 hours at 30 °C; a 7 minute difference, whereas τ_2 is 4.2 hours at 50°C and >1500 hours at 30 °C; a 1400 hour difference.

Previous studies found that the folding of an intramolecular HTS G-quadruplex at 25 °C, after the addition of cations necessary for G-tetrad formation, takes place within

20 milliseconds [59] to 1.5 minutes [60], with evidence of kinetically favored intermediate folds over the course of folding in multiple studies.[38, 57-59, 62, 70, 72, 117] In the 100% ChCl-urea DES, folding of *Htelo1* after quick cooling from its thermally denatured state is much slower ($\tau_1 \sim 1$ hr), with intermediate folded states being adopted for extended periods (up to several months). Even more remarkable is that even though the DES is a liquid at 20 °C, refolding of *Htelo1* to its thermodynamically favored state in the DES at this temperature requires approximately six months!

To further explore the energetics associated with the folding of *Htelo1*, the results from the above analysis were transposed to an Arrhenius plot. (Figure 4.13)

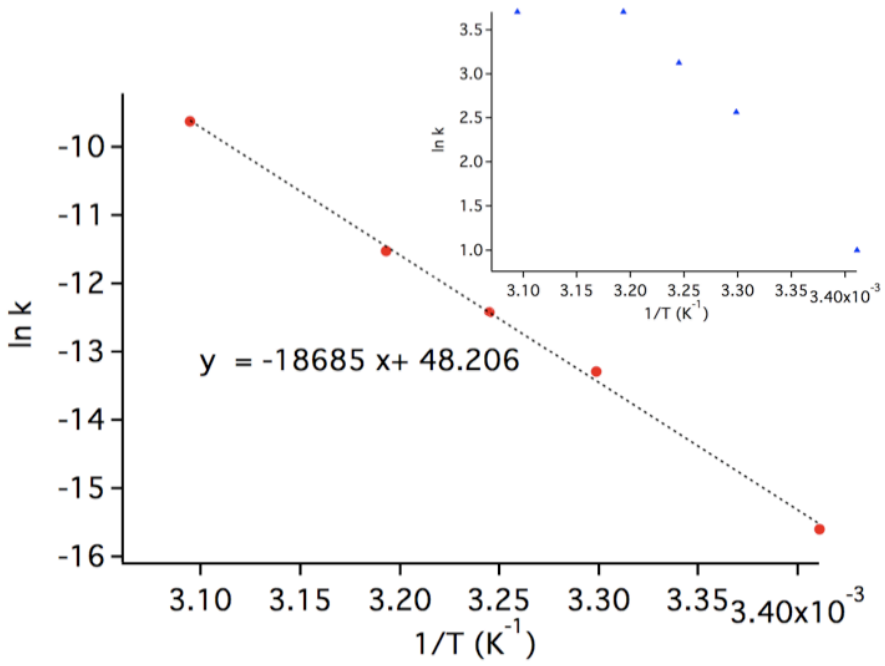

Figure 4.13 Arrhenius plot of *Htelo1* refolding rates in 100% DES. Red circles represent τ_2;(inset) Blue triangles represent τ_1. Linear fit indicated by black dashed line. Activation energy barrier calculated from slope of the linear fit.

The observed activation barrier for the follow on transition to the thermodynamically favored parallel structure is 155.4 $kJ \cdot mol^{-1}$. This value is somewhat consistent with previously reported values of Heddi and Phan (136 $kJ \cdot mol^{-1}$)[1], where they monitored the transition of *Htelo1* aqueous forms to the PEG 200 induced parallel form. However, it is unknown if the results are comparable due to the possible differences between our intermediate structure and their beginning aqueous structures.

The tremendous slowdown of the *Htelo1* folding, which is *very* surprising for an intramolecular system, is indicative of a diffusion-controlled process. As such, the remarkable difference between kinetic rates in aqueous buffer vs. DES should be attributed in part to decreased diffusion rates, which are inversely related to solvent viscosity through the Stokes-Einstein equation. Therefore, on a qualitative level, the increased solvent viscosity of the DES appears to slow refolding transition times (τ_2) as predicted by Kramers rate theory.[77] This hypothesis could help explain the tremendous temperature dependence observed for time constant τ_2 of *Htelo1* for conversion between its kinetically favored state and the parallel fold in 100% DES; which could partly be due to a sizeable enthalpy barrier, but also due to a large decrease in the rate of DNA chain diffusion as a result of the DES viscosity decreasing by about a factor of 10 from 20 °C to 50 °C (*i.e.*, from ca. 1100 cP to ca. 100 cP respectively).[110]

In contrast, τ_2 (the first folding event of *Htelo1* after quick cooling) has only a slight dependence on temperature *and* upon inspection of Figure 4.13 exhibits non-Arrhenius kinetics, which is commonly observed with biopolymer folding reactions. Moreover, τ_1 has only a modest dependence on solvent friction as well. For example, there is only a factor of 1.2 increase in τ_1 at 35 °C compared to 50 °C vs. a factor of 3

decrease in 100% DES viscosity for the same temperature range (ca. 300 cP to ca. 100 cP, respectively).[118] Both the temperature and solvent friction independence in this initial folding reaction indicate that *Htelo1* after quick cooling does not have a diffusion-limited component that requires appreciable solvent rearrangement; nor is the primary contribution to the free energy barrier enthalpic in nature. Instead, the initial activation energy has a major entropic component likely associated with internal friction.[77] This is consistent with kinetic studies that hypothesize the initial folding of HTS DNA resembles globular protein "hydrophobic collapse".[59]

From these results we can conclude that during the early G-quadruplex folding stage, the DNA chains effectively "zipper" together to form transient hairpins with significant internal interactions. These internal rearrangements most likely control the initial folding speed, and as the results show, do not require significant solvent movement and is relatively temperature independent.

4.3 Evidence for a solvent-selected G-quadruplex folding pathway.

The folding of *Htelo1* after quick cooling resulted in the trapping of an intermediate state for hours to months, before conversion back to the parallel-stranded fold. In order to further explore the choline chloride and urea solvent effects and DES viscosity contribution to *Htelo1* folding dynamics the same experiment was carried out in 40% PEG 200 solution. In contrast to the pathway observed in 100% ChCl-urea DES, *Htelo1* in 40% PEG 200 returned to the parallel fold in less than two minutes at 20 °C (Figure. 4.14).

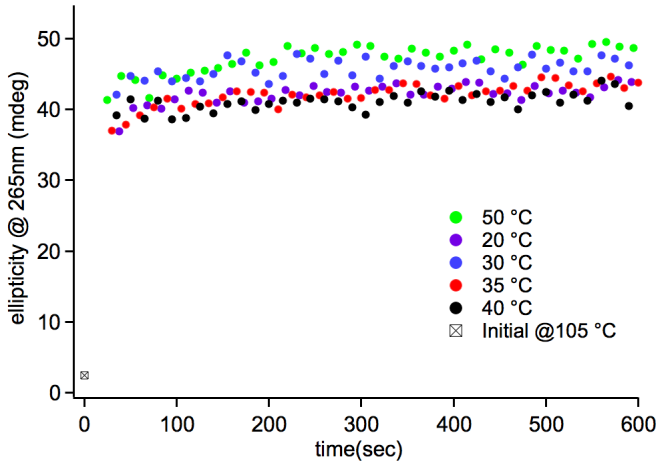

Figure 4.14 Quick cool kinetic analysis of *Htelo1* in 40% PEG200. Ellipticity was monitored at 265 nm as a function of time for *Htelo1* samples in the 40% PEG200 (v/v) at different temperatures after quick-cooling from 105 ºC (-.65 °C/s). Data point at 105 ºC, time 0, was obtained prior to quick cooling. All samples were 1 mM in nucleotide and contained 100 mM KCl and 20 mM potassium phosphate buffer, pH 7.

Due to the time resolution limits of these CD-monitored experiments, a quantitative comparison of folding rates between *Htelo1* in 100% DES and 40% PEG 200 was not possible. However, if *Htelo1* folded to the same intermediate state when quick cooled in the 40% PEG 200 solution as in the 100% ChCl-urea DES, the rate increase for exiting this intermediate state would be on the order of 5 x 10^4 (*i.e.*, $\tau_{2DES}/\tau_{PEG} > 1500$ hr/2 min). Consequently, the observed rate cannot entirely be attributed to the difference in the viscosities of the two solvents as they only differ by a factor of 200 at room temperature. Therefore, a possible explanation is that the folding pathway of *Htelo1* is also solvent dependent and the 100% DES directs *Htelo1* to a state that is not accessed during folding in 40% PEG 200. This effect may be a result of the high viscosity of the 100% DES and/or the solvent effects of choline chloride and urea.[77] Specifically, solvent molecules in the DES (choline and urea) could interact with the G-quadruplex

more powerfully than water or PEG 200. This interaction could increase the solvent friction experienced by nucleic acid chains during strand reorientation, thereby slowing the second transition or refolding of *Htelo1*.

CHAPTER 5

HUMAN TELOMERE SEQUENCE DNA DYNAMICS ARE CONTROLLED BY DIFFUSION

5.1 Abstract

In this chapter viscosity is used as a tool to probe the dynamics of HTS DNA refolding. It is discovered that the refolding kinetics of *Htelo1* G-quadruplex are in fact diffusion controlled. Moreover, the rates of refolding in the presence of various viscogenic agents scale proportionally with dynamic viscosity in accordance with Kramers rate theory. Finally, it is hypothesized that the unique solvent properties of the ChCl-urea DES are responsible for the greater than expected slowing of rates during the refolding reaction.

5.2 Solvent viscosity slows HTS DNA refolding in accord with Kramers rate theory.

The extremely long time constants observed for *Htelo1* folding have not been previously seen for *intramolecular* G-quadruplexes in aqueous solution. Studies of protein folding have shown that structural switches slow significantly with increasing solvent viscosity.[83, 84, 88, 89] Such observations can be explained by Kramers rate theory, as discussed in Chapter 1.[76, 119, 120] Briefly, as a reminder, molecular movements that involve solvent rearrangement will decrease inversely with the friction

experienced between the folding molecule and the solvent. Often, the rates of diffusion-controlled reactions are found to vary linearly with solvents that have viscosities greater than water, (*i.e.*, >1 cP) as the diffusion of a particle in a solvent, according to the Stokes-Einstein equation, scales directly with dynamic viscosity of the solvent.[77, 78] The viscosity of the ChCl-urea DES solvent is approximately 1000 cP [118]; high enough to expect solvent friction to decrease the rate of G-quadruplex refolding. However, in order to test the relative contributions of solvent effects versus viscosity and determine the suitability of Kramers rate theory to explain the slow kinetics of *Htelo1* refolding in the ChCl-urea DES, it is necessary to compare refolding time constants for the transition of *Htelo1* between the same two structural states in solvents with different viscosity. Furthermore, since the barrier of the transition between the two states is relatively high, population changes at positions along the reaction coordinate may be effected by the different nature of solvents. Therefore, in an effort test whether the increase in relaxation time results only from increased solvent viscosity different viscogens must be utilized.

Heddi and Phan measured time constants for the transition of *Htelo1* from its aqueous folded state to its parallel structure in 40% PEG 200 by transferring an aliquot of PEG 200 to an aqueous solution containing *Htelo1*.[1] In order to carry out the same refolding experiment, and compare the results, ChCl-urea and PEG 200-glycerol aqueous mixtures were utilized. It was determined in Chapter 3 (Figure 3.21) that ≥ 85% ChCl-urea DES (w/w with water) favors the parallel G-quadruplex as the thermodynamically favored structure. A similar determination was needed for the amount of added glycerol viscogen. Figure 5.1 displays that ≤ 30% glycerol with 40% PEG 200 (v/v) is sufficient

for the formation of the parallel G-quadruplex as the thermodynamically favored structure of *Htelo1*.

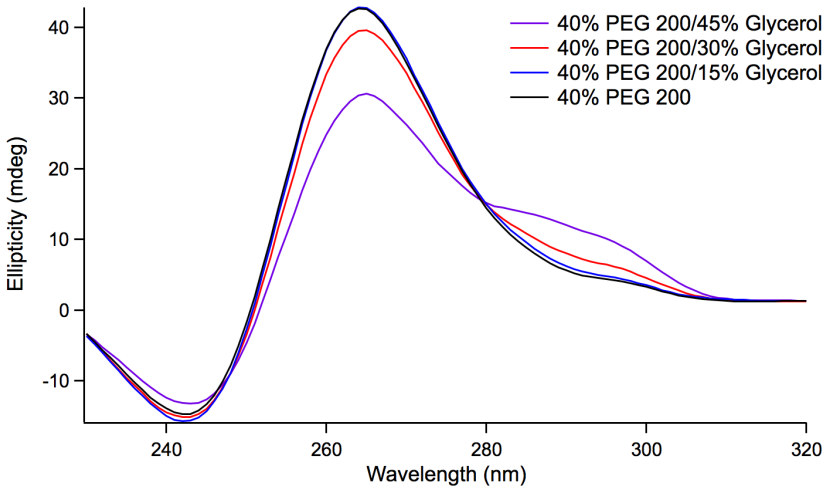

Figure 5.1 CD spectra of DNA with the HTS-derived sequence d[$TAG_3(TTAG_3)_3$] (*Htelo1*) in various solvents. DES sample was 1 mM in nucleotide and contained 100 mM KCl and 20 mM potassium phosphate buffer, pH 7. Percentages in figure legend represent v/v with water. Spectra were recorded at 20 °C after samples were equilibrated.

For isothermal refolding studies, samples were prepared by mixing one part of aqueous stock solution containing *Htelo1* with respective parts ChCl-urea DES or PEG 200-glycerol as added viscogens. Monitoring the refolding of *Htelo1* samples maintained at 30, 40, 50 and 60 °C was accomplished through the use of CD spectroscopy. Time-course CD spectra for the 40 °C samples are shown in Figures 5.2-5.5. Isoelliptic points at ≈250 and ≈280 nm imply that a two-state transition takes place over time, between the aqueous state structures and the parallel structure, with no significant intermediate states. Similar time-course CD spectra for 30, 50 and 60 °C are provided in Appendix A.

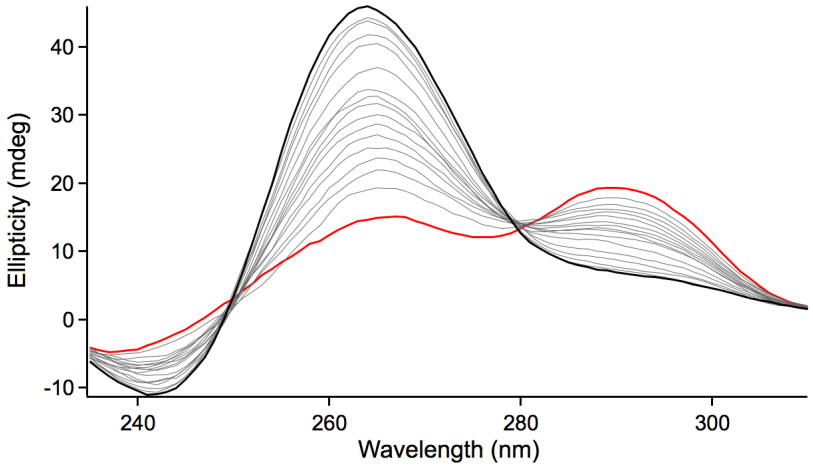

Figure 5.2 Time dependent CD spectra of *Htelo1* following transfer to 90% ChCl-urea DES (w/w). Initial spectrum after mixing and transfer to instrument at 40 °C is shown in red. Sample was 1 m*m* in nucleotide; 100 m*m* KCl and 20 m*m* potassium phosphate, pH 7.

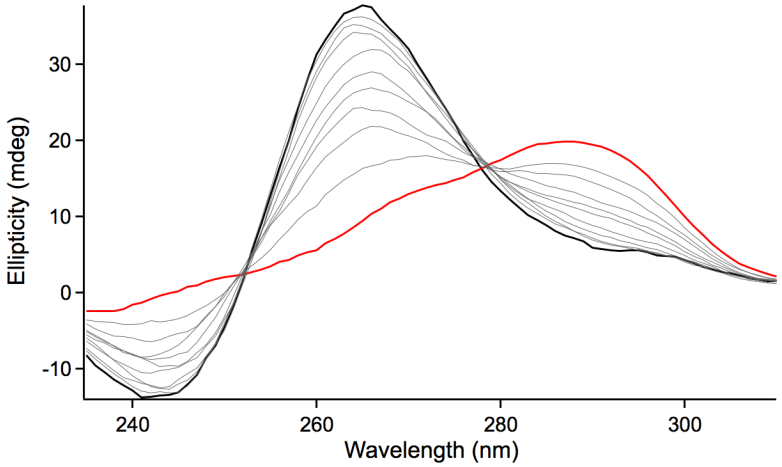

Figure 5.3 Time dependent CD spectra of *Htelo1* following transfer to 40% PEG 200 (v/v). Initial spectrum after mixing and transfer to instrument at 40 °C is shown in red. Sample was 1 mM in nucleotide; 100 mM KCl and 20 mM potassium phosphate, pH 7.

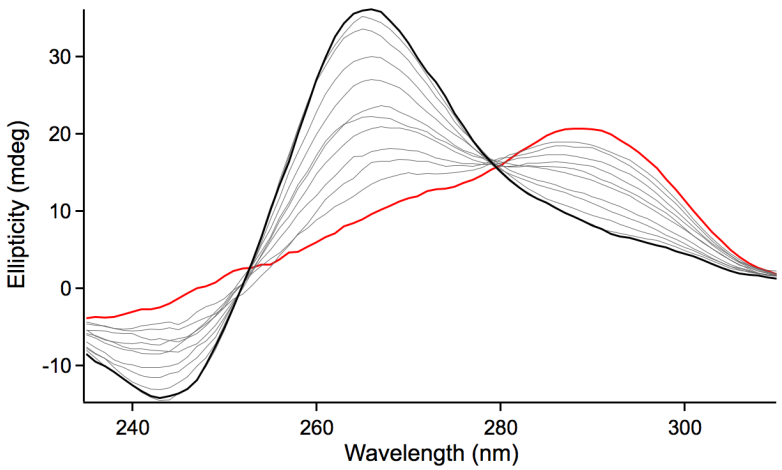

Figure 5.4 Time dependent CD spectra of *Htelo1* following transfer to 40% PEG 200 / 30% Glycerol (v/v). Initial spectrum after mixing and transfer to instrument at 40 °C is shown in red. Sample was 1 mM in nucleotide; 100 mM KCl and 20 mM potassium phosphate, pH 7.

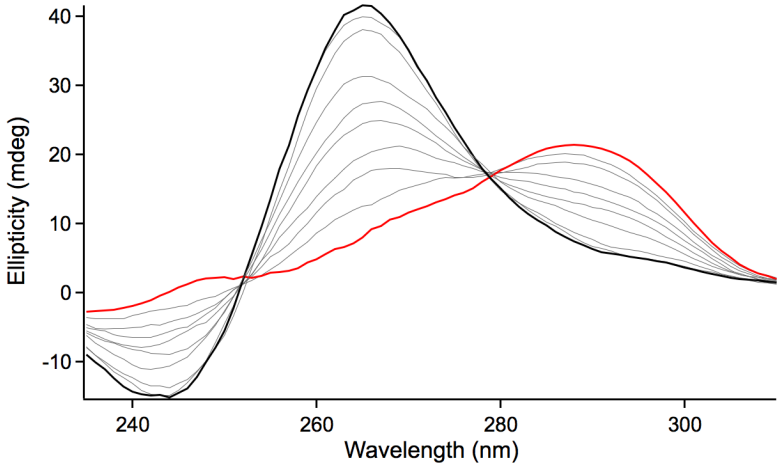

Figure 5.5 Time dependent CD spectra of *Htelo1* following transfer to 40% PEG 200 / 15% Glycerol (v/v). Initial spectrum after mixing and transfer to instrument at 40 °C is shown in red. Sample was 1 mM in nucleotide; 100 mM KCl and 20 mM potassium phosphate, pH 7.

In an effort to more rigorously verify the two state assumptions, a dual wavelength parametric test of the CD data was performed (Figures 5.6, 5.8, 5.10 and

5.12). Upon inspection of the residual analysis from the linear fit to the data in the 90% DES conditions (Figure 5.7) one observes that the transition of *Htelo1* deviates from a two-state conversion during the early and late stages of refolding at all temperatures measured except 60 °C. Deviations are also observed in the 40% PEG 200/30% glycerol conditions at 30 °C (Figure 5.11) and the 40% PEG 200/15% glycerol conditions at 50 °C and 60 °C (Figure 5.13). In contrast to all other folding conditions, the 40% PEG 200 solvent displays no significant deviation from a two-state transition at the temperatures observed indicating a concerted mechanism of refolding.

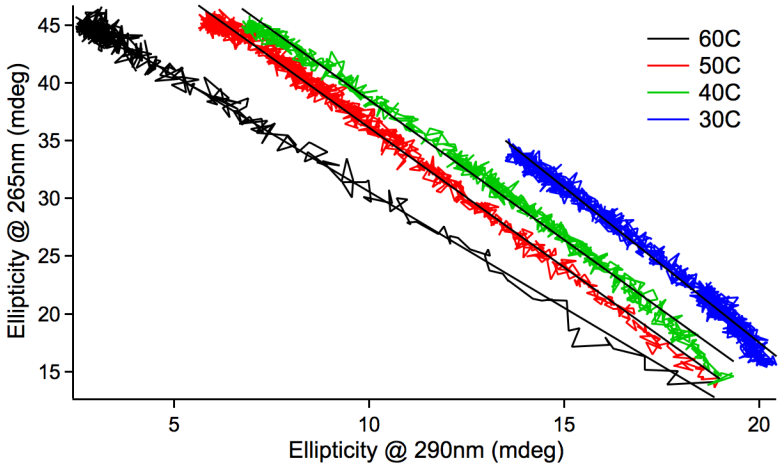

Figure 5.6 Parametric plot of 265 nm *vs.* 290 nm for *Htelo1* transition following addition of 90% ChCl/urea DES (w/w) at various temperatures. 30 °C and 60 °C data were offset for clarity. Solid black lines represent linear fit of the respective data.

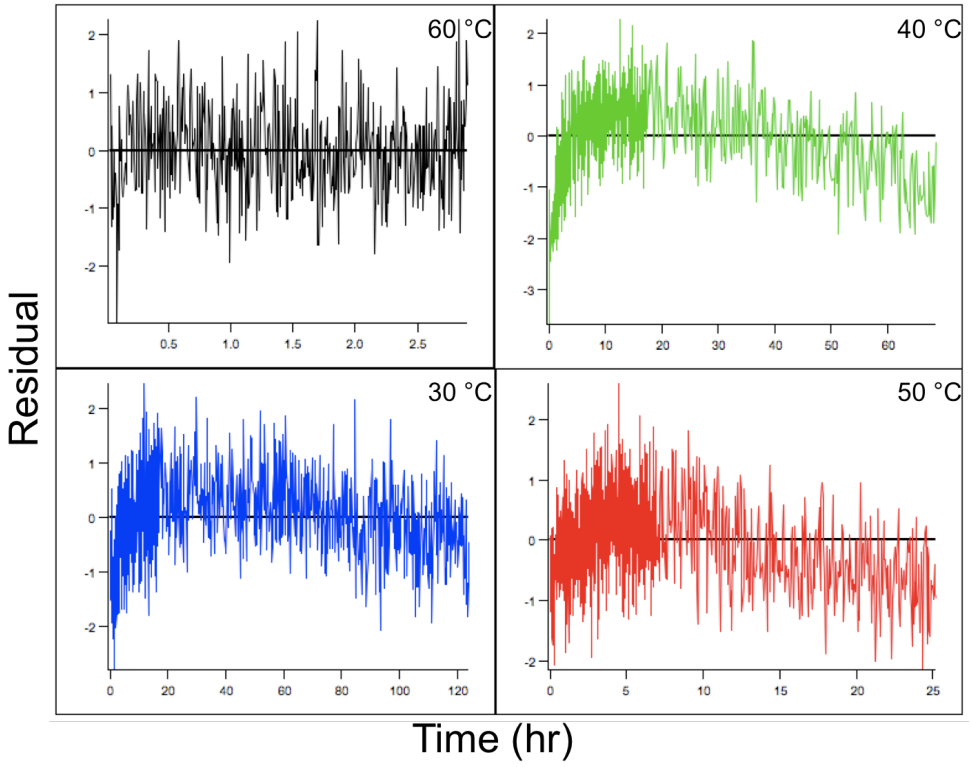

Figure 5.7 Residual analysis of the linear fit in Figure 5.6 as a function of time.

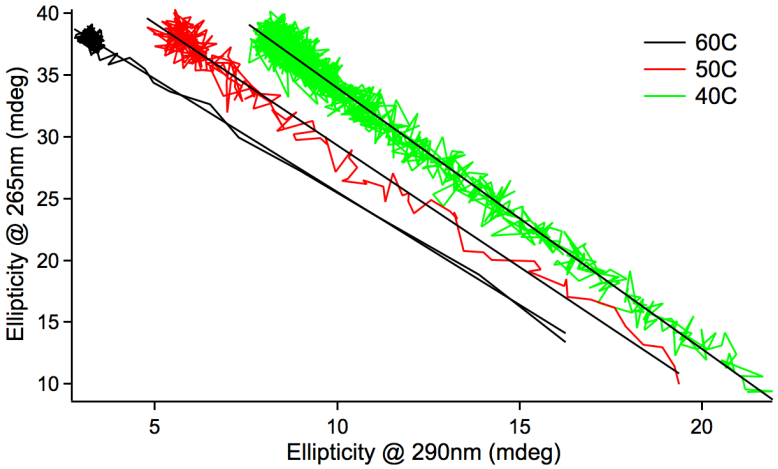

Figure 5.8 Parametric plot of 265 nm *vs.* 290 nm for *Htelo1* transition following addition of 40% PEG 200 (v/v) at various temperatures. 40 °C and 60 °C data were offset for clarity. Solid black lines represent linear fit of the respective data.

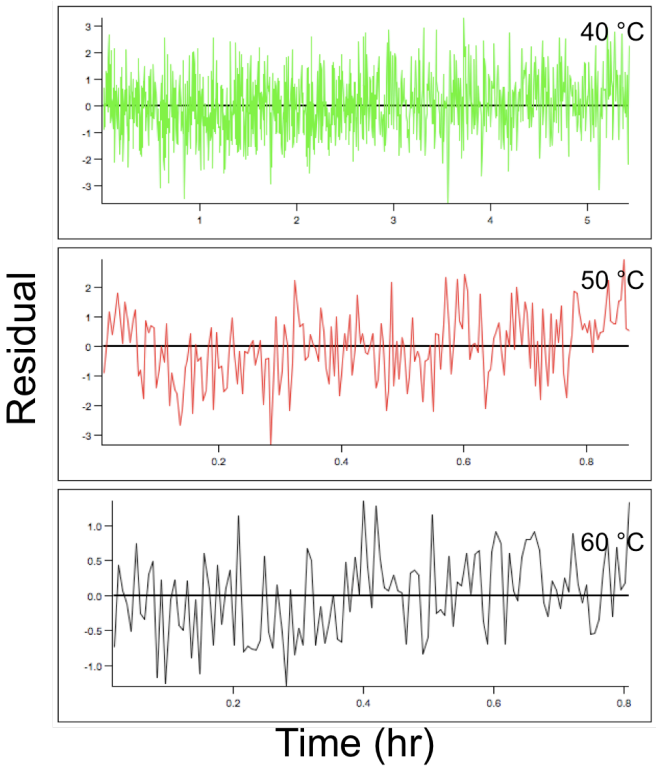

Figure 5.9 Residual analysis of the linear fit in Figure 5.8 as a function of time.

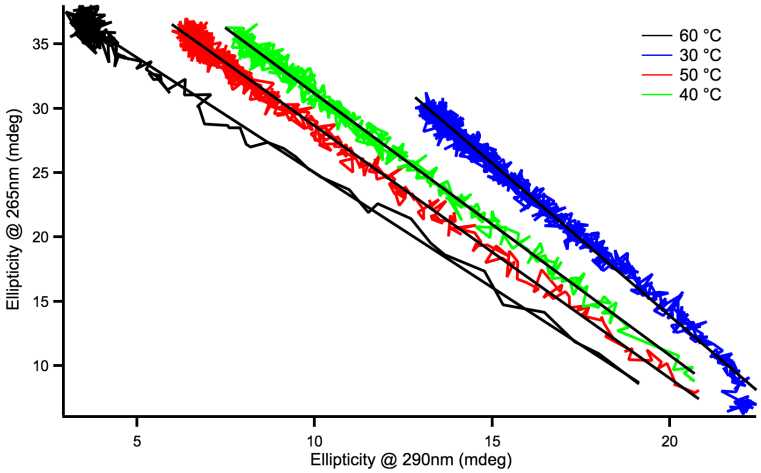

Figure 5.10 Parametric plot of 265 nm *vs.* 290 nm for *Htelo1* transition as a function of time following addition of 40% PEG 200 / 30% Glycerol (v/v) at various temperatures. 40 °C and 60 °C data were offset for clarity. Solid black lines represent linear fit of the respective data.

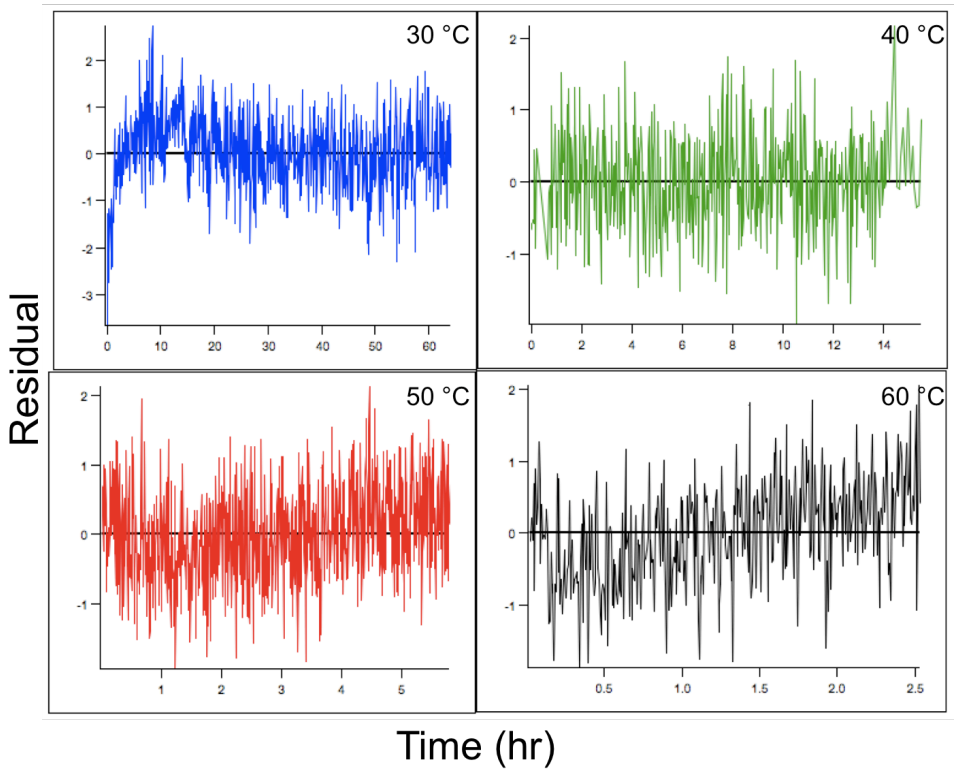

Figure 5.11 Residual analysis of the linear fit in Figure 5.10 as a function of time.

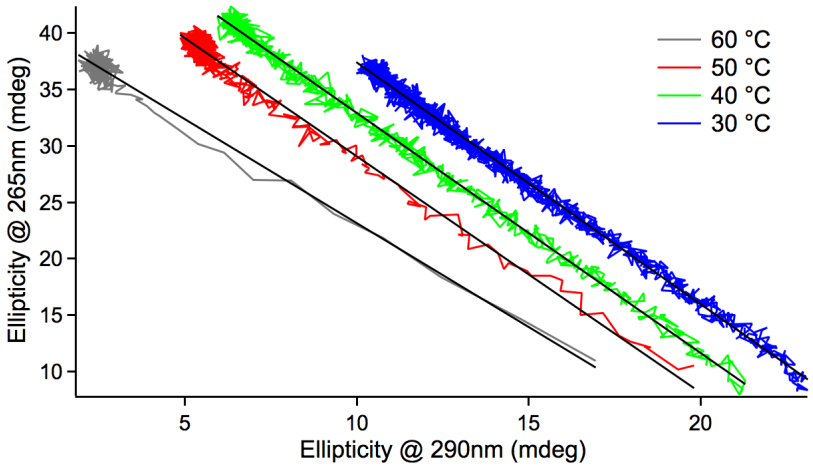

Figure 5.12 Parametric plot of 265 nm *vs.* 290 nm for *Htelo1* transition as a function of time following addition of 40% PEG 200 / 15% Glycerol (v/v) at various temperatures. 40 °C and 60 °C data were offset for clarity. Solid black lines represent linear fit of the respective data.

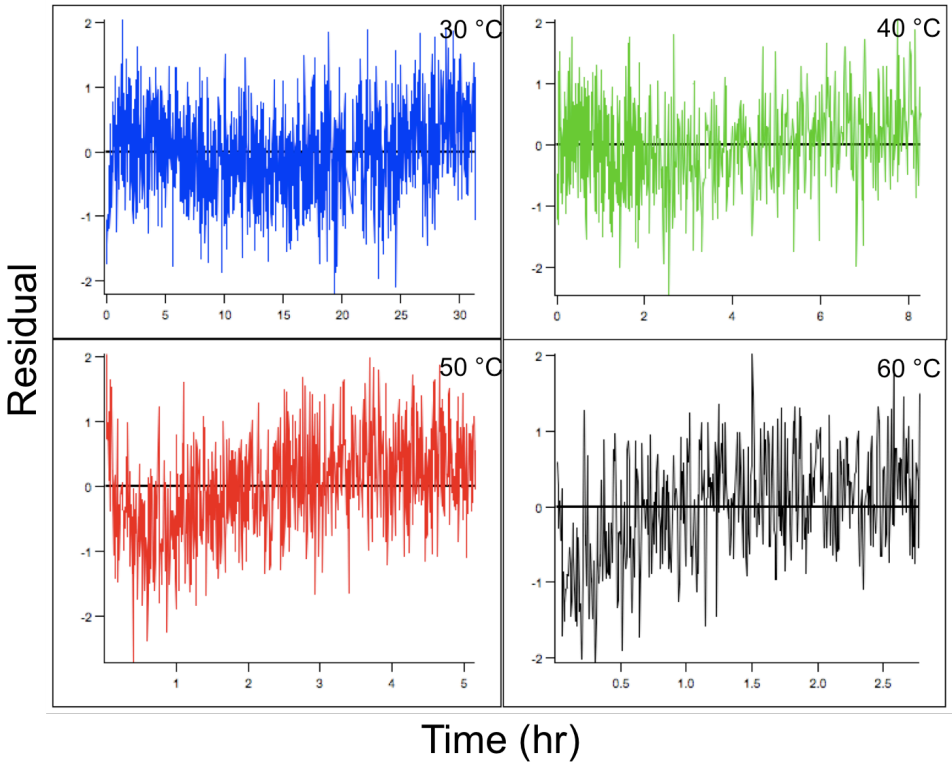

Figure 5.13 Residual analysis of the linear fit in Figure 5.12 as a function of time.

Curve fitting of plots of 265 nm CD signal intensity *vs*. time under the various conditions (Figures 5.14-5.17) revealed principal time constants for conversion between aqueous folded states and the parallel structures. These values are reported in Table 5.1.

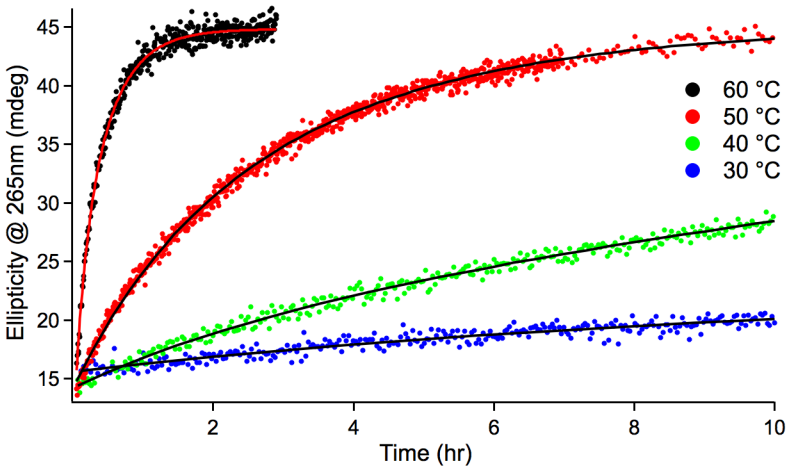

Figure 5.14 CD signal intensity at 265 nm as a function of time for *Htelo1* refolding following transfer to 90% ChCl-urea DES (w/w). Least-squares fits with double exponential functions are shown as solid lines. Samples were 1 m*m* in nucleotide; 100 m*m* KCl and 20 m*m* potassium phosphate, pH 7.

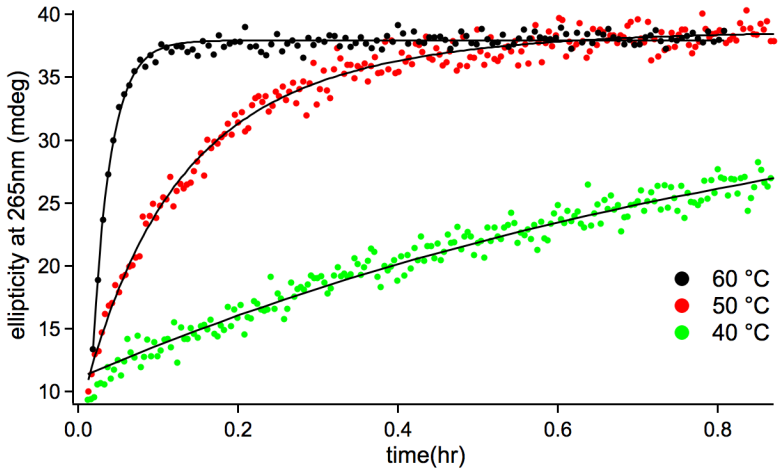

Figure 5.15 CD signal intensity at 265 nm as a function of time for *Htelo1* refolding following transfer to 40% PEG 200 (v/v). Least-squares fits with single exponential functions are shown as solid lines. Samples were 1 mM in nucleotide; 100 mM KCl and 20 mM potassium phosphate, pH 7.

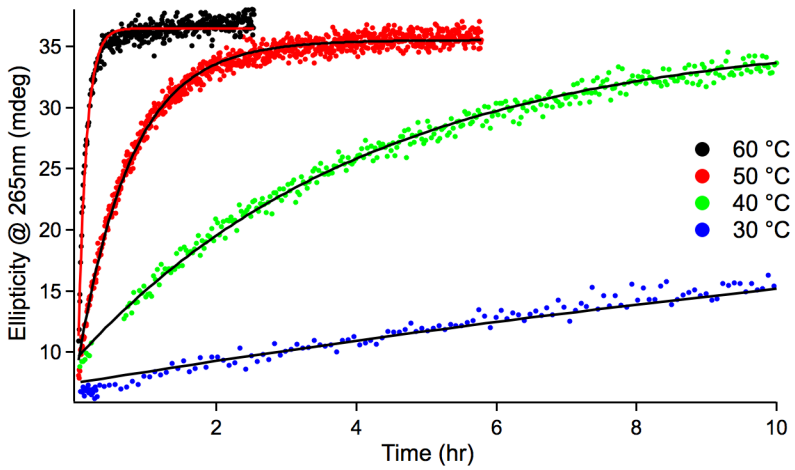

Figure 5.16 CD signal intensity at 265 nm as a function of time for *Htelo1* refolding following transfer to 40% PEG 200 / 30% glycerol (v/v). Least-squares fits with single exponential functions are shown as solid lines. Samples were 1 mM in nucleotide; 100 mM KCl and 20 mM potassium phosphate, pH 7.

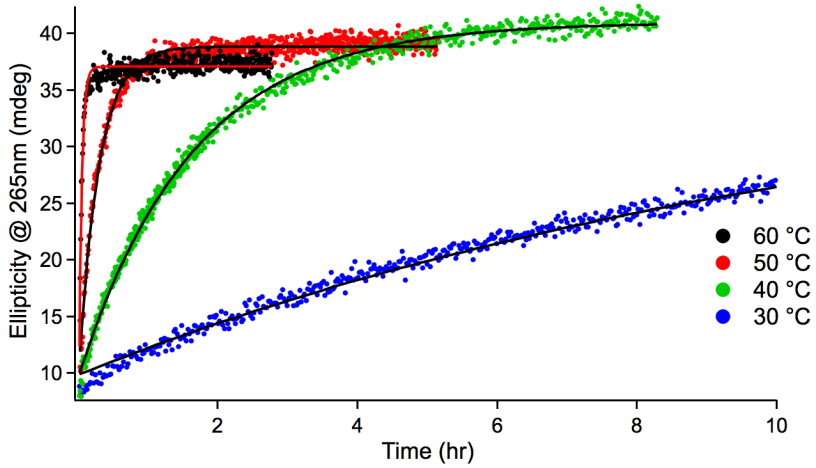

Figure 5.17 CD signal intensity at 265 nm as a function of time for *Htelo1* refolding following transfer to 40% PEG 200 / 15% glycerol (v/v). Least-squares fits with single exponential functions are shown as solid lines. Samples were 1 mM in nucleotide; 100 mM KCl and 20 mM potassium phosphate, pH 7.

Table 5.1 Time constants for *Htelo1* refolding in various solvents

Temperature (°C)	τ_1 (hr) 90% ChCl-urea DES[a]	τ_2 (hr) 90% ChCl-urea DES[a]	τ (hr) 40% PEG 200[b]	τ (hr) 40% PEG 200 / 30% glycerol[b]	τ (hr) 40% PEG 200/ 15% glycerol[b]
60	0.14	0.44	0.23	0.15	0.04
50	1.51	3.39	0.14	0.75	0.29
40	2.44	21.47	0.97	4.22	1.62
30	5.55	94.08	4.10	26.26	11.66

[a] Time constants obtained by double exponential fit of ellipticity at 265nm *vs.* time
[b] time constants obtained by exponential fit of ellipticity at 265nm *vs.* time

Fitting of the 90% ChCl-urea DES curves within a standard deviation of the data required a double exponential function, as a minor fraction of *Htelo1* (estimated to be <10% based on percentage change in CD spectra) made the transition to the parallel structure with a time constant that was an order of magnitude less than the major transition (τ_1, Table 5.1). As noted above, the parametric plot analysis of *Htelo1* conversion in 90% DES displayed a slight deviation from a two-state transition (Figure 5.6). These observations are confirmatory of previous inferences that *Htelo1* exists in more than one folded state in an aqueous solution.[1] Moreover, these analyses show that the free energy barrier of transition to the parallel fold is substantially less for at least one minor species in the aqueous solution, compared to the other folded species in the same sample.

In contrast, the differential rates of conversion are not observed in similar experiments with the less viscous 40% PEG 200 solvent; the CD signal intensity at 265nm vs. time (Figure 5.15) does not require the use of a double exponential fit.

Moreover, the two-state assumption in the 40% PEG 200 holds after examination by a parametric plot analysis (Figure 5.8). Additionally, the differential rates of conversion are not observed with the added 30-15% glycerol to the 40% PEG 200, however, the parametric analysis shows a deviation from a two-state transition at lower temperatures in the case of 30% glycerol, and higher temperatures in the 15% glycerol.

A possible explanation for these anomalies could be that the interaction of *Htelo1* with PEG 200 allows all aqueous forms of the G-quadruplex to convert via a concerted reaction with the same transition rates. Another possible explanation is that the increased viscosity of the 90% ChCl-urea solvent allowed a sequential mechanism to be observed alongside the differential rates of refolding that occur between the various aqueous structures of *Htelo1* on the time-scale possible in this study. This conclusion is reinforced by the observed deviation from a two-state transition and less accurate fitting with a single exponential exhibited by *Htelo1* in the 30% glycerol / 40% PEG 200 solution conditions at 30 °C. The divergence from a two state transition of the 15% glycerol / 40% PEG 200 refolding conditions at the beginning of the refolding event at increased temperatures is also unexpected. It is likely that this observation is an artifact of data collection due to the time interval constraints during the faster refolding events leading to an erroneous linear regression analysis.

To further investigate the kinetic parameters of the system in various solvent conditions the refolding rates were analyzed through the use of an Arrhenius plot (Figure 5.18). The fit of the data points to the Arrhenius equation yielded apparent energetic barrier heights that are summarized in Table 5.2. For comparison, the rates obtained by Heddi and Phan for the refolding of *Htelo1* in 40% PEG 200 indicate a transition barrier

height of 136 kJ/mol.[1] Accordingly, the linear fits of the Arrhenius plots for *Htelo1* refolding in 90% DES, 40% PEG 200, and 40% PEG 200 with 30% and 15% glycerol have very similar slopes (Figure 5.18).

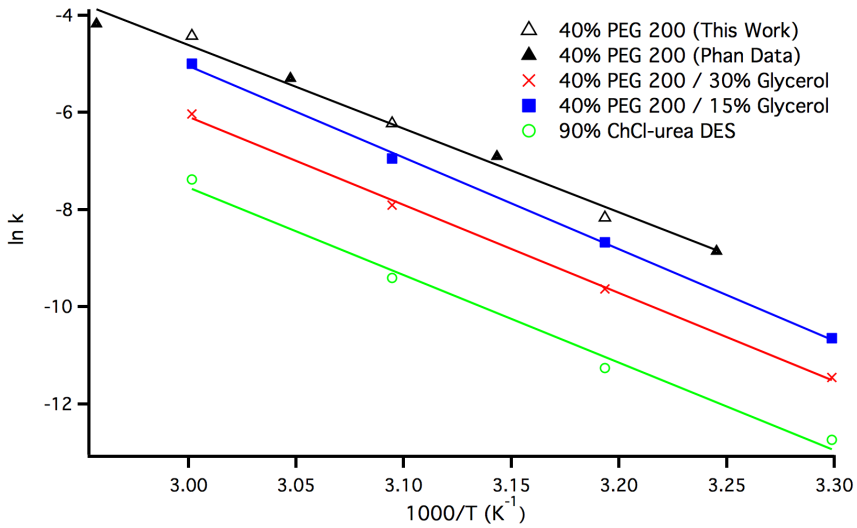

Figure 5.18 Arrhenius plot comparison for *Htelo1* transition kinetics from aqueous structures to the parallel fold in multiple solvents. Black triangles indicate kinetic data from Heddi and Phan [1] for refolding in 40% PEG 200. Open triangles are data from the current study for *Htelo1* refolding in 40% PEG 200. DES Samples contained 1 m*m* DNA, 100 m*m* KCl, 20 m*m* potassium phosphate, pH 7. PEG and PEG/glycerol samples contained 100 mM KCl, 20 mM potassium phosphate, pH 7.

Table 5.2 Apparent energy associated with transition barriers of *Htelo1* refolding in various solvents

Solvent	E_a (kJ/mol)
90% ChCl-urea DES	150.1
40% PEG 200 (combined data)*	143.3
40% PEG 200 / 30% glycerol	150.0
40% PEG 200 / 15% glycerol	156.7

* linear fit obtained from both this work's data and Heddi and Phan data[1]

The similar slopes but different vertical placements of the various solvent's Arrhenius plots suggest a substantial difference in the pre-exponential constant of the Arrhenius equations that describe the different refolding rates. As mentioned in Chapter 1, for folding reactions in the strong friction regime, Kramers rate theory and the Stokes-Einstein equation predict that the pre-exponential constant of the Arrhenius equation will decrease linearly with viscosity.[77] That is, the Arrhenius equation can be written as equation 1.2, seen in Chapter 1. To examine the consistency of this form of the Arrhenius equation with *Htelo1* refolding, the natural log of refolding rates were re-plotted *vs*. 1000/T as viscosity-adjusted rates (*i.e*. ln (η/τ); Figure 5.19). The adjusted activation energies associated with the linear fit of these viscosity-corrected rates are displayed in Table 5.3.

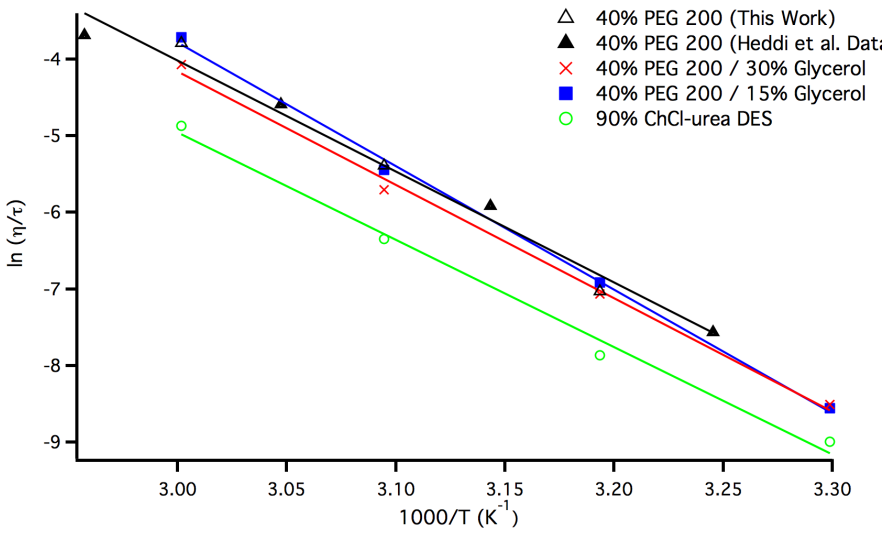

Figure 5.19 Arrhenius plot comparison of *Htelo1* DNA transition kinetics in various solvents with added viscogens. Rates are scaled according to the viscosity of each solvent at each temperature. Black triangles indicate kinetic data from Heddi and Phan [1] for refolding in 40% PEG 200. Open triangles are data from the current study for *Htelo1* refolding in 40% PEG 200. DES Samples contained 1 m*m* DNA in nucleotide, 100 m*m* KCl, 20 m*m* potassium phosphate, pH 7. PEG and PEG/glycerol samples contained 100 mM KCl, 20 mM potassium phosphate, pH 7.

Table 5.3 Apparent energy associated with transition barriers of *Htelo1* refolding in various solvents after correction for viscosity

Solvent	E_a (kJ/mol)
90% ChCl-urea DES	116.4
40% PEG 200 (combined data)*	120.3
40% PEG 200 / 30% glycerol	123.0
40% PEG 200 / 15% glycerol	134.1

* linear fit obtained from both this work's data and Heddi and Phan data[1]

The approximately twenty-percent decrease in the apparent activation barrier in all of the solvents illustrates the influence of temperature-dependent solvent viscosity on the apparent enthalpy of the transition state barrier height. The closer vertical placement of the PEG and PEG/glycerol plots imply that the barrier crossing is a simple process where the friction coefficient is proportional to the solvent's dynamic viscosity. However, a factor of 2.5 still remains between the 90% DES plot and the others, implying that this viscogen alters the free energy surface. In order to verify if the relevant reaction friction is proportional to the viscosity, a plot of τ vs. η should be linear with zero intercept. Figures 5.20-5.24 display these plots at various temperatures.

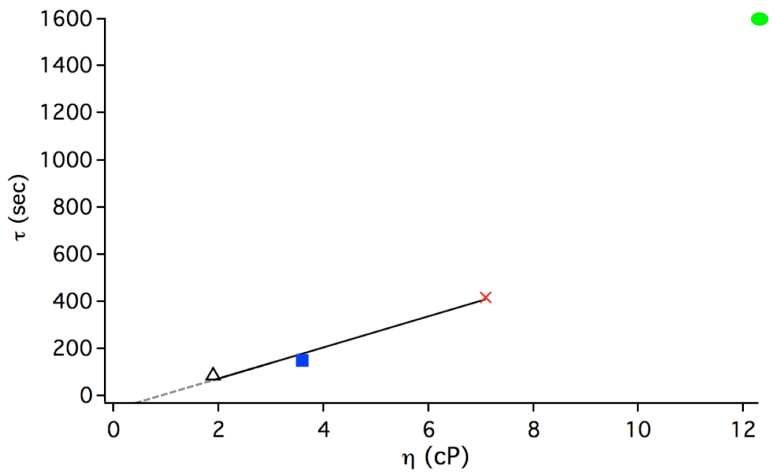

Figure 5.20 Plot of *Htelo1* refolding rate constants (τ) vs. dynamic viscosity (η) at 60 °C. The black open triangle is the observed rate in 40% PEG 200; The blue square is the observed rate in 40% PEG 200 / 15% glycerol; the red x is the observed rate in 40% PEG 200 / 30% glycerol; the green circle is the observed rate in 90% ChCl-urea DES. All samples contained 1 mM (m*m* for DES) DNA in nucleotide, 100 mM (m*m* for DES) KCl, and 20 mM (m*m* for DES) potassium phosphate buffer, pH 7. Linear fit was only obtainable by utilizing rates of *Htelo1* refolding in glycerol and PEG solutions.

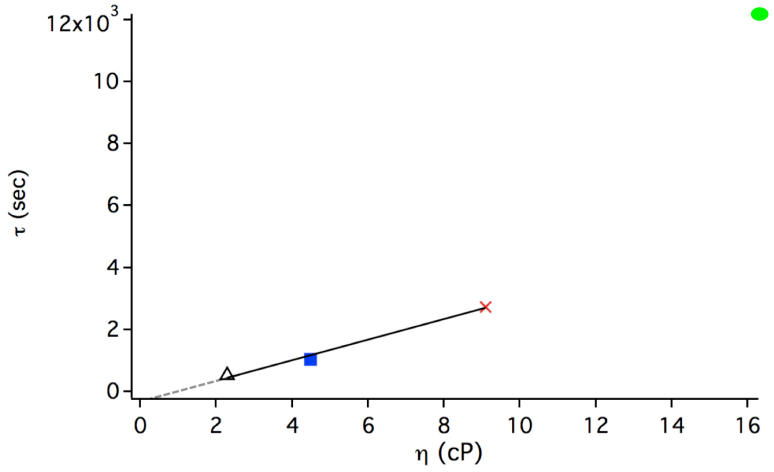

Figure 5.21 Plot of *Htelo1* refolding rate constants (τ) vs. dynamic viscosity (η) at 50 °C. The black open triangle is the observed rate in 40% PEG 200; The blue square is the observed rate in 40% PEG 200 / 15% glycerol; the red x is the observed rate in 40% PEG 200 / 30% glycerol; the green circle is the observed rate in 90% ChCl-urea DES. All samples contained 1 mM (m*m* for DES) DNA in nucleotide, 100 mM (m*m* for DES) KCl, and 20 mM (m*m* for DES) potassium phosphate buffer, pH 7. Linear fit was only obtainable by utilizing rates of *Htelo1* refolding in glycerol and PEG solutions.

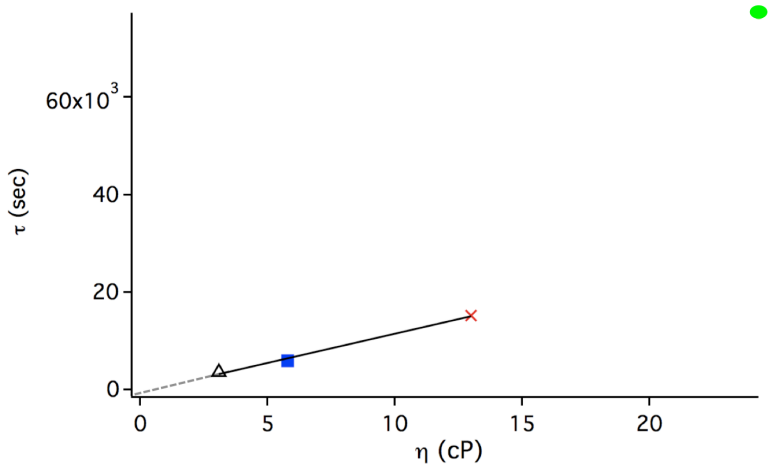

Figure 5.22 Plot of *Htelo1* refolding rate constants (τ) vs. dynamic viscosity (η) at 40 °C. The black open triangle is the observed rate in 40% PEG 200; The blue square is the observed rate in 40% PEG 200 / 15% glycerol; the red x is the observed rate in 40% PEG 200 / 30% glycerol; the green circle is the observed rate in 90% ChCl-urea DES. All samples contained 1 mM (m*m* for DES) DNA in nucleotide, 100 mM (m*m* for DES) KCl, and 20 mM (m*m* for DES) potassium phosphate buffer, pH 7. Linear fit was only obtainable by utilizing rates of *Htelo1* refolding in glycerol and PEG solutions.

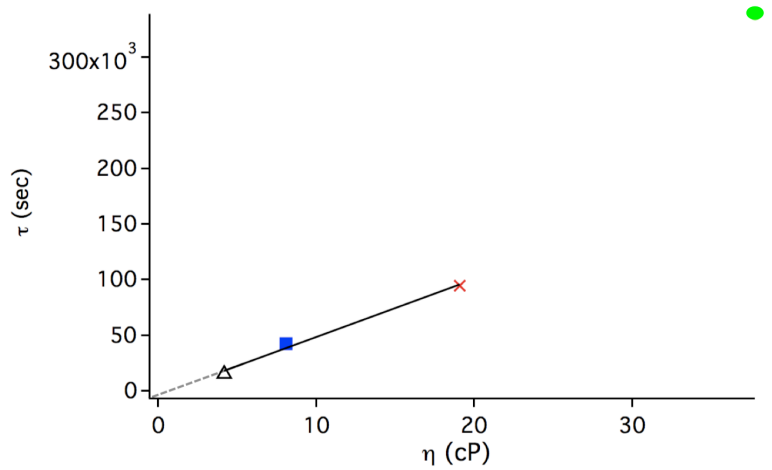

Figure 5.23 Plot of *Htelo1* refolding rate constants (τ) vs. dynamic viscosity (η) at 30 °C. The black open triangle is the observed rate in 40% PEG 200; The blue square is the observed rate in 40% PEG 200 / 15% glycerol; the red x is the observed rate in 40% PEG 200 / 30% glycerol; the green circle is the observed rate in 90% ChCl-urea DES. All samples contained 1 mM (m*m* for DES) DNA in nucleotide, 100 mM (m*m* for DES) KCl, and 20 mM (m*m* for DES) potassium phosphate buffer, pH 7. Linear fit was only obtainable by utilizing rates of *Htelo1* refolding in glycerol and PEG solutions.

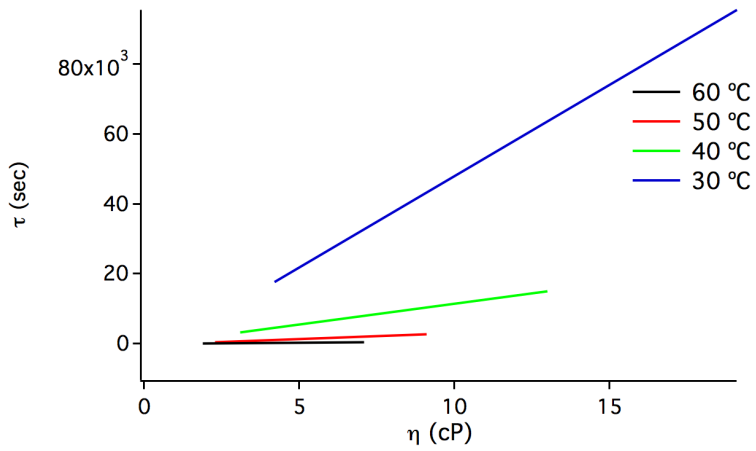

Figure 5.24 Combined plots of *Htelo1* refolding rate linear fits at all temperatures observed. All samples contained 1mM (m*m* for DES) DNA in nucleotide, 100 mM (m*m* for DES) KCl, and 20 mM (m*m* for DES) potassium phosphate buffer, pH 7. Linear fit excluded 90% DES solution rates.

As expected, in the case of the glycerol/PEG solutions, the plots are linear and exhibit a zero intercept at lower temperatures and therefore higher viscosities (Figures 5.22 and 5.23). Moreover, the temperature variations have a substantial effect on the slopes in Figure 5.24, supporting the conclusion that refolding is influenced by solvent viscosity, as the viscosities of the viscogens utilized vary strongly with temperature. In contrast, a linear fit was not obtainable when using the rates of *Htelo1* refolding in the 90% DES conditions. Specifically, as observed in Figure 5.19, only a factor of 10 of the 25-fold difference in *Htelo1* refolding rates in 90% DES can be attributed to solvent viscosity.

Most studies of protein folding kinetics as a function of solvent viscosity have shown less than an inverse dependence of folding rate with solvent viscosity, especially at lower viscosities and with faster folding molecules.[78, 79, 85, 87, 90-92] That is, $k \propto 1/\eta^n$, with $n < 1$. Typically, the exponent of viscosity approaches unity with increasing

viscosity.[78] In contrast, *Htelo1* refolding in 90% DES has a greater than expected increase in refolding time. One possibility for this difference is an over estimation of the solvent viscosity that is experienced by the G-quadruplex in its immediate (microscopic) vicinity. Previous studies showed that large polymers do not significantly affect the rate of small molecule diffusion in a fluid.[94] However, a microscopic viscosity analysis of PEG 200 displayed a good correlation between dynamic viscosity and microscopic viscosity making the over estimation of PEG 200 viscosity unlikely.[111] Another explanation is that the solvent friction experienced by *Htelo1* increases more than linearly with the macroscopic dynamic viscosity of 90% ChCl-urea. In this case, the actual solvent friction could be greater than predicted by solvent viscosity if solvent molecules (e.g., choline) associate with the nucleic acid are more strongly than water and thereby increase the effective size of HTS DNA structures (e.g. loops) that require rearrangement of bulk solvent molecules for refolding. This heterogeneous reaction friction effect could increase the "roughness" of the free energy surface, thereby accounting for the additional factor of 2.5 decrease in rates observed in the 90% DES solvent.

Another possible explanation is that different viscogens could affect the equilibrium enthalpy of folding and thereby alter the transition energy barrier due to a change in the enthalpy of activation. A 7 °C increase in T_m's between the 40% PEG 200 and 90% DES conditions supports this hypothesis, (Figures 3.11 and 3.8 respectively) however, the observed activation energies from the Arrhenius analysis are the same between the two solvents, (within experimental error, Table 5.3) indicating that the rate-limiting folding transition barriers are the same and stability effects are not the main cause of the greater than expected slowdown of refolding rates in 90% DES. Moreover,

the T_m's observed in the refolding conditions with glycerol as an added viscogen are higher than that observed for 40% PEG 200, (Figures 5.25 and 5.26), but an increase in folding rates is not observed in these two solvents. Therefore, the refolding transition state ensembles of *Htelo1* are likely congruent between the various solvents and the probable explanation for the greater than expected slowdown of refolding in 90% DES is caused by increased heterogeneous reaction friction due to the solvent properties of the ChCl-urea DES.

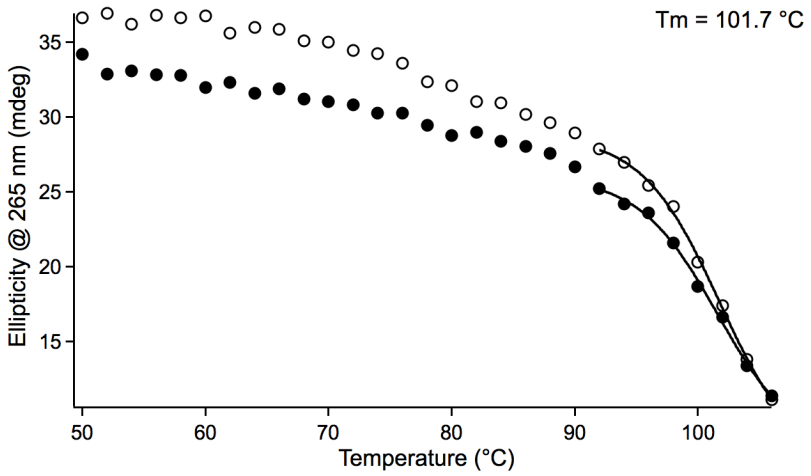

Figure 5.25 Heating and cooling traces of d[$TAG_3(TTAG_3)_3$] (*Htelo1*) in the 40% PEG 200 / 30% glycerol (v/v with water) generated by monitoring CD intensity at 265 nm as a function of temperature. Heating/cooling rates were approximately 0.34 °C/min. Samples were 1 mM in nucleotide and contained 100 mM KCl and 20 mM potassium phosphate buffer, pH 7. Heating traces shown with open circles; cooling traces shown filled circles. Sigmoidal fits of traces after attempted baseline correction to obtain T_m values are shown with black lines. T_m value, displayed on the figure is an estimate. The melting point of the G-quadruplex is too high in these conditions to be accurately determined due to the lack of an upper melting baseline.

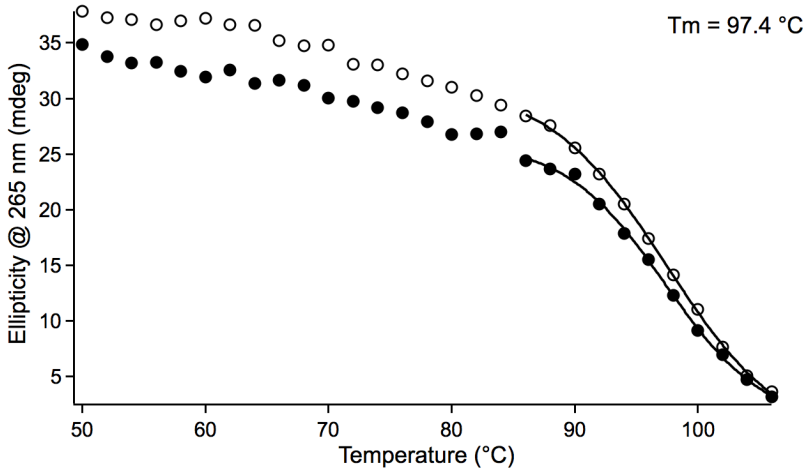

Figure 5.26 Heating and cooling traces of d[$TAG_3(TTAG_3)_3$] (*Htelo1*) in the 40% PEG 200 / 15% glycerol (v/v with water) generated by monitoring CD intensity at 265 nm as a function of temperature. Heating/cooling rates were approximately 0.34 °C/min. Samples were 1 mM in nucleotide and contained 100 mM KCl and 20 mM potassium phosphate buffer, pH 7. Heating traces shown with open circles; cooling traces shown filled circles. Sigmoidal fits of traces after attempted baseline correction to obtain T_m values are shown with black lines. T_m value, displayed on the figure is an estimate. The melting point of the G-quadruplex is too high in these conditions to be accurately determined due to the lack of an upper melting baseline.

Overall, the comparison of the time constants associated with the *Htelo1* structural transition from its mixed stranded folded state in aqueous solution to its parallel fold in 90% ChCl-urea DES or 40% PEG 200 with added glycerol with time constants for the same transition in 40% PEG 200 only, provide solid evidence that G-quadruplex folding can be altered by solvent friction in accordance with Kramers rate theory. Likewise, analysis of DNA hairpin folding rates, which takes place on the tens of μs time scale, were found to follow an approximately $\boldsymbol{k \propto \eta^{-1}}$ relationship upon addition of glycerol as a viscogen.[73, 74] Despite differences in the details of the present study and past studies of protein or nucleic acid folding/refolding, the data presented here demonstrates that Kramers rate theory is valid for describing the effect of solvent

viscosity on the macromolecular folding of G-quadruplex DNA over multiple orders of magnitude. It also appears that the unique properties of the choline-chloride and urea DES increase the solvent friction effects over other viscogens.

CHAPTER 6

CONCLUSION

During the course of this study, it was determined that the human telomere sequence in anhydrous ChCl-urea DES adopts a parallel-stranded "propeller" G-quadruplex topology similar to that observed in 40% PEG 200 solution and in the crystal state. The exact physiological form of human telomere sequence G-quadruplex DNA is still unclear, however, the results of this investigation confirms observations that HTS G-quadruplex conformation is greatly influenced by water activity.

Additionally, this work demonstrates that the HTS G-quadruplex is vulnerable to significant kinetic control in alternative solvents with increased viscosity. Specifically, it was discovered that the high solvent friction of an anhydrous ChCl-urea DES alters the pathway of HTS folding from the thermally denatured state, thereby entrapping kinetic intermediates on the order of months at room temperature. This behaviour has not been observed for HTS G-quadruplex in aqueous solutions.

Furthermore, by probing the viscosity dependence of *Htelo1* refolding rates in different viscogens, it was determined that the HTS DNA G-quadruplex is subject to diffusion control in accordance with Kramers rate theory. Moreover, the present study demonstrates that Kramers rate expression is valid over an additional 5 orders of magnitude from 1 second in protein folding studies to over 94 hours for *Htelo1* refolding. Empirical evidence also showed that the ChCl-urea DES slowed the refolding reaction rates even more than anticipated ($1/\tau \sim \eta^{-n}$; $n>1$), indicating that a significant portion of

the friction experienced in the system is a result of the distinctive properties of the solvent and its interaction with *Htelo 1*.

These discoveries highlight the fact that studies into G-quadruplex dynamics should consider solvent friction effects. Additionally, it is reasonable to assume that many other nucleic acid topologies will be found to show similar behaviour in high viscosity solvents. For this reason, it is important to note that further insights into the dynamics of nucleic acid secondary structure, might be obtained through the use viscogenic cosolvents and application of Kramers rate theory.

APPENDIX A

SUPPLEMENTARY FIGURES FOR CHAPTER 5

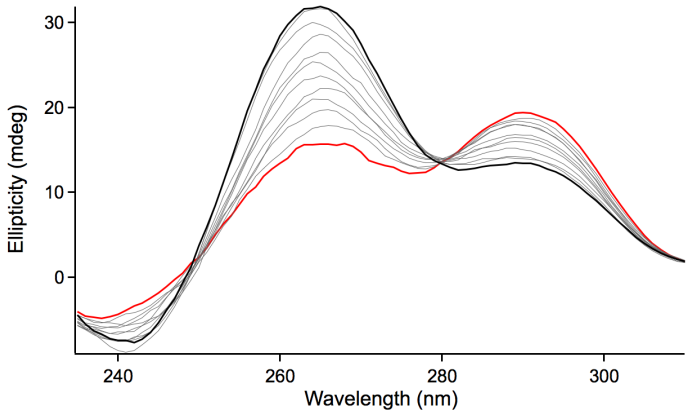

Figure A.1 Time dependent CD spectra of *Htelo1* following transfer to 90% ChCl-urea DES (w/w). Initial spectrum after mixing and transfer to instrument at 30 °C is shown in red. Sample was 1 m*m* in nucleotide; 100 m*m* KCl and 20 m*m* potassium phosphate, pH 7.

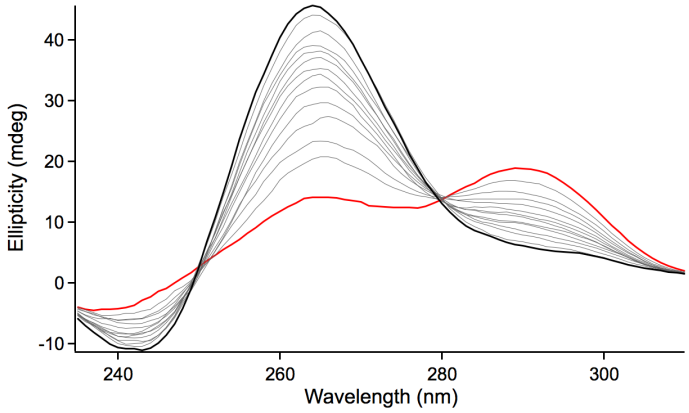

Figure A.2 Time dependent CD spectra of *Htelo1* following transfer to 90% ChCl-urea DES (w/w). Initial spectrum after mixing and transfer to instrument at 50 °C is shown in red. Sample was 1 m*m* in nucleotide; 100 m*m* KCl and 20 m*m* potassium phosphate, pH 7.

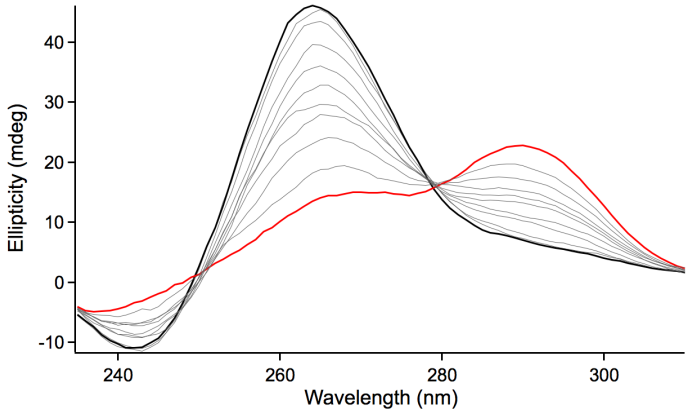

Figure A.3 Time dependent CD spectra of *Htelo1* following transfer to 90% ChCl-urea DES (w/w). Initial spectrum after mixing and transfer to instrument at 60 °C is shown in red. Sample was 1 m*m* in nucleotide; 100 m*m* KCl and 20 m*m* potassium phosphate, pH 7.

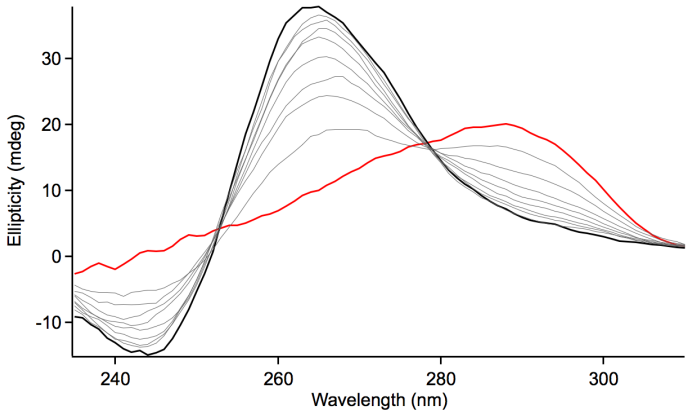

Figure A.4 Time dependent CD spectra of *Htelo1* following transfer to 40% PEG 200 (v/v). Initial spectrum after mixing and transfer to instrument at 50 °C is shown in red. Sample was 1 mM in nucleotide; 100 mM KCl and 20 mM potassium phosphate, pH 7.

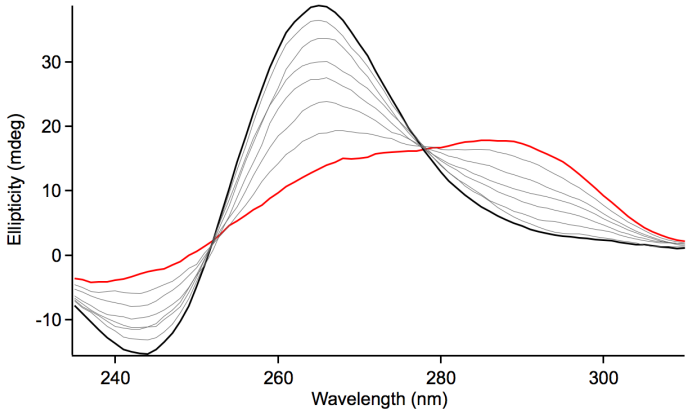

Figure A.5 Time dependent CD spectra of *Htelo1* following transfer to 40% PEG 200 (v/v). Initial spectrum after mixing and transfer to instrument at 60 °C is shown in red. Sample was 1 mM in nucleotide; 100 mM KCl and 20 mM potassium phosphate, pH 7.

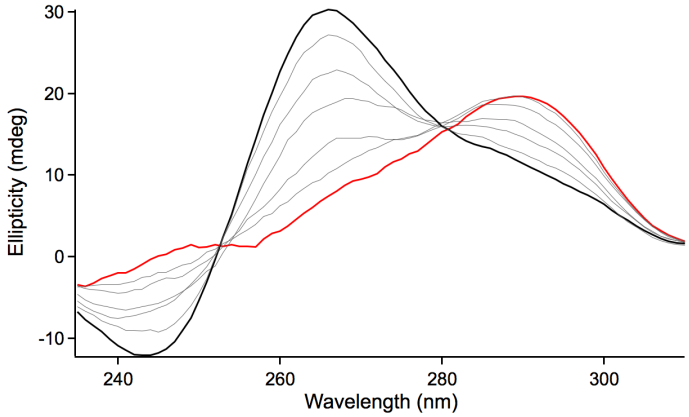

Figure A.6 Time dependent CD spectra of *Htelo1* following transfer to 40% PEG 200 / 30% Glycerol (v/v). Initial spectrum after mixing and transfer to instrument at 30 °C is shown in red. Sample was 1 mM in nucleotide; 100 mM KCl and 20 mM potassium phosphate, pH 7.

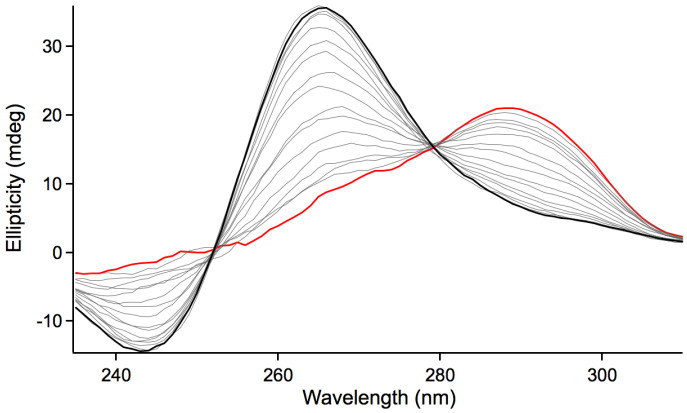

Figure A.7 Time dependent CD spectra of *Htelo1* following transfer to 40% PEG 200 / 30% Glycerol (v/v). Initial spectrum after mixing and transfer to instrument at 50 °C is shown in red. Sample was 1 mM in nucleotide; 100 mM KCl and 20 mM potassium phosphate, pH 7.

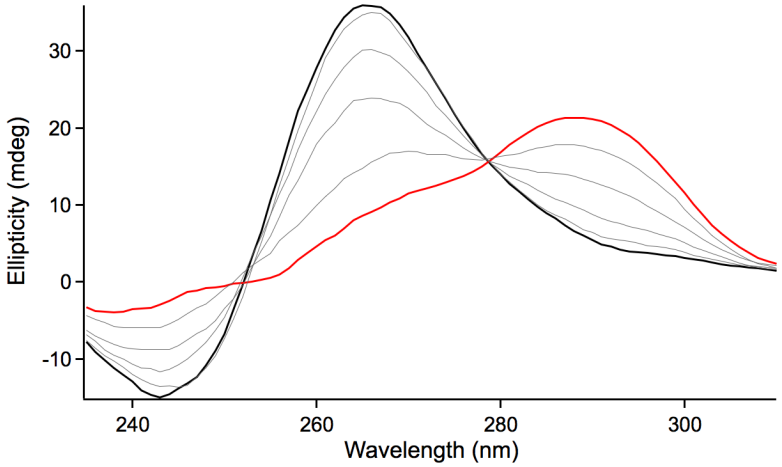

Figure A.8 Time dependent CD spectra of *Htelo1* following transfer to 40% PEG 200 / 30% Glycerol (v/v). Initial spectrum after mixing and transfer to instrument at 60 °C is shown in red. Sample was 1 mM in nucleotide; 100 mM KCl and 20 mM potassium phosphate, pH 7.

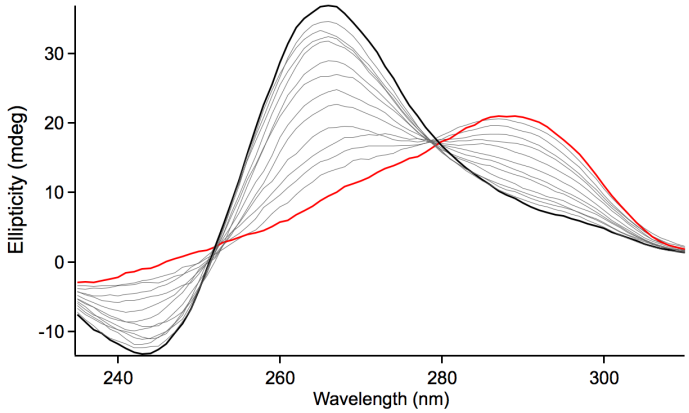

Figure A.9 Time dependent CD spectra of *Htelo1* following transfer to 40% PEG 200 / 15% Glycerol (v/v). Initial spectrum after mixing and transfer to instrument at 30 °C is shown in red. Sample was 1 mM in nucleotide; 100 mM KCl and 20 mM potassium phosphate, pH 7.

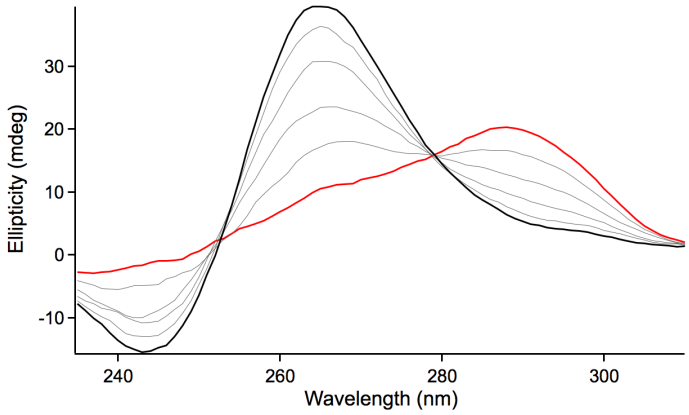

Figure A.10 Time dependent CD spectra of *Htelo1* following transfer to 40% PEG 200 / 15% Glycerol (v/v). Initial spectrum after mixing and transfer to instrument at 50 °C is shown in red. Sample was 1 mM in nucleotide; 100 mM KCl and 20 mM potassium phosphate, pH 7.

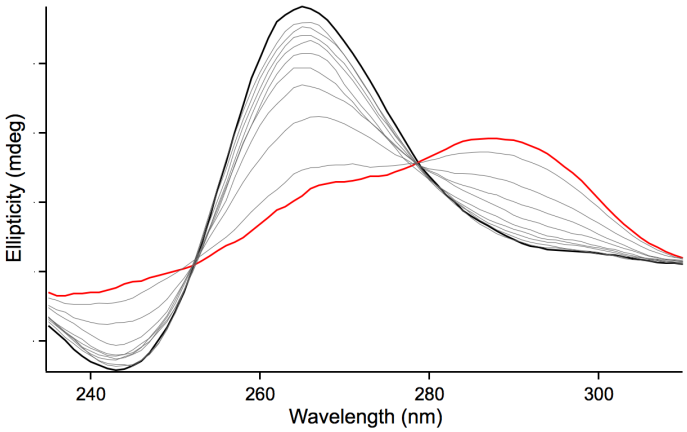

Figure A.11 Time dependent CD spectra of *Htelo1* following transfer to 40% PEG 200 / 15% Glycerol (v/v). Initial spectrum after mixing and transfer to instrument at 60 °C is shown in red. Sample was 1 mM in nucleotide; 100 mM KCl and 20 mM potassium phosphate, pH 7.

REFERENCES

1. Heddi, B. and A.T.n. Phan, *Structure of Human Telomeric DNA in Crowded Solution.* Journal of the American Chemical Society, 2011. **133**(25): p. 9824-9833.

2. Miller, M.C., et al., *Hydration Is a Major Determinant of the G-Quadruplex Stability and Conformation of the Human Telomere 3′ Sequence of d(AG3(TTAG3)3).* Journal of the American Chemical Society, 2010. **132**(48): p. 17105-17107.

3. Vorlíčková, M., et al., *Intramolecular and intermolecular guanine quadruplexes of DNA in aqueous salt and ethanol solutions.* Biopolymers, 2007. **86**(1): p. 1-10.
4. Kuimova, M.K., et al., *Molecular Rotor Measures Viscosity of Live Cells via Fluorescence Lifetime Imaging.* Journal of the American Chemical Society, 2008. **130**(21): p. 6672-6673.

5. Gellert, M., M.N. Lipsett, and D.R. Davies, *Helix Formation by Guanylic Acid.* Proceedings of the National Academy of Sciences, 1962. **48**(12): p. 2013-2018.

6. Phan, A.T., *Human telomeric G-quadruplex: structures of DNA and RNA sequences.* FEBS J, 2010. **277**(5): p. 1107-17.

7. Neidle, S. and S. Balasubramanian, *Quadruplex nucleic acids*. RSC biomolecular sciences2006, Cambridge: RSC Pub. xiv, 301 p.

8. McEachern, M.J., A. Krauskopf, and E.H. Blackburn, *Telomeres and their control.* Annu Rev Genet, 2000. **34**: p. 331-358.

9. de Lange, T., *How Telomeres Solve the End-Protection Problem.* Science, 2009. **326**(5955): p. 948-952.

10. Moyzis, R.K., et al., *A highly conserved repetitive DNA sequence, (TTAGGG)n, present at the telomeres of human chromosomes.* Proc Natl Acad Sci U S A, 1988. **85**(18): p. 6622-6.

11. Meyne, J., R.L. Ratliff, and R.K. Moyzis, *Conservation of the human telomere sequence (TTAGGG)n among vertebrates.* Proc Natl Acad Sci U S A, 1989. **86**(18): p. 7049-53.

12. Siddiqui-Jain, A., et al., *Direct evidence for a G-quadruplex in a promoter region and its targeting with a small molecule to repress c-MYC transcription.* Proceedings of the National Academy of Sciences, 2002. **99**(18): p. 11593-11598.

13. Kim, N.W., et al., *Specific Association of Human Telomerase Activity with Immortal Cells and Cancer.* Science, 1994. **266**(5193): p. 2011-2015.

14. Hanahan, D. and R.A. Weinberg, *Hallmarks of Cancer: The Next Generation.* Cell, 2011. **144**(5): p. 646-674.

15. Neidle, S., *Human telomeric G-quadruplex: The current status of telomeric G-quadruplexes as therapeutic targets in human cancer.* FEBS Journal, 2010. **277**(5): p. 1118-1125.

16. Mergny, J.L. and C. Helene, *G-quadruplex DNA: a target for drug design.* Nature medicine, 1998. **4**(12): p. 1366-7.

17. Silva, M.W., *Geometric formalism for DNA quadruplex folding.* Chemistry-a European Journal, 2007. **13**(35): p. 9738-9745.

18. Parkinson, G.N., M.P. Lee, and S. Neidle, *Crystal structure of parallel quadruplexes from human telomeric DNA.* Nature, 2002. **417**(6891): p. 876-80.

19. Wang, Y. and D.J. Patel, *Solution Structure of the Human Telomeric Repeat D[Ag(3)(T(2)Ag(3))3] G-Tetraplex.* Structure, 1993. **1**(4): p. 263-282.

20. Luu, K.N., et al., *Structure of the human telomere in K(+) solution: An intramolecular (3+1) G-quadruplex scaffold.* J Am Chem Soc, 2006. **128**(30): p. 9963-9970.

21. Dai, J.X., et al., *Structure of the Hybrid-2 type intramolecular human telomeric G-quadruplex in K+ solution: insights into structure polymorphism of the human telomeric sequence.* Nucleic Acids Res, 2007. **35**(15): p. 4927-4940.

22. Matsugami, A., et al., *Structure of a human telomeric DNA sequence stabilized by 8-bromoguanosine substitutions, as determined by NMR in a K+ solution.* FEBS Journal, 2007. **274**(14): p. 3545-3556.

23. Phan, A.T., et al., *Structure of two intramolecular G-quadruplexes formed by natural human telomere sequences in K+ solution.* Nucleic Acids Res, 2007. **35**(19): p. 6517-25.

24. Lim, K.W., et al., *Structure of the human telomere in K+ solution: a stable basket-type G-quadruplex with only two G-tetrad layers.* J Am Chem Soc, 2009. **131**(12): p. 4301-9.

25. Dai, J.X., et al., *Structure of the intramolecular human telomeric G-quadruplex in potassium solution: a novel adenine triple formation.* Nucleic Acids Res, 2007. **35**(7): p. 2440-2450.

26. Lim, K.W., et al., *Sequence variant (CTAGGG)n in the human telomere favors a G-quadruplex structure containing a G.C.G.C tetrad.* Nucleic Acids Res, 2009. **37**(18): p. 6239-48.

27. Li, J., et al., *Not so crystal clear: the structure of the human telomere G-quadruplex in solution differs from that present in a crystal.* Nucleic Acids Res, 2005. **33**(14): p. 4649-59.

28. Xue, Y., et al., *Human telomeric DNA forms parallel-stranded intramolecular G-quadruplex in K+ solution under molecular crowding condition.* J Am Chem Soc, 2007. **129**(36): p. 11185-91.

29. Miyoshi, D., H. Karimata, and N. Sugimoto, *Hydration Regulates Thermodynamics of G-Quadruplex Formation under Molecular Crowding Conditions.* J Am Chem Soc, 2006. **128**(24): p. 7957-7963.

30. Chang, C.-C., et al., *Detection of Quadruplex DNA Structures in Human Telomeres by a Fluorescent Carbazole Derivative.* Anal Chem, 2004. **76**(15): p. 4490-4494.

31. Fletcher, T.M., et al., *Effect of DNA Secondary Structure on Human Telomerase Activity†.* Biochemistry, 1998. **37**(16): p. 5536-5541.

32. Oganesian, L. and T.M. Bryan, *Physiological relevance of telomeric G-quadruplex formation: a potential drug target.* BioEssays, 2007. **29**(2): p. 155-165.

33. Hänsel, R., et al., *The parallel G-quadruplex structure of vertebrate telomeric repeat sequences is not the preferred folding topology under physiological conditions.* Nucleic Acids Res, 2011.

34. Renciuk, D., et al., *Arrangements of human telomere DNA quadruplex in physiologically relevant K+ solutions.* Nucleic Acids Res, 2009. **37**(19): p. 6625-34.

35. Zhang, D.-H., et al., *Monomorphic RNA G-Quadruplex and Polymorphic DNA G-Quadruplex Structures Responding to Cellular Environmental Factors.* Biochemistry, 2010. **49**(21): p. 4554-4563.

36. Paeschke, K., et al., *Telomere end-binding proteins control the formation of G-quadruplex DNA structures in vivo.* Nature Structural & Molecular Biology, 2005. **12**(10): p. 847-854.

37. Xu, Y., Y. Noguchi, and H. Sugiyama, *The new models of the human telomere d[AGGG(TTAGGG)3] in K+ solution.* Bioorg. Med. Chem., 2006. **14**: p. 5584-5591.

38. Lee, J.Y., et al., *Extreme conformational diversity in human telomeric DNA.* Proc Natl Acad Sci U S A, 2005. **102**(52): p. 18938-18943.

39. Miyoshi, D. and N. Sugimoto, *Molecular crowding effects on structure and stability of DNA.* Biochimie, 2008. **90**(7): p. 1040-1051.

40. Mergny, J.L., A.T. Phan, and L. Lacroix, *Following G-quartet formation by UV-spectroscopy.* FEBS letters, 1998. **435**(1): p. 74-8.

41. Phan, A.T. and J.L. Mergny, *Human telomeric DNA: G-quadruplex, i-motif and Watson-Crick double helix.* Nucleic Acids Res, 2002. **30**(21): p. 4618-25.

42. Lane, A.N., et al., *Stability and kinetics of G-quadruplex structures.* Nucleic Acids Res, 2008. **36**(17): p. 5482-515.

43. Gu, J., J. Leszczynski, and M. Bansal, *A new insight into the structure and stability of Hoogsteen hydrogen-bonded G-tetrad: an ab initio SCF study.* Chemical Physics Letters, 1999. **311**(3–4): p. 209-214.

44. Gray, R.D. and J.B. Chaires, *Linkage of cation binding and folding in human telomeric quadruplex DNA.* Biophysical Chemistry, 2011. **159**(1): p. 205-209.

45. Vorlickova, M., et al., *Guanine tetraplex topology of human telomere DNA is governed by the number of (TTAGGG) repeats.* Nucleic Acids Res, 2005. **33**(18): p. 5851-60.

46. Li, W., et al., *Characterization and thermodynamic properties of quadruplex/duplex competition.* Febs Letters, 2002. **526**(1-3): p. 77-81.

47. Venczel, E.A. and D. Sen, *Parallel and Antiparallel G-DNA Structures from a Complex Telomeric Sequence.* Biochemistry, 1993. **32**(24): p. 6220-6228.

48. Aaron E. Engelhart, J.P., Ozgul Persil and Hud, Nicholas V., *Metal Ion Interactions with G-Quadruplex Structures*, in *Nucleic Acid-Metal Ion Interactions*, N.V. Hud, Editor 2008, RCS Publishing. p. 154-179.

49. Balagurumoorthy, P. and S.K. Brahmachari, *Structure and Stability of Human Telomeric Sequence.* J. Biol. Chem., 1994. **269**(34): p. 21858-21869.

50. Risitano, A. and K.R. Fox, *Stability of intramolecular DNA quadruplexes: Comparison with DNA duplexes.* Biochemistry, 2003. **42**(21): p. 6507-6513.

51. Hud, N.V., et al., *The selectivity for K+ versus Na+ in DNA quadruplexes is dominated by relative free energies of hydration: A thermodynamic analysis by H-1 NMR.* Biochemistry, 1996. **35**(48): p. 15383-15390.

52. Phillips, K., et al., *The crystal structure of a parallel-stranded guanine tetraplex at 0.95 angstrom resolution.* J Mol Biol, 1997. **273**(1): p. 171-182.

53. Guedin, A., et al., *How long is too long? Effects of loop size on G-quadruplex stability.* Nucleic Acids Research, 2010. **38**(21): p. 7858-7868.

54. Strahan, G.D., M.A. Keniry, and R.H. Shafer, *NMR structure refinement and dynamics of the K+-[d(G3T4G3)]2 quadruplex via particle mesh Ewald molecular dynamics simulations.* Biophys J, 1998. **75**(2): p. 968-81.

55. Keniry, M.A., et al., *Solution structure of the Na+ form of the dimeric guanine quadruplex [d(G3T4G3)]2.* European Journal of Biochemistry, 995. **233**(2): p. 631-43.

56. Lu, M., Q. Guo, and N.R. Kallenbach, *Thermodynamics of G-tetraplex formation by telomeric DNAs.* Biochemistry, 1993. **32**(2): p. 598-601.

57. Xue, Y., et al., *Kinetic and Thermodynamic Control of G-Quadruplex Folding.* Angewandte Chemie International Edition, 2011. **50**(35): p. 8046-8050.

58. Phan, A.T. and D.J. Patel, *Two-repeat human telomeric d(TAGGGTTAGGGT) sequence forms interconverting parallel and antiparallel G-quadruplexes in solution: distinct topologies, thermodynamic properties, and folding/unfolding kinetics.* J Am Chem Soc, 2003. **125**(49): p. 15021-7.

59. Gray, R.D. and J.B. Chaires, *Kinetics and mechanism of K+- and Na+-induced folding of models of human telomeric DNA into G-quadruplex structures.* Nucleic Acids Res, 2008. **36**(12): p. 4191-203.

60. Zhao, Y., et al., *Determining the folding and unfolding rate constants of nucleic acids by biosensor. Application to telomere G-quadruplex.* J Am Chem Soc, 2004. **126**(41): p. 13255-13264.

61. Ying, L.M., et al., *Studies on the structure and dynamics of the human telomeric G quadruplex by single-molecule fluorescence resonance energy transfer.* Proc. Natl. Acad. Sci. USA, 2003. **100**(25): p. 14629-14634.

62. Green, J.J., et al., *Kinetics of unfolding the human telomeric DNA quadruplex using a PNA trap.* J Am Chem Soc, 2003. **125**(13): p. 3763-7.

63. Okamoto, K., et al., *G-quadruplex structures of human telomere DNA examined by single molecule FRET and BrG-substitution.* Bioorg Med Chem, 2008. **16**(14): p. 6873-6879.

64. Mashimo, T., et al., *Folding Pathways of Human Telomeric Type-1 and Type-2 G-Quadruplex Structures.* J Am Chem Soc, 2010. **132**(42): p. 14910-14918.

65. Ambrus, A., et al., *Human telomeric sequence forms a hybrid-type intramolecular G-quadruplex structure with mixed parallel/antiparallel strands in potassium solution.* Nucleic Acids Research, 2006. **34**(9): p. 2723-2735.

66. Zhang, Z.J., et al., *Structure of a two-G-tetrad intramolecular G-quadruplex formed by a variant human telomeric sequence in K(+) solution: insights into the interconversion of human telomeric G-quadruplex structures.* Nucleic Acids Res, 2010. **38**(3): p. 1009-1021.

67. Zimmerman, S.B. and S.O. Trach, *Estimation of macromolecule concentrations and excluded volume effects for the cytoplasm of Escherichia coli. J. Mol. Biol.*, 1991. **222**(3): p. 599-620.

68. Ellis, R.J. and A.P. Minton, *Cell biology: Join the crowd.* Nature, 2003. **425**(6953): p. 27-28.

69. Zhou, H.-X., G. Rivas, and A.P. Minton, *Macromolecular Crowding and Confinement: Biochemical, Biophysical, and Potential Physiological Consequences.* Annual Review of Biophysics, 2008. **37**(1): p. 375-397.

70. Gray, R.D., J. Li, and J.B. Chaires, *Energetics and Kinetics of a Conformational Switch in G-Quadruplex DNA.* Journal of Physical Chemistry B, 2009. **113**(9): p. 2676-2683.

71. Xu, L., S. Feng, and X. Zhou, *Human telomeric G-quadruplexes undergo dynamic conversion in a molecular crowding environment.* Chem Commun (Camb), 2011. **47**(12): p. 3517-9.

72. Gray, R.D., et al., *Characterization of a K(+)-Induced Conformational Switch in a Human Telomeric DNA Oligonucleotide Using 2-Aminopurine Fluorescence.* Biochemistry, 2010. **49**(1): p. 179-194.

73. Wallace, M.I., et al., *Non-Arrhenius kinetics for the loop closure of a DNA hairpin.* Proc Natl Acad Sci U S A, 2001. **98**(10): p. 5584-9.

74. Ansari, A. and S.V. Kuznetsov, *Is Hairpin Formation in Single-Stranded Polynucleotide Diffusion-Controlled?* The Journal of Physical Chemistry B, 2005. **109**(26): p. 12982-12989.

75. Uzawa, T., et al., *The Length and Viscosity Dependence of End-to-End Collision Rates in Single-Stranded DNA.* Biophys J, 2009. **97**(1): p. 205-210.

76. Kramers, H.A., *Brownian motion in a field of force and the diffusion model of chemical reactions.* Physica, 1940. **7**: p. 284-304.

77. Hagen, S.J., *Solvent viscosity and friction in protein folding dynamics.* Curr Protein Pept Sci, 2010. **11**(5): p. 385-95.

78. Ansari, A., et al., *The role of solvent viscosity in the dynamics of protein conformational changes.* Science, 1992. **256**(5065): p. 1796-8.

79. Best, R.B. and G. Hummer, *Diffusive Model of Protein Folding Dynamics with Kramers Turnover in Rate.* Phys Rev Lett, 2006. **96**(22): p. 228104.

80. Portman, J.J., S. Takada, and P.G. Wolynes, *Microscopic theory of protein folding rates. II. Local reaction coordinates and chain dynamics.* Journal of Chemical Physics, 2001. **114**(11): p. 5082-5096.

81. Frauenfelder, H., et al., *Protein folding is slaved to solvent motions.* Proc Natl Acad Sci U S A, 2006. **103**(42): p. 15469-15472.

82. Jacob, M., et al., *Diffusion control in an elementary protein folding reaction.* Proceedings of the National Academy of Sciences, 1997. **94**(11): p. 5622-5627.

83. Jacob, M., et al., *Diffusional barrier crossing in a two-state protein folding reaction.* Nat Struct Biol, 1999. **6**(10): p. 923-6.

84. Plaxco, K.W. and D. Baker, *Limited internal friction in the rate-limiting step of a two-state protein folding reaction.* Proc Natl Acad Sci U S A, 1998. **95**(23): p. 13591-6.

85. Qiu, L. and S.J. Hagen, *A Limiting Speed for Protein Folding at Low Solvent Viscosity.* J Am Chem Soc, 2004. **126**(11): p. 3398-3399.

86. Plotkin, S.S. and J.N. Onuchic, *Understanding protein folding with energy landscape theory. Part I: Basic concepts.* Q Rev Biophys, 2002. **35**(2): p. 111-67.

87. J, S., *Viscosity dependence of intramolecular activated processes.* Chemical Physics, 1988. **120**(2): p. 187-197.

88. Ramos, C.H., S. Weisbuch, and M. Jamin, *Diffusive motions control the folding and unfolding kinetics of the apomyoglobin pH 4 molten globule intermediate.* Biochemistry, 2007. **46**(14): p. 4379-89.

89. Perl, D., et al., *Thermodynamics of a diffusional protein folding reaction.* Biophysical Chemistry, 2002. **96**(2–3): p. 173-190.

90. Jas, G.S., W.A. Eaton, and J. Hofrichter, *Effect of Viscosity on the Kinetics of α-Helix and β-Hairpin Formation.* The Journal of Physical Chemistry B, 2000. **105**(1): p. 261-272.

91. Pabit, S.A., H. Roder, and S.J. Hagen, *Internal friction controls the speed of protein folding from a compact configuration.* Biochemistry, 2004. **43**(39): p. 12532-8.

92. Bieri, O., et al., *The speed limit for protein folding measured by triplet-triplet energy transfer.* Proc Natl Acad Sci U S A, 1999. **96**(17): p. 9597-601.

93. Yedgar, S., et al., *Viscosity dependence of O2 escape from respiratory proteins as a function of cosolvent molecular weight.* Biophys J, 1995. **68**(2): p. 665-70.

94. Blacklow, S.C., et al., *Triosephosphate isomerase catalysis is diffusion controlled. Appendix: Analysis of triose phosphate equilibria in aqueous solution by 31P NMR.* Biochemistry, 1988. **27**(4): p. 1158-67.

95. Ladurner, A.G. and A.R. Fersht, *Upper limit of the time scale for diffusion and chain collapse in chymotrypsin inhibitor 2.* Nat Struct Biol, 1999. **6**(1): p. 28-31.

96. Ardhammar, M.N., B., Kurucsev, T., *Circular Dichroism: Principles and Applications*. Second ed, ed. N. Berova, Nakanishi, K., Woody, R.W.2000: John Wiley & Sons, Inc. 741-768.

97. Berova, N., L. Di Bari, and G. Pescitelli, *Application of electronic circular dichroism in configurational and conformational analysis of organic compounds.* Chem Soc Rev, 2007. **36**(6): p. 914-31.

98. Masiero, S., et al., *A non-empirical chromophoric interpretation of CD spectra of DNA G-quadruplex structures.* Organic & Biomolecular Chemistry, 2010. **8**(12): p. 2683-92.

99. Paramasivan, S., I. Rujan, and P.H. Bolton, *Circular dichroism of quadruplex DNAs: Applications to structure, cation effects and ligand binding.* Methods, 2007. **43**(4): p. 324-331.

100. Karsisiotis, A.I., et al., *Topological Characterization of Nucleic Acid G-Quadruplexes by UV Absorption and Circular Dichroism.* Angewandte Chemie, 2011. **123**(45): p. 10833-10836.

101. Burge, S., et al., *Quadruplex DNA: sequence, topology and structure.* Nucleic Acids Research, 2006. **34**(19): p. 5402-5415.

102. Kypr, J. and M. Vorlickova, *Graphical analysis of circular dichroic spectra distinguishes between two-state and gradual alterations in DNA conformation.* Gen Physiol Biophys, 1986. **5**(4): p. 415-21.

103. Wallimann, P., et al., *Dual wavelength parametric test of two-state models for circular dichroism spectra of helical polypeptides: anomalous dichroic properties of alanine-rich peptides.* J Am Chem Soc, 2003. **125**(5): p. 1203-20.

104. Hendler, R.W. and R.I. Shrager, *Deconvolutions based on singular value decomposition and the pseudoinverse: a guide for beginners.* Journal of Biochemical and Biophysical Methods, 1994. **28**(1): p. 1-33.

105. Haq, I., B.Z. Chowdhry, and J.B. Chaires, *Singular value decomposition of 3-D DNA melting curves reveals complexity in the melting process.* European Biophysics Journal, 1997. **26**(6): p. 419-426.

106. Viswanath, D.S., Ghosh, T.K., Prasad, D.H.L., Dutt, N.V.K., Rani, K.Y., *Viscosity of Liquids: Theory, Estimation, Experiment, and Data*. Vol. XIV. 2007, Dordrecht, The Netherlands: Springer. 662.

107. Batchelor, G.K., *An Introduction To Fluid Dynamics*1967, Cambridge, UK: Cambridge University Press. 545.

108. Goins, A.B., H. Sanabria, and M.N. Waxham, *Macromolecular crowding and size effects on probe microviscosity.* Biophys J, 2008. **95**(11): p. 5362-73.

109. Kuimova, M.K., et al., *Imaging intracellular viscosity of a single cell during photoinduced cell death.* Nat Chem, 2009. **1**(1): p. 69-73.

110. Abbott, A.P., et al., *Novel solvent properties of choline chloride/urea mixtures.* Chem Commun (Camb), 2003(1): p. 70-1.

111. Bhanot, C., et al., *Dynamic viscosity versus probe-reported microviscosity of aqueous mixtures of poly(ethylene glycol).* The Journal of Chemical Thermodynamics, 2012. **45**(1): p. 137-144.

112. Abbott, A.P., R.C. Harris, and K.S. Ryder, *Application of hole theory to define ionic liquids by their transport properties.* Journal of Physical Chemistry B, 2007. **111**(18): p. 4910-3.

113. Abbott, A.P., et al., *Deep eutectic solvents formed between choline chloride and carboxylic acids: Versatile alternatives to ionic liquids.* Journal of the American Chemical Society, 2004. **126**(29): p. 9142-9147.

114. Mamajanov, I., et al., *DNA and RNA in anhydrous media: duplex, triplex, and G-quadruplex secondary structures in a deep eutectic solvent.* Angewandte Chemie, 2010. **49**(36): p. 6310-4.

115. Jang, Y.H., et al., *pKa Values of Guanine in Water: Density Functional Theory Calculations Combined with Poisson−Boltzmann Continuum−Solvation Model.* The Journal of Physical Chemistry B, 2002. **107**(1): p. 344-357.

116. Yim, S.D., et al., *Decomposition of Urea into NH3 for the SCR Process.* Industrial & Engineering Chemistry Research, 2004. **43**(16): p. 4856-4863.
117. Chaires, J.B., *Human telomeric G-quadruplex: thermodynamic and kinetic studies of telomeric quadruplex stability.* FEBS Journal, 2010. **277**(5): p. 1098-1106.

118. Abbott, A.P., et al., *Novel solvent properties of choline chloride/urea mixtures.* Chemical Communications, 2003(1): p. 70-71.

119. Hanggi, P., P. Talkner, and M. Borkovec, *Reaction-rate theory - 50 years after Kramers.* Reviews of Modern Physics, 1990. **62**(2): p. 251-341.

120. Hynes, J.T., *Chemical-reaction dynamics in solution.* Annual Review of Physical Chemistry, 1985. **36**: p. 573-597.